ABSTRACT

Title of Document: THE DELIVERY OF IGF-1 FOR SKELETAL MUSCLE REGENERATION WITHIN ABDOMINAL WALL HERNIAS

Erin Elizabeth Falco, Doctor of Philosophy, 2009

Directed By: Associate Professor, Dr. John P. Fisher, Fischell Department of Bioengineering

At an ever increasing pace, synthetic biomaterials are being developed with specific functionalities for tissue engineering applications. These biomaterials possess properties including biocompatibility, mechanical strength, and degradation as well as functionalities such as specific cell adhesion and directed cell migration. However, synthetic polymers are often not completely biologically inert and may non-specifically react with the surrounding *in vivo* environment. An example of this reactivity is the release of acidic degradation products from hydrolytically degradable polymers based upon an ester moiety. These degradation products can lower the local pH and incite an inflammatory response as well as increase scaffold degradation rate. Therefore there has been a concerted effort in the research community to develop alternatives.

In order to address this concern, a novel class of biomaterials based upon a cyclic acetal unit has been developed and investigated for both soft and hard tissue

repair. This work specifically looks at a cyclic acetal biomaterial based on a 5-ethyl-5-(hydroxymethyl)-β,β-dimethyl-1,3-dioxane-2-ethanol diacrylate (EHD) monomer as a scaffold for abdominal wall hernia repair.

Abdominal wall hernias are a growing concern for clinicians today as they occur in approximately 10% of all patients that undergo an abdominal procedure. Despite many advances in repair techniques, both wound healing and skeletal muscle regeneration is limited in many cases. This results in both a decrease in abdominal wall tissue function as well as a hernia recurrence rate of up to 50%.

To address this high recurrence rate this project aims to create a functional gene delivery scaffold from the EH monomer. Scaffolds with different architectures were fabricated and skeletal muscle myoblast cell compatibility, material properties and protein and gene delivery rates were all investigated.

THE DELIVERY OF IGF-1 FOR SKELETAL MUSCLE REGENERATION WITHIN ABDOMINAL WALL HERNIAS

By

Erin Elizabeth Falco

Dissertation submitted to the Faculty of the Graduate School of the
University of Maryland, College Park, in partial fulfillment
of the requirements for the degree of
Doctor of Philosophy
2009

Advisory Committee:
Professor John P Fisher, Chair
Professor William E. Bentley
Professor Srinivasa R. Raghavan
Professor Sameer B. Shah
Professor Lyle Isaacs

Dedication

I would like to dedicate this to my parents Anthony and Nancy Falco who have had unwavering supported for me through all of the ups and downs of this journey.

Without them I would never have made it this far.

I love you.

Acknowledgements

First and foremost I would like to thank my family for their endless support. Without them I would never have made it this far. This was truly a group effort at times and it's something that "we" have earned.

Next I would like to thank my advisor Dr. John P. Fisher without whom I would not have been able to complete this work. His assistance and support in showing me the big picture often helped me to put things into better perspective. In addition, I would like to thank Dr. J. Scott Roth whose collaboration helped lead the way for this project, as well as Dr. Abhay Pandit for imparting as much knowledge about plasmid DNA as possible on me in my short stay in his lab at NCBES.

I would also like to thank my committee members, Dr. William Bentley, Dr. Srinivasa Raghavan, Dr. Lyle Isaacs and Dr. Sameer Shah. Your comments given to me during my Masters Degree defense, PhD proposal and individual discussions have been very helpful in shaping this work.

Without the help of several undergrads throughout the way, this work would not be what it is today. Eve Rubinstein, Aubrey Francisco and Erik Li have worked hard for me and I hope this work makes them as proud as it makes me.

Finally I would like to thank my friends both in the Tissue Engineering and Biomaterials Lab and various labs on campus and abroad. Without you and your support, this experience would not have been nearly as amazing as it was. I don't know quite how to thank you.

Table of Contents

Dedication ii
Acknowledgements iii
Table of Contents iv
List of Tables vii
List of Figures viii
Chapter 1: Introduction 1
Chapter 2: Recent Developments in Cyclic Acetal Biomaterials for Tissue Engineering Applications 3
- Introduction 3
- Current Degradable Biomaterials 5
  - Polyesters 5
  - Polyanhydrides 7
- Cyclic Acetal Biomaterials 8
  - EH Networks 9
  - EH-PEG Hydrogels 14
  - Poly[poly(ethylene glycol)-co-cyclic acetal] (PECA) Hydrogels 18
- Polyacetals and Polyketals 20
- Conclusions 23
- Acknowledgements 24

Chapter 3: Skeletal Muscle Tissue Engineering Approaches to Abdominal Wall Hernia Repair 25
- Introduction 25
- Abdominal Wall Morphology 26
  - Abdominal Wall Physiology and Function 26
  - Musculature Development and Regeneration 28
- Anatomy of Hernia Formation 29
  - A Mechanism for Herniation 29
  - Wound Healing in Hernias 30
- Overview of Current Clinical Solutions 32
  - Clinical Approaches to Treat Abdominal Hernias 32
  - Criteria for Repair Techniques 33
  - Xenografts 34
  - Allografts 35
  - Autografts 36
  - Prosthetic Meshes 37
- Tissue Engineering Approaches to Treat Defects 39
  - Next Generation Polymeric Scaffolds 40
- Conclusions 41
- Acknowledgments 41

Chapter 4: Project Summary 42
Chapter 5: EH Networks as a Scaffold for Skeletal Muscle Regeneration in Abdominal Wall Hernia Repair 44

Introduction 44
Materials and Methods 48
Materials 48
EH Network Synthesis 48
Skeletal Myoblast Isolation and Harvest 49
Dynamic Mechanical Analysis 50
Skeletal Myoblast Attachment 51
Dosed IGF-1 Induced Myoblast Proliferation 51
Adsorbed IGF-1 Release Profile and its Effect on Myoblast Proliferation 52
Statistical Analysis 53
Results 53
Discussion 59
Conclusions 63
Acknowledgments 64
Chapter 6: Fabrication and Characterization of Porous EH Scaffolds and EH-PEG Bilayers 65
Introduction 65
Materials and Methods 67
Materials 67
5-ethyl-5-(hydroxymethyl)-β,β-dimethyl-1,3-dioxane-2-ethanol diacrylate Synthesis 68
Solid EH Network Formation 69
Solution Formed Porous EH Monolayer Formation 69
Solid PEG Monolayer Formation 70
EH-PEG Bilayer Production 71
Scanning Electron Microscopy 71
Degradation Study 72
Mechanical Analysis 72
Results 73
Discussion 80
Conclusions 85
Acknowledgments 86
Chapter 7: Porous EH Monolayers and EH-PEG Bilayers as a Gene Delivery Device for Abdominal Wall Hernias Repair 87
Introduction 87
Materials and Methods 90
Materials 90
5-ethyl-5-(hydroxymethyl)-β,β-dimethyl-1,3-dioxane-2-ethanol diacrylate Synthesis 90
Slurry Formed Porous EH Monolayer Formation 92
Solution Formed Porous EH Monolayer Formation 92
EH-PEG Bilayer Production 93
Scanning Electron Microscopy 94
Single Gene Lipoplex Formation 94
Dose Dependent SG Lipoplex Release from SLRY EH Monolayers 94
IGF-1 GFP Fusion Plasmid Construction 95

Fusion Gene Complex Formation 96
Fusion Gene Lipoplex Formation 96
Transfection Efficiency and Dose Dependence 96
Architecture Guided FG Complex Release 97
Statistical Analysis 97
Results 98
Discussion 103
Conclusions 108
Acknowledgments 108
Chapter 8: Summary 110
References 113

List of Tables

Table 7.1: The percent mass lost during leaching for two different SLRY and a SOLN EH monolayer. It was found that the SOLN fabrication technique produced scaffolds with higher pore interconnectivity than the SLRY fabrication technique. 105

List of Figures

Figure 2. 1: Chemical structure of 5-ethyl-5-(hydroxymethyl)-β,β-dimethyl-1, 3-dioxane-2-ethanol diacrylate (EHD) cyclic acetal networks and its degradation products (22). 10
Figure 2. 2: (A) The percent mass lost from EH scaffolds and (B) change in solvent pH during *in vitro* degradation. All porous groups displayed similar degradation over 28 days with a more dramatic degradation than the solid EH networks. Results also confirmed the near constant solvent pH throughout the 28 day degradation study, demonstrating the lack of acidic degradation products by the CABs. Values represent means and associated standard deviation (n=5). 13
Figure 2. 3: Chemical reaction between poly(ethylene glycol) diacrylate (PEGDA) and 5-ethyl-5-(hydroxymethyl)-β,β-dimethyl-1, 3-dioxane-2-ethanol diacrylate (EHD) to form EH-PEG hydrogels (58). 15
Figure 2. 4: Synthetic route for PECA and PECA hydrogels (60). 19

Figure 5. 1: (A) Chemical structure of the monomer 5-ethyl-5-(hydroxymethyl)-β,β-dimethyl-1,3dioxane-2-ethanol diacrylate (EHD). (B) Chemical structure of the resulting crosslinked EH network. (C) An EH network sheet made with a 0.58M BP solution. 45
Figure 5. 2: Complex modulus as a function of initiator concentration. A frequency sweep of 1–100 Hz was run on a Q-800 dynamic mechanical analyzer (TA Instruments) with parameters of 37°C and 15 μm amplitude. Results for 10 Hz are reported in this graph. 54
Figure 5. 3: Myoblast cell attachment on EH networks with varied initiator concentrations. All groups were found to be statistically similar. 55
Figure 5. 4: Total number of cells attached to EH networks after 3 and 5 days. It was shown in this study that only the IGF-1 groups at day 5 were statistically different from all groups in both time points. 56
Figure 5. 5: (A) Total IGF-1 released from the surface of the EH network. The 10 ng loading group showed a significantly lower amount of IGF-1 released than the 50 and 150 ng loading groups. The 50 and 150 ng groups were statistically similar for all time points except 2 and 48 h. (B) Percent IGF-1 release from the surface of the EH network. The 10 ng loading group released a significantly higher percent of the loaded IGF-1 than the 150 ng loading group. The 50 ng group released the highest percent of the loaded IGF-1 and was statistically different from both the 10 ng and 50 ng loading groups. 57
Figure 5. 6: Total number of cells attached to IGF-1 loaded EH networks after 3 and 5 days. It was shown in this study that only the networks that contained 50 and 150 ng of IGF-1 had more cells attached at day 3 than the 10 ng and control groups. It was also found that by day 5 all groups had leveled off and were statistically similar. 58

Figure 6. 1: (A) SEM image of the surface (top) and cross section (bottom) of a solid EH network (B) SEM image of the surface (top) and cross section (bottom) of a 75 wt% SOLN EH monolayer (C) SEM image of the surface (top) and cross section (bottom) of a 80 wt% SOLN EH monolayer. 74
Figure 6. 2: Percent mass change of solid EH networks, 75 and 80 wt% SOLN EH monolayers and 75 and 80 wt% EH-PEG bilayers degraded in PBS buffer over 85 days. The 75 and 80 wt% EH-PEG bilayers did not lose a significant percent of its mass over the course of this study. The solid EH networks lost 12.290 ± 0.663 % of their mass which was statistically different than at day 1, but was not statistically different than the 75 and 80 wt% bilayers. The 75 and 80 wt% SOLN EH monolayers lost the most percent mass having lost 29.209 ± 7.181 % and 25.028 ± 5.920 % respectively. 75
Figure 6. 3: pH change of PBS buffer solution from solid EH networks, 75 and 80 wt% SOLN EH monolayers and 75 and 80 wt% EH-PEG bilayers degraded over 85 days. The pH of the 75 wt% SOLN EH networks did not vary significantly over the course of the study. The solid EH networks and the 80 wt% SOLN EH monolayers however did show a significant decrease in pH to 6.98 ± 0.06 and 7.01 ± 0.06 respectively at day 85. Both of the 75 and 80 wt% EH-PEG bilayer groups showed the largest drops in pH from 7.4 to 5.87 ± 0.14 and 6.406 ± 0.17 respectively. 77
Figure 6. 4: The Young's modulus was found for 75 and 80 wt% SOLN EH monolayers, 75 and 80 wt% EH-PEG bilayers and a solid PEG control network. Results indicate the modulus for the 75 wt% SOLN EH monolayers was statistically higher than the 75 wt% EH-PEG bilayers and 80 wt% SOLN EH monolayers. In addition, the modulus for the 80 wt% EH-PEG bilayers and solid PEG control networks were statistically lower than all of the other groups. EH UP refers to when the force was being applied to the EH layer and PEG UP refers to when the force was being applied to the PEG layer. 78
Figure 6. 5: The flexural strength was found for 75 and 80 wt% SOLN EH monolayers, 75 and 80 wt% EH-PEG bilayers and a solid PEG control network. Results indicate the 75 wt% SOLN EH monolayers, 75 wt% EH-PEG bilayers and the 80 wt% SOLN EH monolayers were not statistically different. In addition it was found that the 80 wt% EH-PEG bilayers and solid PEG control network was significantly lower than all of the other groups. EH UP refers to when the force was being applied to the EH layer and PEG UP refers to when the force was being applied to the PEG layer. 79

Figure 7. 1: (A) Image of a 75 wt% porous SLRY EH monolayer. (B) SEM image of the surface of a 75 wt% SLRY EH monolayer. (C) SEM image of the cross section of a 75 wt% SLRY EH monolayer. (D) Higher

magnification SEM image of pores in a 75 wt% SLRY EH monolayer. 99
Figure 7. 2: (A) Image of an 80 wt% SOLN EH monolayer. (B) 10x magnification of an 80 wt% SOLN EH monolayer. (C) SEM image of the surface of an 80 wt% SOLN EH monolayer. (D) SEM image of the cross section of an 80 wt% SOLN EH monolayer. (E) Higher magnification SEM image of a single pore in an 80 wt% SOLN EH monolayer. 100
Figure 7. 3: Total SG plasmid DNA released from a 75 wt% porous SLRY EH monolayer. The 25 μg loading group released the most plasmid at 24 h followed by the 10 μg and 5 μg loading groups respectively. The 25 μg and 10 μg loading groups were statistically higher than the 5 μg loading groups at all time points. They were not statistically different from each other until the 2 h time point. 101
Figure 7. 4: (A) GFP expression within hSkMMs seeded at a density of 20,000 cells/well. (B) GFP expression within hSkMMs seeded at a density of 40,000 cells/well. (C) GFP expression within fused hSkMMs in culture. (D) Amount of IGF-1 produced from transfected hSkMMs. The general trend shows that there is a slight dose response over the DNA range used. In addition the lipoplexes and the complexes performed similarly at all doses. The 5 μg FuGENE complex group was statistically higher than the control group. 102
Figure 7. 5: Total IGF-1 GFP plasmid release from SOLN EH monolayers and bilayers. Trends showed that 80 wt% SOLN EH monolayers released more plasmid than the 75 wt% SOLN EH monolayers. It was also observed that the porous bilayers released more plasmid than their monolayer counterparts. 103

Chapter 1: Introduction

Synthetic biomaterials are often used clinically in the repair of both soft and hard tissues. These materials can be tailored to exhibit physical properties that mimic the desired tissue as well as chemical properties that promote a desired biological function. One drawback of these materials however is that they are not always biologically inert. Once implanted they can induce an inflammatory response which can hinder healing. This reaction occurs more strongly in degradable materials. Most degradable materials take advantage of the hydrolytically degradable ester moiety, however this unit produces acidic byproducts. This can lead to an increased inflammatory response as well as an increase in scaffold degradation. Therefore there has been significant research into developing materials that have more biocompatible properties. One such class of materials incorporates a cyclic acetal monomer in place of an ester. This cyclic acetal unit degrades hydrolytically into neutral diol and aldehyde byproducts. This makes it an attractive choice for tissue repair strategies.

Specifically, this work investigates the use of a cyclic acetal biomaterial for the regeneration of skeletal muscle within an abdominal wall defect. Abdominal wall hernias are an increasing problem in the United States with many cases going unreported and untreated. Current repair techniques include xenografts, allografts and prosthetic meshes. Despite these techniques, the hernia recurrence rate is as high as 50%.

To address this issue, scaffolds were fabricated from the cyclic acetal monomer 5-ethyl-5-(hydroxymethyl)-β,β-dimethyl-1,3-dioxane-2-ethanol diacrylate (EHD). First the mechanical and biological compatibility of solid EH networks was

investigated. Solid EH networks were fabricated and mechanical properties, cellular attachment and insulin-like growth factor 1 (IGF-1) protein release and viability were tested. Second, the structural architecture of the EH scaffolds was altered to produce more desirable mechanical and physical properties. To determine the effect changing scaffold architecture, the degradation and buffer pH change, as well as Young's modulus and flexural strength were examined. Third, the utility of these scaffolds as a gene delivery device was evaluated. Specifically, the effect of the scaffold architecture on the release of a green fluorescent protein (GFP) plasmid as well as an IGF-1 GFP fusion gene plasmid was studied. Overall, this work provides a comprehensive look at the design and characterization of an EH scaffold for skeletal muscle regeneration within an abdominal wall hernia defect.

Chapter 2: Recent Developments in Cyclic Acetal Biomaterials for Tissue Engineering Applications*

Introduction

Biomaterials fabricated from synthetic polymers have been exhaustively developed so as to possess both biocompatible and bioactive properties for biomedical and tissue engineering applications.[1-3] Depending upon each application, a newly developed polymer needs to meet a specific set of requirements. As a result, numerous studies have tailored polymers for individual applications by precisely controlling their chemical and physical properties.[4-8] For example, synthetic polymers have been fabricated into specific shaped materials with desired pore morphologies to promote tissue in-growth.[9-11] Indeed, a number of synthetic polymers have been successfully developed, and are now used widely in clinical applications.[12, 13]

A major advantage of synthetic polymers is that they may be modified to support the incorporation of drugs, chemical moieties, cells, implants and devices, as well as micro- and macro-molecules.[14-16] Furthermore, specific biological functions can be pre-programmed into polymer materials by incorporating any of a variety of molecules, including ligands, hormones, proteins, peptides, nucleotides, drugs, enzymes, vectors, and antibodies.[17-19] Together, these physical and biological properties can create an optimal biomaterial whose main function is to act as a tissue

* This chapter was published as the following article: Falco, E.E., M. Patel, and J.P. Fisher, *Recent developments in cyclic acetal biomaterials for tissue engineering applications.* Pharm Res, 2008. **25**(10): p. 2348-56

substitute. With the diversity of matrix components available, however, it may be possible for the polymeric biomaterial to provide additional functionalities so as to ultimately act as a tissue replacement, or engineered tissue. *In vivo*, polymeric biomaterials should facilitate cellular proliferation and differentiation, as precursors to the synthesis of a new organic extracellular matrix. To successfully promote cellular and tissue regeneration, synthetic polymers must first work in concert with the surrounding tissue, and thus elicit a short and mild inflammatory response. The surrounding tissue response is especially critical in the development of degradable polymeric biomaterials. In particular, these biomaterials should possess degradation properties that do not lead to a long and pronounced inflammatory reaction.[20, 21]

Recently, a number of investigators have shifted their focus to fabricating degradable, biomedical polymers that produce less toxic degradation products, therefore decreasing the inflammatory response of the surrounding tissue. For example, synthetic polymers based upon degradable units such as acetals, cyclic acetals, and ketals have been developed and shown to degrade via hydrolysis to produce hydroxyl and carbonyl terminals.[22-24] While the specific chemical structure of each degradation product is monomer and reaction specific, the products are typically alcohols, carbonyls, aldehydes, and ketones. This review will discuss the current research, development, and potential applications of newly developed acetal, cyclic acetal, and ketal based polymers. Further, this review will describe some of the encouraging physical, chemical, and biological properties of the resulting polymeric biomaterials, making them attractive candidates for a wide range of tissue engineering and drug delivery applications.

Current Degradable Biomaterials

Polymeric biomaterials vary widely both in material properties and applications. Tissue engineering applications require the consideration of properties such as biocompatibility, mechanical strength, and degradation. In the related field of drug delivery, however, the emphasis on mechanical strength is often replaced with the ability to release bioactive molecules. Overall, the importance given to each property is often application dependant and while many materials fulfill individual needs, there is still a requirement for a universally ideal material.

Polyesters

Polymers based upon a repeating ester unit are probably the most widely investigated biomaterials for biomedical and tissue engineering applications. Polyesters have been found to be largely biocompatible, along with possessing a wide range of mechanical and degradation properties. The simplest polyester is poly(glycolic acid) (PGA). PGA can easily be synthesized via the ring-opening polymerization of glycolide.[25] PGA is most notably used in the clinical setting as resorbable sutures, but is currently being investigated in several other biomedical applications.[26] PGA is a hydrophilic polymer which has a highly crystalline structure.[26] PGA degrades via bulk degradation, where mass loss occurs throughout the material while initial dimensions (or volume) of the material remains mostly constant.[27] Due to the mass loss, PGA materials exhibit a significant decrease in mechanical strength as the material degrades.[26, 28, 29] In an effort to increase PGA's

utility and slow its degradation, PGA is often used as a co-polymer with poly (L-lactic acid) (PLLA) or poly(D,L-lactic acid) (PLA).

PLLA and PLA are structurally similar to PGA, with the exception of the presence of a chiral methyl group. PLLA and PLA have a semi-crystalline structure and are hydrophobic in nature. The increased hydrophobicity leads to an increase in degradation rate compared to PGA.[26, 30-32] To increase the hydrophilicity of PLLA and slow the degradation rate of PGA, co-polymers with PLLA have been developed, such as the widely investigated poly(D,L-lactic-co-glycolic acid) (PLGA). A significant clinical application of the PLGA copolymers is in drug delivery, where injectable PLGA microspheres are utilized to deliver leuprolide acetate in a controlled profile.[30-32]

Poly(ε-caprolactone) (PCL) is a semi-crystalline polymer similar to PLA.[26] PCL has been extensively used for drug delivery applications due to its high permeability to drugs and long term sustainability *in vivo*.[26, 33, 34] The bulk degradation of PCL is a slow process on the order of one to three years. In an attempt to increase its degradation rate, PCL has been increasingly used in the synthesis of co-polymers and polymer blends with poly(ethylene glycol) (PEG), poly (ethylene oxide) (PEO), poly(hydroxybutyrate-co-hydroxyvalerate) (PHBHV), PLLA and PLGA.[35-38]

Poly(propylene fumarate) (PPF) is a linear polyester which hydrolytically degrades into fumaric acid and propylene glycol.[39] Due to the presence of carbon-carbon double bonds within the repeating unit of PPF, PPF may be covalently crosslinked to fabricate a rigid biomaterial. Previous studies have demonstrated that

PPF crosslinking may be initiated by either thermal or photo activated initiators.[40, 41] The physical properties of the PPF crosslinked networks, including the rate of degradation, are heavily influenced by the fabrication procedure.[26, 42] Particulate materials, including carbon nanotubes, have been incorporated within PPF to increase its mechanical strength, especially critical in bone tissue engineering applications.[43-45] *In vivo* studies of both the tissue response to PPF and the functionality of PPF scaffolds have indicated that the polymer promotes a mild inflammatory response similar to other polyester materials.[46, 47]

Polyanhydrides

Polyanhydrides are synthesized from diacid monomers, as opposed to the polyesters' single acid monomer, and they degrade hydrolytically at the anhydride linkages into diacid products. Polyanhydrides are especially desirable due to their surface erosion degradation properties.[26, 48, 49] Surface erosion occurs from the surface of the material, as opposed to bulk degradation which occurs throughout the material. Biomaterials that degrade through a surface mechanism retain their density, as mass is lost from the surface. The degradation rate of polyanhydrides has been shown to be largely controlled by the polymer backbone structure. Since the mechanical properties of polyanhydrides are generally modest, co-polymers and crosslinked polyanhydrides have been developed for bone tissue engineering applications.[26, 50] Polyanhydrides have also been used clinically as drug delivery materials.[26, 51, 52]

While polyesters and polyanhydrides are all widely characterized and under development for biomedical applications, they are not biologically inert and may non-specifically react with the surrounding *in vivo* environment.[53] Polyesters and polyanhydrides, as well as other similarly structured polymers, degrade via hydrolysis and give rise to products with carboxylic acid terminal groups. Thus their degradation may create an acidic regenerative environment which can prolong the inflammatory response and accelerate the degradation of the material, leading to premature loss of mechanical and structural properties.[54, 55] Previous studies have also shown that accumulation and increased concentration of acidic degradation products can induce tissue toxicity.[28, 29, 56] To address these issues, a new class of synthetic, polymeric biomaterials based upon degradable units such as acetals, cyclic acetals, and ketals have been developed.[22, 24, 53]

Cyclic Acetal Biomaterials

Cyclic acetal biomaterials (CAB) are a novel class of biomaterials consisting of a six member ring structure based upon a cyclic acetal unit. The cyclic acetal unit hydrolytically degrades, forming products terminated with diol and carbonyl end groups. Recent studies have described the development of CAB's for tissue engineering applications.[22, 57-59]

CABs are most easily fabricated by radical polymerization of the monomer 5-ethyl-5-(hydroxymethyl)-β,β-dimethyl-1,3-dioxane-2-ethanol diacrylate (EHD). Although available commercially through the early 2000s, to the best of our knowledge the EHD monomer is no longer commercially available. However, the

EHD monomer may be easily synthesized in approximately 4 days.[60] Briefly, isobutyraldehyde and formaldehyde are reacted with potassium carbonate. The product is then extracted using chloroform and is washed with water and brine. The resulting solution is dried under vacuum overnight, producing the solid product, 3-hydroxy-2,2-dimethylpropionaldehyde (HDP). HDP is then reacted with trimethylolpropane in 1 M hydrochloric acid. The solution is neutralized with sodium hydroxide and the resulting product, hydrolyzed EHD (HEHD), is extracted, washed with water and brine, purified by ether precipitation, and then dried overnight under vacuum. Finally acrylate terminal groups are added to the monomer. Here, HEHD is combined with triethylamine and acryloyl chloride. The final EHD product is extracted, washed, and purified by silica chromatography.[60]

It should be noted here that although the EHD monomer does allow for the fabrication of a polymer network whose backbone is formed by hydrolytically degradable cyclic acetal units, the use of acrylates in the crosslinking chemistry will form degradation products with terminal carboxylic acids. Future development of CABs will attempt to eliminate the acrylate based crosslinking chemistry, and therefore completely remove acidic degradation products.

EH Networks

A number of disparate biomaterials may be fabricated from the EHD monomer. The simplest material is a EH network, where the EHD monomer is radically polymerized in to a network, using the initiator benzoyl peroxide (BP) and the accelerant N,N-dimethyl-p-toluidine (DMT) (Fig. 1).

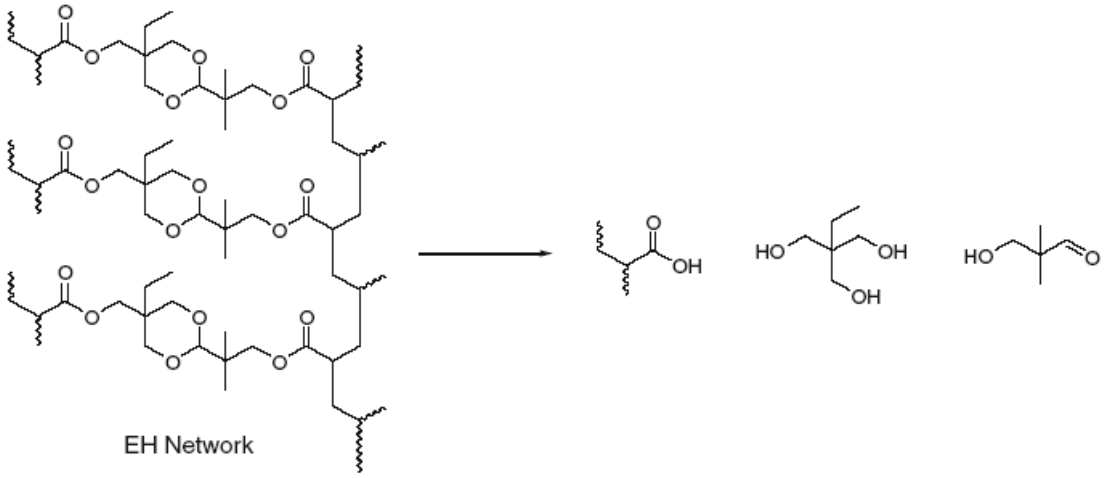

Figure 2. 1: Chemical structure of 5-ethyl-5-(hydroxymethyl)-β,β-dimethyl-1, 3-dioxane-2-ethanol diacrylate (EHD) cyclic acetal networks and its degradation products (22).

A recent study focused on the effects of initiator, accelerant, and diluent content on the physical properties of the EH networks.[22] Investigated properties included gelation time, reaction temperature, swelling degree, sol fraction, swelling degree, and cytotoxicity. Results showed that EH network gelation time varied between 33.3 and 193.9 s, with the gelation time decreasing with increased BP content. Maximum reaction temperature also increases from 31.9°C to 109.0°C with an increase in BP content. These gelation times and reactions temperatures are similar to the clinically relevant range for injectable biomaterials, however the utility of EH networks as an injectable biomaterial has not been fully investigated. Overall, results indicated that initiator and accelerant had the greatest effect upon the rate of reaction, as demonstrated by gelation time and maximum reaction temperature.[22] As EH networks are hydrophobic, they do not swell in water, however swelling in organic solvent can be utilized to describe network formation. Results showed that EH network swelling varied between 29.9% and 48.3%, while network sol fraction

varied from 22.0% to 45.0%. The results demonstrated that diluent content had the greatest effect upon swelling degree and sol fraction, and therefore most significantly affected the extent of the network forming reaction. Finally, results also indicated that EH networks could support the adhesion and viability of osteoprogenitor cells. There was a significant difference in osteoprogenitor cell viability between all experimental groups and the tissue culture polystyrene control at 4 h, however viability at 8 h was comparable to the control for the experimental group containing high amounts of initiator and diluent. Thus, the results imply that EH networks can be fabricated with controlled properties and also support osteoprogenitor cell adhesion and viability.[22]

Additional investigations have characterized the degradation of the EHD monomer as well as EH networks. In terms of the monomer, EHD was degraded under acidic conditions (pH 2 and pH 4) and the solvent was analyzed for the degradation products of trimethylolpropane and HDP using 1H NMR. Results showed that at temperatures of 65°C, 80°C and 90°C these products were indeed realized, and that their release followed first order kinetics.[60]

Since the monomer does demonstrate hydrolytic degradation, the degradation rate of both porous and non-porous EH networks was evaluated. Macroporous EH scaffolds were prepared using a leachable porogen strategy. Briefly, macroporous networks were fabricated by incorporating a NaCl porogen (70, 75, and 80 wt%) into the EHD monomer solution prior to cross-linking. EH networks were formed around the crystals by radical polymerization, and the porogen was removed by water leaching. The results confirmed that while degradation occurred in all networks, the

rate of degradation was enhanced with the addition of the macropores (Fig. 2a). Solid EH networks, which are highly hydrophobic and resist water absorption, lost approximately 3.5% of their mass after 28 days. By incorporating macropores however, the degradation rate was dramatically increased, with the EH scaffolds displaying approximately 10% mass degradation after 28 days. The degradation rate was not found to be dependent on porogen content, however with only 10% mass lost for these groups after 28 days it should be noted that further testing is needed to determine the length of time required for complete degradation of the scaffolds. As described above, the use of acrylate chemistry in the formation of the EH networks will result in the formation of degradation products with terminal carboxylic acid groups. To investigate the acidity of the EH network degradation products, the pH of the solvent was monitored throughout the study and the solvent was not refreshed during the experimental time. The results demonstrated that the degradation of the EH networks was not associated with a significant pH change over the course of the 28 day study (Fig. 2b). Thus the study concluded that EH scaffolds hydrolytically degrade and produce minimal acidic products upon hydrolysis.

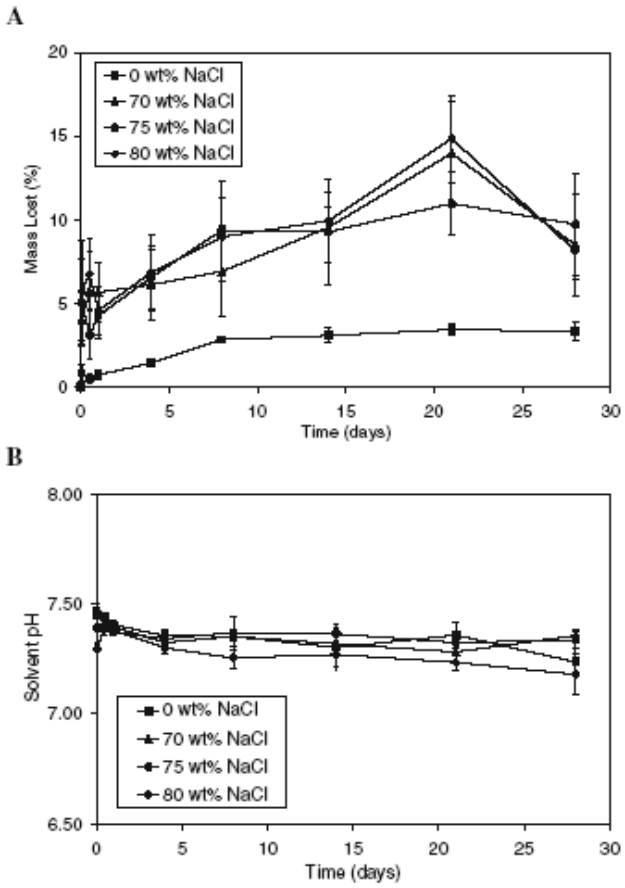

Figure 2. 2: (A) The percent mass lost from EH scaffolds and (B) change in solvent pH during *in vitro* degradation. All porous groups displayed similar degradation over 28 days with a more dramatic degradation than the solid EH networks. Results also confirmed the near constant solvent pH throughout the 28 day degradation study, demonstrating the lack of acidic degradation products by the CABs. Values represent means and associated standard deviation (n=5).

An initial application of EH networks has been in the area of skeletal muscle regeneration. Here, EH networks would act as platform for the recruitment of satellite cells, the proliferation and differentiation of satellite cells into myoblasts, and the ultimate formation of myotubes and myofibers. Therefore, initial studies examined the attachment and proliferation of putative myoblasts upon EH networks

as well as the myoblastic response to EH network's release of insulin-like growth factor 1 (IGF-1).[59] To begin, two EH networks formed from 0.34 and 0.58 M initiator solutions were tested for myoblast attachment at 4 and 6 h. Both networks displayed a myoblast attachment similar to tissue culture polystyrene at both time points. Further testing was done to investigate the ability of the EH network to release growth factors and stimulate myoblast proliferation.[59] IGF-1 was absorbed onto the networks' surface at concentrations of 0, 10, 50 and 150 ng/network, and then primary myoblasts were seeded onto the growth factor coated networks and grown in growth media for 3 and 5 days. Results indicated that on day 3, the IGF-1 loaded networks significantly increased myoblast proliferation in the highest loaded networks, and that the maintenance of this increased proliferation requires continuous IGF-1 release. Overall, this work demonstrated that EH networks support myoblast attachment as well as IGF-1 induced myoblast proliferation.[59]

EH-PEG Hydrogels

In order to form a water swellable network based upon a cyclic acetal monomer, poly(ethylene glycol) was incorporated into the EH network polymerization reaction resulting in EH-PEG hydrogels (Fig. 3).[57, 58, 61]

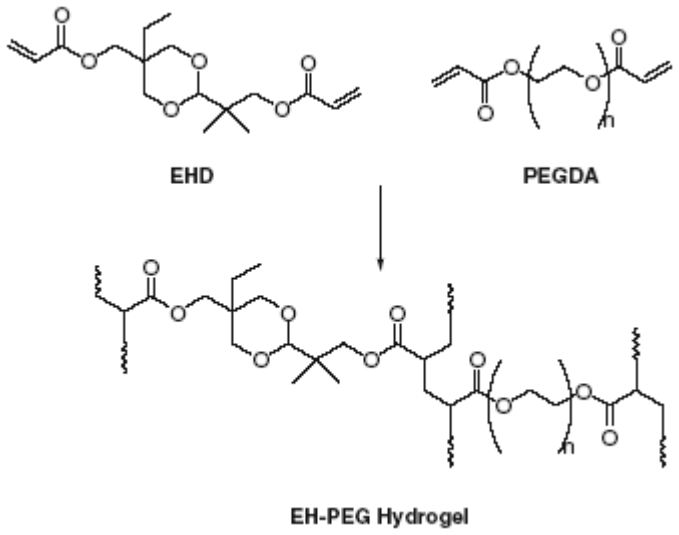

Figure 2. 3: Chemical reaction between poly(ethylene glycol) diacrylate (PEGDA) and 5-ethyl-5-(hydroxymethyl)-β,β-dimethyl-1, 3-dioxane-2-ethanol diacrylate (EHD) to form EH-PEG hydrogels (58).

EH-PEG hydrogels were synthesized with varying molar ratios of EHD to PEGDA as well as with varying monomer concentrations so as to then investigate their effects upon the physical properties of the resulting hydrogel.[58] Results showed that the EH-PEG hydrogel swelling degree was particularly dependent on the monomer concentration, with swelling increasing as monomer concentration decreased. Initiator concentration did not appear to have a significant effect on the swelling degree of EH-PEG hydrogels. Results also demonstrated that low initiator concentrations did not produce sufficient amounts of radicals to propagate thorough crosslinking reactions. This lead to a higher sol fraction, due to unreacted monomers left within the gel.[58] A study of water contact angle was also performed to examine the hydrophilicity of the surface of the EH-PEG hydrogels, with results indicating that the water contact angle decreased as the ratio of PEGDA increased. Thus, the

addition of PEGDA strongly influenced the hydrophilicity of the material, due to its hydrophilic EH polymer main chain.[58] Finally, the range of contact angle values was within the range of 50° to 75° where cell adhesion is generally thought to be promoted.[62, 63] This study concluded that the EH-PEG hydrogels can be easily fabricated with controllable properties and that these biomaterials may be suited for cell transplantation applications.[58]

In order to investigate the utility of EH-PEG hydrogels as cell carriers, a series of studies were also undertaken to examine the viability and function of embedded osteoprogenitor cells.[57] Specifically, this work examined (1) the effect of radical initiators on viability and metabolic activity of osteoprogenitor cells in monolayer, (2) the ability of the osteoprogenitor cells to differentiate after initiator exposure, and (3) the viability of osteoprogenitor cells embedded in the EH-PEG hydrogels. EH-PEG hydrogels were fabricated using the water-soluble redox, radical initiation system of ammonium persulfate (APS) and N,N,N′,N′-tetramethylethylenediamine (TEMED). To assess the effect of the initiator system on the metabolic activity, osteoprogenitor cells were cultured with the initiators at concentrations of 10, 15, and 20 mM and analyzed using a standard toxicology kit. Results indicate similar levels of metabolic activity between the 10, 15 mM, and control groups at early times and decreased activity for the 20 mM group. The effect of the initiator system on the differentiation of osteoprogenitor cells was examined by short exposure to the initiator system followed by culture in osteogenic media; differentiation was assayed by the expression of alkaline phosphatase. Results indicate that exposure to low concentrations of the initiation system does not affect the ability of the cell population

to osteodifferentiate. Lastly, osteoprogenitor cells were embedded in EH-PEG hydrogels, cultured in media for 7 days, and analyzed for viability using a fluorescent live/dead assay. Results quantitatively showed that the majority of the osteoprogenitor cell population was viable up to 7 days. This work indicated that the EH-PEG hydrogel system is a viable approach for cell carrier applications.

Finally, a recent study demonstrated the utility of EH-PEG hydrogels to repair craniofacial defects.[61] The goals of the study were to repair the defect while studying tissue response to EH-PEG hydrogels and the extent of bone repair after loading the hydrogels with bone morphogenetic protein- 2 (BMP-2). Results indicated a mild tissue response to the EH-PEG hydrogels and minimal cellular invasion around the implant. Prior to the *in vivo* study, BMP-2 release from the hydrogels was studied *in vitro*, demonstrating that the EH-PEG hydrogels do indeed release bioactive BMP-2 over the course of 12 h.[61] For the *in vivo* study, two experimental groups (EH-PEG hydrogels containing either 0.25 or 2.5 μg BMP-2) and an unloaded EH-PEG hydrogel control group were implanted into an orbital defect created in the rabbit animal model. Histological results after 7 days indicated no difference in bone growth near the construct between both experimental groups. However, at 28 days the EH-PEG hydrogel containing 2.5 μg BMP-2 demonstrated higher levels of bone growth compared to the experimental and control groups. The results of this work demonstrated that EH-PEG hydrogels can be used for delivery of BMP-2 *in vivo* for bone tissue engineering applications.[61]

Poly[poly(ethylene glycol)-co-cyclic acetal] (PECA) Hydrogels

Although EH-PEG hydrogels have a number of attractive properties for biomedical applications, there may be a need to fabricate water swellable, cyclic acetal based networks with a more defined, and therefore more controllable, macromolecular structure. Thus, a hydrogel formed from a copolymer of EHD and PEG may be advantageous, when compared to the random network of polymerized monomers and short chained polymers that form EH-PEG hydrogels. To this end, the copolymer poly[poly(ethylene glycol)-co-cyclic acetal] (PECA) and the resulting PECA hydrogels have been developed. The PECA copolymer is synthesized by copolymerization of the EHD cyclic acetal monomer with PEG polymers (Fig. 4).[60] More specifically, EHD is first dissolved in tetrahydrofuran with sodium hydride at 0°C. Next, poly(ethylene glycol) (Mn=600 g/mol) ditosylate is added at 50°C. Water is added to the mixture, and then all solvents are removed by reduced pressure. The resulting PECA copolymer is dissolved in ethyl acetate, filtered, and then further purified by silica chromatography. The hydroxyl groups of the product were transformed into acrylate groups by acryloyl chloride and triethylamine. Diacrylated PECA was then crosslinked using APS and TEMED to form PECA hydrogels.

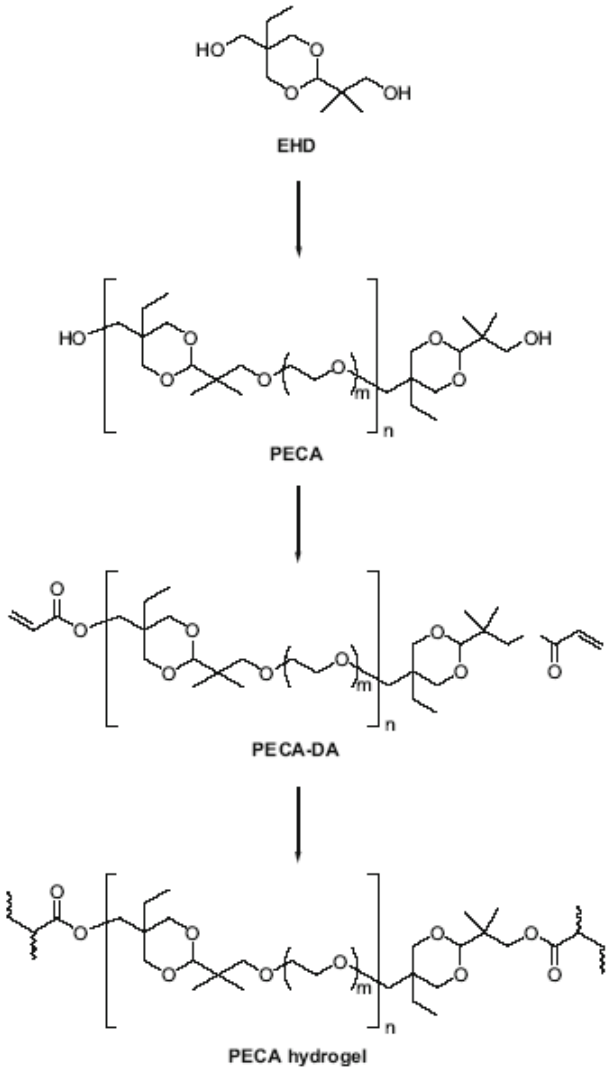

Figure 2. 4: Synthetic route for PECA and PECA hydrogels (60).

A series of studies investigated the effect of PEG length on the properties of the PECA copolymer as well as the resulting PECA hydrogels.[60] Results confirmed that PECA hydrogels could be readily fabricated with water contents in excess of 90 wt%. The swelling and sol fraction of PECA hydrogels were found to be dependent on the initial PEG chain length, initiator concentration, and polymer concentration. Swelling degree increased as the PECA concentration decreased, due to the mobility

of the polymer chains during gelation and the crosslink density of hydrogels. Swelling degree also increased with an increase in PEG chain length due to the decreased hydrogel crosslinking. Degradation rate of the cyclic acetal segments was found to be dependent on the solvent acidity and temperature, where degradation rate increased with a decrease in temperature and acidity due to dependence of cyclic acetal hydrolysis upon hydronium ion concentration.[60] When the cyclic acetal segments were degraded under simulated physiological conditions, the pH of the surrounding environment remained constant. Studies also showed that the dry weight of PECA hydrogels decreased by 30% after 5 months of *in vitro* degradation. Thus, this study revealed that both swelling ratio and degradation rate of PECA hydrogels were easily controlled, and well suited for future drug delivery and tissue engineering applications.[60]

Polyacetals and Polyketals

Another group of novel synthetic polymers includes the polyacetals and polyketals. The utility of biomaterials based upon polyacetals and polyketals are not limited to tissue regeneration, but are also useful in applications ranging from drug delivery to orthopedic implants. These biomaterials are often modified specifically to their desired function during synthesis using alcohols, ethers, aldehydes, and ketones.[64] Consequentially, the degradation products can also be tailored to consist of alcohols, aldehydes, and ketones, none of which significantly change the local tissue pH. Due to the variety of methods and reactants available for synthesis, there are near limitless applications for these biomaterials.

The majority of the work with polyacetal and polyketal based biomaterials is focused on drug delivery and tumor targeting. Current cancer therapeutics are often delivered systemically as opposed to selectively, leading to high levels of the drug found in tissues far from the intended site. Polyacetal and polyketal based biomaterials can take advantage of the fact that the local environment within a tumor has a lower pH than the surrounding tissue, and therefore induce the release of drugs at these sites, due to pH dependent degradation.[24, 65] A number of studies have recently shown that degradation and drug release rates are accelerated when in a low pH environment.[23, 24, 66, 67] This targeted release allows the carrier to remain in the blood and not release the therapeutic drug until it is taken up into the tumor, significantly decreasing administration of the drug to local healthy tissues.[66] Also, the pH dependent behavior allows for the carrier to remain in the system longer than current carriers, and therefore deliver more therapeutic agent to the tumor.[68] Additionally, by altering the reactants, carriers that have a Mw < 40,000 g/mol can be produced, allowing for the renal exclusion of degradation products.[66]

Using the same principles, polyacetal and polyketal based biomaterials can be tailored to target other chronic illnesses. For example, macrophages can be targeted by these biomaterials for the delivery of anti-inflammatory drugs. The distinct pH difference between the blood (pH 7.4), endosome (pH 6.5), and lysosome (pH 5.5) allows for polyacetal and polyketal based biomaterial degradation within a specific compartment of the targeted cell.[69, 70] Taking the delivery one step further, Vicent et al. has shown that the therapeutic agent can be directly incorporated into the

backbone of these polyacetal and polyketal polymer carriers.[66] Through hydrolysis, the drug is freed as the polymer backbone is degraded.

Another application of polyacetal and polyketal based biomaterials is to create specialized structures that are polyfunctional. For example, Lemcoff and Fuchs showed that it is possible to create dendrimeric diacetals that had several potential uses, including guest inclusion, self assembly, and channel formation with controlled degradation.[71] These structures are unique in the fact that each generation of the dendrimer is available for independent removal and can contain functional macromolecules that would become free upon degradation.[71] This could be utilized in a multifaceted approach with each generation containing a different macromolecule. Gillies et al. have also used these polyacetal and polyketal based dendrimer structures to create potential drug carriers.[72] They have synthesized linear-dendritic block copolymers containing acetal degradable units that self assembled into micelles. To investigate the use of these micelles as controlled release drug carriers, studies were performed with Nile Red dye as a model. It was found that this dye, which was protected within the micelle's core, was subsequently released as the acetal groups were hydrolyzed and the micelle dispersed, therefore showing a degradation controlled release.[72]

Polyacetals have also been used clinically in several orthopedic implants, most notably the Freeman all-polymer knee replacement and hip resurfacing prostheses.[73, 74] Current studies have discussed work on surface wear of hip joints and mechanical properties of these materials.[73-75] A recent study published by Lee and Choi demonstrated that the properties of a porous polyacetal block were similar

to that of bone.[76] These studies have displayed the diverse function that these materials have in every aspect of tissue engineering.

Conclusions

Current synthetic biomaterials for tissue engineering applications are sufficient, yet they are far from ideal. Biomaterials based upon polyesters and polyanhydrides possess distinctive properties and are used extensively in clinical practice. While synthetic biomaterials can be tailored to meet many tissue engineering and drug delivery needs, many are not biologically inert. In an effort to develop alternative materials, extensive research is being done to synthesize polymers that have more desirable degradation properties. Cyclic acetals are an increasingly versatile group of materials that can be utilized for both soft and hard tissue repair. Properties of cyclic acetal biomaterials have been controlled by varying fabrication parameters to create highly hydrophobic EH networks. These networks have been shown to support a viable osteoprogenitor and myoblast cell population. Alternatively, water swellable EH-PEG hydrogels were able to sustain an encapsulated osteoprogenitor cell population for up to 7 days *in vitro* as well as deliver BMP-2 to bone *in vivo*. Finally, in an effort to create a more organized hydrogel structure EHD and PEG were copolymerized to form PECA. PECA hydrogels have been shown to be a favorable material for both drug delivery and tissue engineering applications. Other groups of biomaterials are based upon polyacetals and polyketals, and have been shown potential in drug delivery applications due to their pH dependent degradation properties. The development of

alternative synthetic polymers, such as those described here is a critical step for the future success of many tissue engineering and drug delivery applications.

Acknowledgements

This work was supported by the Arthritis Foundation through an Arthritis Investigator Award to JPF, the National Science Foundation through a CAREER Award to JPF (#0448684), and the State of Maryland Department of Business and Economic Development.

Chapter 3: Skeletal Muscle Tissue Engineering Approaches to Abdominal Wall Hernia Repair*

Introduction

Hernia repair is one of the most frequently performed operations with estimates of approximately one million operations annually in the United States alone.[77-80] Groin hernias represent the vast majority of these hernia repairs with a preponderance of these being performed in men. It has been estimated that approximately four out of every 1,000 men will need hernia repair surgery.[81] These overwhelming numbers put abdominal hernias among the most common pathological conditions affecting humans. Furthermore, it is believed that these numbers are most likely underestimated.[82, 83]

Ventral hernias represent a significant proportion of abdominal wall hernias. These hernias occur on the anterior abdominal wall and may be congenital or acquired. They account for 36 percent of hernia repairs and this number is increasing every year.[77] Incisional hernias represent a subset of ventral hernias occurring in patients that have undergone a prior abdominal operation. These incisional hernias occur when the skeletal muscle and fascia around an incision site is weakened and can no longer support the pressure generated within the abdominal cavity resulting in a rupture. These hernias occur in up to 10% of patients that undergo abdominal incisions.

---

* This chapter was published as the following article: Falco, E.E., J.S. Roth, and J.P. Fisher, *Skeletal muscle tissue engineering approaches to abdominal wall hernia repair.* Birth Defects Res C Embryo Today, 2008. **84**(4): p. 315-21.

Hernias most commonly present as an uncomfortable protuberance of the abdominal wall. The protrusion typically represents abdominal viscera which have protruded through the confines of the abdominal cavity. Although uncommon, the herniated abdominal contents may become entrapped or incarcerated. Viscera incarcerated within a hernia may result initially in discomfort with progression to ischemia and death of the involved organs. If untreated, a strangulated hernia may result in the loss of the organ or possibly the death of the patient.

Current treatment methods for abdominal wall hernias involve the placement of prosthetic biomaterials, xenografts, or allografts. Despite these available techniques, the incidence of recurrence varies from 20 to 50%.[84] There is no definitive best biomaterial, graft, or technique for the repair of abdominal hernias. The choice of repair is generally dictated by the background, training and experience of the operating surgeon. This review summarizes the mechanisms of abdominal hernia formation, provides an overview of the current practices for hernia repair and considers the role of skeletal muscle regeneration strategies for the treatment of hernias.

Abdominal Wall Morphology

Abdominal Wall Physiology and Function

The abdominal wall is made up of six layers: skin, subcutaneous fascia, musculature, transversalis fascia, preperitoneal tissue and peritoneum.[85] The skin is composed of two layers: the epidermis and the dermis. The epidermis, which is the uppermost layer of skin, is made up of nonvascularized endothelial cells that form

from the inside outward. Just beneath this layer is the dermis, which functions as a collagenaous connective tissue layer that contains capillaries, lymphatics, and nerve ending, as well as, the hair follicles, sebaceous glands, sweat glands and their ducts, and smooth muscle fibers.[86] This connective tissue layer recurs along with adipose tissue in most of the layers of the abdominal wall. The subcutaneous fascia, transversalis fascia and preperitoneal layers all contain connective tissue with varying amounts of fat cells and fat stores which vary in thickness gradually with position along the abdominal wall.[87] The musculature is made up of the transverus abdominis, internal oblique, external oblique and rectus abdominis muscle groups.[85] Each muscle group consists of uniquely arranged muscle fibers specific to its required motor function. These groups work in concert to provide the mechanical strength and flexibility necessary to move the torso of the body and to carry out the vital function of the abdominal wall: to counteract the large pressure force exerted by the internal organs. Lastly, the peritoneum is a serous membrane that lines both the abdominal wall and internal organs, allowing for movement of the organs within the abdominal cavity. Abdominal hernias commonly affect the last four layers of the abdominal wall as well as the incorporated connective tissues and muscular fasciae. Loss of this musculature is critical as the muscles provide the majority of the abdominal walls mechanical strength. Once lost it is replaced only with connective and scar tissues which leave the site vulnerable to continual defects.

Musculature Development and Regeneration

Skeletal muscle provides the bulk of the mechanical strength, mobility, and flexibility to not just the abdominal wall but to almost all the mobile parts of the body making it a tissue of great interest. Since muscle is such a dense tissue, its defects often exceed the limits of nutrient diffusion and therefore have a relatively complicated regeneration scheme. Not only must the physical muscle be regenerated, but the surrounding nerves and vasculature must also be repaired in order for proper functionality to return.

Skeletal muscle fiber development and regeneration are similar processes. In development mononuclear myoblasts line up parallel to one another and fuse to produce multinucleated myotubes. The myotubes share the cytoplasm of incorporated myoblasts and their nuclei are disbursed along its length. Once the myotubes are formed they go through a maturation process, during which they become innervated and vascularized, resulting in myofibers.[88] Myofibers are then bound together by connective tissues to provide strength to the muscle. When electrically stimulated the myofibers contract simultaneously leading to the most distinctive characteristic exhibited by skeletal muscle: voluntary movement. The parallel alignment of the myoblasts during fusion is the key to what gives the myofibers their ability to produce the force necessary for movement and strength.

If trauma occurs to the fibers, muscle regeneration and repair begins with the activation of the progenitor cells, known as satellite cells.[89-91] These mononuclear cells are present in all types of muscle, and in skeletal muscle they reside between the basal lamina and the myofiber it encapsulates. While they are not always found in the

same density in all skeletal muscles, they are often found spaced throughout the myofiber with which they reside. [88] It has been found that these cells are not directly associated with the myofiber, as was shown by the presence of a gap between the plasma membrane of the myofiber and the membrane of the satellite cell. This gap can range in size from 15-60 nm with little protrusion of the basal lamina into the space. [88] It is possible that this space is what allows the cells to migrate freely and as necessary. Once activated, the satellite cells migrate to the site of the defect and proliferate. The newly produced cells can return to quiescence and replenish the satellite cell reserve or remain activated and migrate to the site of the defect to regenerate the muscle. Within the defect they can align parallel to the injured myofiber or fuse to each other to develop new and repaired myotubes. These myotubes again undergo the maturation process of innervation and vascularization to become functioning myofibers. There are several diseases and conditions that can affect the repair and regeneration processes of the skeletal muscle: one of which is abdominal wall hernias.

Anatomy of Hernia Formation

A Mechanism for Herniation

Abdominal hernias occur when the structural integrity of the abdominal wall is compromised resulting in a loss of tissue function.[92, 93] During normal activities such as exercising, laughing, coughing, lifting, standing and sitting upright there is a significant increase in the internal pressure force applied to the abdominal wall.[83, 92] Normally this excess pressure is equally distributed along the abdominal wall,

however when abnormalities are present in the abdominal wall tissue the musculature can bulge or tear under the stress effectively relieving the increased pressure and resulting in a hernia.

Discontinuities in the abdominal tissue can occur as a result of several mechanisms. Hernias often result from direct trauma to the abdomen resulting in the disruption of the underlying musculature. This can occur through blunt force trauma, high-energy transfer events [94] or through physical penetration, such as bullet and knife wounds.[92] The common thread in all cases is the loss of the skeletal muscle and therefore loss of mechanical stability within an area of the abdominal wall. Regardless of the source, these injuries stimulate a wound healing response. It is widely thought that herniation results from both the mechanical instabilities as well as inadequate wound healing at the injury site. [84, 93]

Wound Healing in Hernias

Recently, in an effort to better anticipate and resolve herniation in patients, research has been done into the wound healing of both primary and recurring hernias. In normal wound healing an inflammatory response is incited and blood fills the defect, allowing proteins to form a provisional matrix. This matrix provides a scaffold to facilitate wound healing by helping direct incoming cells, proteins and signals and aid in the remodeling of the scar tissue. Once the matrix is formed, acute inflammation begins with the infiltration of fluid, plasma proteins and various leukocytes.[95] Macrophages specifically have been shown to help to direct tissue repair and are vital to proper wound healing.[93] Fibroblasts are then recruited to the

wound site where they proliferate and initiate angiogenesis, collagen synthesis and extra cellular matrix (ECM) production creating granulation tissue.[93, 95] In the final stage of wound healing, the granulation tissue is remodeled and combined with foreign body giant cells to become fibrous scar tissue.[95]

In hernia patients there is evidence that indicates that normal wound healing does not take place. Samples of scar tissue from patients with recurring hernias showed abnormalities in the scar tissue as well as surrounding skin and connective tissues.[93] When compared to normal tissue, the most prominent difference was that the herniated tissue displayed a lower ratio of collagen type I to collagen type III.[84, 93] In wound healing collagen type I is responsible for the mature remodeled ECM that provides tensile strength to the tissue, whereas collagen type III makes up the immature fibrils that form the provisional matrix during inflammation.[84] Therefore, lower ratios of type I to type III collagen result in weaker and less mature scar tissue. For hernia repair this has a significant effect, as the tissue must have the adequate tensile strength to withstand the large pressure changes experienced in the abdominal cavity during everyday activity. Additionally, some reports have shown modified collagen metabolism due to the increased expression of matrix metallo-proteinases, therefore altering the collagen degradation and remodeling processes. This results in a significant difference in scar tissue strength as well as the overall wound strength.[84, 93]

There are several other factors that can increase the probability of primary and recurring hernias as well as alter wound healing. Old age, male gender and a high body mass index all increase a patient's susceptibility to complications, longer

surgery times, larger defects and a higher recurrence rate.[96] Behaviors such as smoking or using steroids and medical conditions such as diabetes mellitus have also been shown to increase the risk of developing primary and recurring incisional hernias.[83, 84, 92, 97] Furthermore, wound infection, surgical technique, and the choice of suture or prosthetic material affects the probability of herniation.[92, 93] Some suture materials and surgical meshes can incite a foreign body reaction leading to chronic inflammation, characterized by the presence of macrophages, monocytes, and lymphocytes with vascularization beginning to occur.[95] This prolonged inflammation hinders granulation tissue formation, leading to decreased mechanical stability and overall wound healing. All together these defects are the leading reasons for the continuously high hernia recurrence rates.

Overview of Current Clinical Solutions

Clinical Approaches to Treat Abdominal Hernias

Currently there is no accepted universal approach to treating abdominal hernias. The most common techniques involve the placement of prosthetic biomaterial meshes, xenografts, or allografts into the defect.[82, 98] The use of these materials has resulted from a necessity to improve upon the poor results of sutured hernia repair. When the native tissue is repaired by suture alone, there is a large tension force exerted on a small area of tissue that is occupied by the suture. As a result, the abdominal wall can tear at the suture point resulting in hernia recurrences. These recurrent hernias typically occur lateral to the initial hernia repair and are often

larger with multiple defects as a result of disruption of the abdominal wall at multiple suture sites. The recurrence rate for this technique approaches 50%.[97]

In an attempt to reduce the risk of recurrences, meshes are secured using a "tension free" approach. The tension free placement helps to reduce healing time and pain.[99-101] These advances have reduced the hernia recurrence rate by as much as 75%. However, the overall recurrence rate is still approximately 24%.[97, 102]

Criteria for Repair Techniques

There are several criteria that surgical implants must meet before they can be considered viable for clinical application. The first is mechanical stability. The prosthesis or tissue that is used for repair must allow for the return of functionality of the tissue. In skeletal muscle this means it must be pliable and able to move with the body, as well as have the mechanical strength to withstand intra-abdominal pressures. These mechanical properties can be tested *in vitro*.

It is essential to understand the systemic reaction to any implanted biomaterial. Wound healing plays an important role in the regaining of functional tissue and any material that supports the growth of bacteria or the harboring of other harmful organisms is not suitable for implantation. Biomaterials must also have a minimal inflammatory response following implantation. It has been shown that devices that can decrease the inflammatory response and body rejection to an implant or suture is a better candidate for repair. In addition, the tissue or prosthesis should support ingrowth of the native tissue to repair the defect, while preventing adhesions to the abdominal viscera.[103]

One major setback to the use of permanent biomaterials is the possibility for the implant to migrate or contract thus rendering it ineffective.[104] Therefore implants that are absorbable in addition to having the aforementioned properties are being studied. This additional quality allows the material to be removed from the system slowly, allowing the hosts tissues to replace the defect as the material degrades. Optimization of these three qualities would give the best outcome for hernia repair.

Xenografts

Xenografts have been used extensively in developing suture material and prosthetic patches. Kangaroo, ox, deer and whale tendons have all been used in the past as prosthetics for repair.[100] Catgut has also been used to form suture material. More recently, porcine small intestine submucosa (SIS) has been studied as a viable material for hernia repair. Badylak et al. describes a production method in which the small intestine is harvested from a pig and the superficial and abluminal muscular layers, as well as the serosa were mechanically removed.[105] The remaining submucosa and basal layer, which contained the ECM's supporting structures, were sterilized using 0.1% peracetic acid.[105] Multiple sections were then pressed together using vacuum to form a stronger and larger scaffold.[105, 106] After a final sterilization with ethylene oxide the SIS is ready for implantation. Once implanted, this scaffold contains growth factors and ECM molecules that attract host cells and begins to reorganize them in such a way that they can create functional tissue. Over time the graft is reabsorbed into the body leaving behind only host tissue. Rauth et al. compared two SIS meshes to a synthetic expanded polytetrafluoroethylene (ePTFE)

mesh which were all commercially available and found that while all implants displayed wound healing and fibrous encapsulation, the wound contraction of the SIS meshes was significantly higher than with the ePTFE.[107] This additional contraction is indicative of stronger more mature collagen network in the fibrous encapsulation. [93], therefore indicating that the SIS is more capable of tissue ingrowth and remodeling than the synthetic ePTFE mesh and thus could result in better long term repair.[107]

While all these materials help restore some functionality of the muscle there are two major limitations: disease transmission and host rejection. While techniques for detecting disease are advancing daily, disease transmission is a significant concern, although occurs rarely. Host rejection is an equally troublesome limitation that can lead to a chronic inflammatory response resulting in incomplete or inefficient healing. However, by removing the cells from the graft, as is done with the porcine SIS, these limitations can be greatly reduced.

Allografts

Allografts are especially useful because the donor tissues that are supplied are more comparable to host tissues. Xu et al. have studied the effectiveness of both commercially available human acellular dermal matrix (HADM or AlloDerm®) and human cellular dermal matrix (HCDM).[108] They found that the absence of cells in the HADM allowed for the infiltration of fibroblasts, spindle-shaped cells, aligned fibers, and a vasculature network but did not illicit a chronic immune response.[108] HCDM on the other hand exhibited a chronic inflammatory response and fibrous encapsulation.[108] In another study Silverman et al. compared a pig allogenic acellular

dermal matrix (ADM) to ePTFE.[109] The ADM showed stronger tissue ingrowth at the implant-tissue interface and also exhibited vasculature ingrowth. However, no significant difference was found in overall hernia repair.[109] Kolker et al. have also investigated the use of the AlloDerm® acellular scaffolds in patients with recurring hernias. They found that after approximately 16 months, there were no recurrences.[110]

Issues related to supply of allografts represent a significant limitation to widespread use of human acellular dermis for hernia repair. Allografts are generally harvested from organ and tissue donors following their death and are accordingly limited in supply. As with xenografts, host rejection remains an issue, however disease transmission risk is considerably lower.[111]

Autografts

With the help of tissue engineering principles, an emerging technique of repair is autografts. These techniques look to use the rebuilding mechanisms inherent in the host's own musculature. As with allografts, Conconi et al. have shown that an autologous acellular matrix can regenerate myofibers that maintain contractile function for up to 60 days *in vivo*.[112] Other techniques are looking into cellular methods for repair. Satellite cells and mesenchymal stem cells (MSC) are just two cell types that have been studied extensively in skeletal muscle development.[89-91, 113-115] These cells are adult stem cells that reside within muscle and bone marrow, respectively. MSCs are similar to satellite cells, as described above, however they have the ability to differentiate into more than one lineage. The most commonly

studied lineages that arise from MSCs are bone and cartilage; however fat, ligament, tendon, muscle and marrow stroma are also thought to be alternate lineages.[115, 116] The ability of these cells to differentiate and fuse into myofibers is a large step in skeletal muscle engineering and possibly hernia repair. Current hernia repair techniques simply replace the musculature with fibrous scar tissue as opposed to muscle.[113] Therefore, it is a hypothesized that these stem cells combined with prosthetic scaffolds or acellular matrices, such as ECM, will result in skeletal tissue regeneration in the defect.

Prosthetic Meshes

The use of prosthetic meshes in the repair of hernias is the most frequently utilized technique. Meshes have been engineered to suit the needs of the surgical repair. Two common synthetic polymers that have been tested are polytetrafluoroethylene (PTFE) and polypropylene (PP). Natural polymers such as sodium hyaluronate (HA) and carboxymethylcellulose (CMC) are also used. By varying percentages of different monomers along with the crosslink density of the polymer, one can change the biodegradability of the polymer. Also, when looking at the processing techniques, different pore sizes, ranging from 3 – 500 μm can be achieved. As well as, pores of different shapes with both random and ordered distributions.[103, 117] Changes to both the bulk and surface morphology allow for more control over the tissue ingrowth *in vivo* and provides a mesh that can exhibit a wide range of mechanical and biological properties. Due to the lack of a previous cellular component there is not the same risk for disease transmission.

Another advantage to using biomaterials in hernia repairs is that they are not as limited in supply as donor tissue or cells. There is also more opportunity for larger defect repairs. This technique is not perfect however. The implant is treated as a foreign body; therefore the risk of inflammatory response is eminent. In this case, fibrosis can occur and provoke adhesions of the abdominal viscera to the defect site.[104] Adhesions lead to conditions such as intestinal obstruction, chronic abdominal hernia repair, and female infertility.[103] This concern is currently being addressed in research as can been seen with the dual layer meshes.[103]

Polytetrafluoroethylene (PTFE) is a hydrophobic, non-biodegradable polymer that is often formed into a fiber mesh and is currently used clinically.[103, 111] By adjusting the crosslink density of the mesh, one can ideally alter the adhesive and tissue ingrowth properties of the mesh, as is done in the Gore-Tex Dual mesh.[103] This mesh is of a bilayer design. One layer has a mesh size of 3 μm and it meant to restrict tissue ingrowth, where as the other layer has a mesh size of greater than 100 μm and is meant to provoke tissue ingrowth. In a study by Gonzalez et al., it was found that this mesh does inhibit tissue ingrowth.[103] However, other studies have shown that this design has a high rate of recurrence, infection and inflammatory response.[118]

Polypropylene (PP) on the other hand is a slightly less hydrophobic, non-biodegradable polymer.[111] It is also formed into meshes that contain macropores. These macropores helps to trigger tissue ingrowth that help improve the surgical integrity and strength of the implant.[103, 104] Nevertheless, PP has no natural defense for adhesion formation. Therefore, the use of non-adhering agents such has hyaluronic acid and carboxymethylcellulose in addition to the PP is currently being

investigated.[104, 119] These glycosaminoglycans not only reduce the number of binding site available on the PP, they also carry a charge, which can affect cell binding. An overall advantage of the PP grafts is that they have a decreased risk of infection and inflammation when compared to the PTFE grafts.[118]

By combining a polymer that has enhanced cell adhesion, to face the musculature, with one that inhibits cell adhesion, to face the abdominal cavity, the ideal abdominal wall implant could be achieved.

Tissue Engineering Approaches to Treat Defects

Tissue engineering is combining cells, signals and scaffolds to restore, maintain, or improve tissue function. By using the methods of engineering and applying them to living systems, great strides have been made in the field of clinical medicine and vast improvements in the quality of life have been achieved. While clinicians are helping to define specific medical needs, researches are focused on defining cell signaling pathways, migration, attachment, proliferation and differentiation of several types of cells, in the regeneration of tissue.[120-122] Together with clinicians, *in vivo* studies can be performed to test the applicability of the *in vitro* techniques being developed from this knowledge. Only though the combination of the functional biology of the system with the system's interaction characteristics can methods or tissues be produced that can replicate or improve that found naturally. For hernia repair the ideal tissue to focus on is skeletal muscle. Current repair techniques focus on improving the organization of scar tissue while restoring some of the mechanical strength that is lost during herniation. While there have been

significant advances over suture techniques alone, the hernia recurrence rate is still high. Therefore the ideal solution would be to restore the native tissue to its original functionality through skeletal muscle regeneration.

Next Generation Polymeric Scaffolds

As mentioned above, polymeric scaffolds allow researchers and clinicians to control the properties of hernia repair meshes. These meshes have demonstrated promising results in hernia repair but are still not ideal. The next generation of clinical products involves controlling the scaffold degradation and surface properties to help restore function to the damaged skeletal muscle tissue. This can be done by optimizing current scaffolds and creating new novel polymers that possess the mechanical properties, surface properties, biocompatibility, and degradation rates that are desired. Current research is investigating micropatterned materials for directed cell migration and growth of skeletal muscle[123, 124], as well as, degradable polymers that can time release growth factors for not only skeletal muscle regeneration [125, 126], but vascularization and innervation as well. To achieve functional skeletal muscle regeneration, all three tissues must be considered. By learning more about the signals and metabolic pathways of these tissues and their progenitor cells, better tools will become available for the optimization of ideal hernia repair devices.

Conclusions

Despite our attempts to lower the rates of primary hernia occurrence and recurrence, this problem has remained largely unchanged for decades. Imperfect wound healing is thought to be the mechanism for herniation however many attempts to control this have been limited in their success. Therefore a tissue engineering approach of regenerating the lost skeletal muscle has been proposed. To achieve the ideal solution however a greater understanding of current biomaterials and their cellular interactions are needed.

Acknowledgments

This work was supported by the National Science Foundation through a CAREER Award to JPF (#0448684).

Chapter 4: Project Summary

Abdominal wall hernias are a common clinical concern. Existing clinical solutions involve the use of synthetic prosthetic meshes that focus primarily on the structural support of the abdominal wall and not defect wound healing. To address both of these concerns this project aims to use a tissue engineering strategy to regenerate skeletal muscle within the abdominal wall defect using a cyclic acetal based scaffold, a skeletal muscle myoblast cell population, and a plasmid encoded for IGF-1.

Initial studies investigated the biocompatibility of a cyclic acetal biomaterial fabricated from 5-ethyl-5-(hydroxymethyl)-β,β-dimethyl-1,3-dioxane-2-ethanol diacrylate (EHD). Three aspects of this scaffold were investigated. First, the mechanical properties of solid EH networks were determined. Second, the attachment, viability, and proliferation of a rat myoblastic cell population was assessed and third the release and functionality of insulin-like growth factor 1 (IGF-1) was evaluated.

Once completed, the scaffold was improved upon by altering the structural architecture of the crosslinked EH networks. To determine this effect on material properties the mass lost and pH change during degradation, the Young's modulus and the flexural strength for five different scaffold architectures were investigated.

Finally, in an effort to encourage skeletal muscle regeneration over scar tissue formation gene delivery methods were employed. More specifically, the effect of scaffold architecture on plasmid delivery was assessed. In addition, a therapeutic

plasmid that expressed IGF-1 was constructed and evaluated in a human skeletal muscle myoblast cell population.

Chapter 5: EH Networks as a Scaffold for Skeletal Muscle Regeneration in Abdominal Wall Hernia Repair*

Introduction

Abdominal wall hernias, and particularly incisional hernias, are a common clinical problem affecting nearly 5 million Americans. Although autografts, allografts, and xenografts are options for the repair of abdominal wall hernias, their relatively high recurrence rates have mostly limited their clinical application.[105, 106, 127-130] The most common approach for incisional hernia repair involves the implantation of a synthetic or natural prosthetic mesh. Synthetic prosthetic materials, including polypropylene, polytetrafluoroethylene, and various polyesters, are most often used, while natural polymers, such as sodium hyaluronate and carboxymethylcellulose, may be used in conjunction with these prosthetic materials so as to augment the tissue response to the implant materials. As synthetic prosthetic meshes have mostly controllable physical properties, including pliability and strength, as well as pore size, shape, and distribution, the fabrication can be tailored for a specific clinical application.[103, 117] Nevertheless, synthetic materials are associated with significant disadvantages, such as a prolonged inflammatory response, prosthetic infections, and fistula formation.[118, 130, 131] Furthermore, the potential for mesh migration or shrinkage may render them ineffective.[104] As a result of these

* This chapter was published as the following article: Falco, E.E., J.S. Roth, and J.P. Fisher, *EH Networks as a scaffold for skeletal muscle regeneration in abdominal wall hernia repair*. J Surg Res, 2008. **149**(1): p. 76-83.

disadvantages, the current incidence of hernia recurrence after intervention ranges from 32% to 63%.[132]

As an answer to the current clinical need for better hernia repair, we propose that a degradable biomaterial scaffold, which promotes the regeneration of abdominal skeletal muscle, may be an attractive approach. Here, the implanted scaffold would guide the regeneration of load bearing skeletal muscle through facilitated myoblast proliferation and maturation. To this end, we have engineered a scaffold, termed an EH network, made from the cyclic acetal monomer 5-ethyl- 5-(hydroxymethyl)-β,β-dimethyl-1,3-dioxane-2-ethanol diacrylate (Fig. 1).

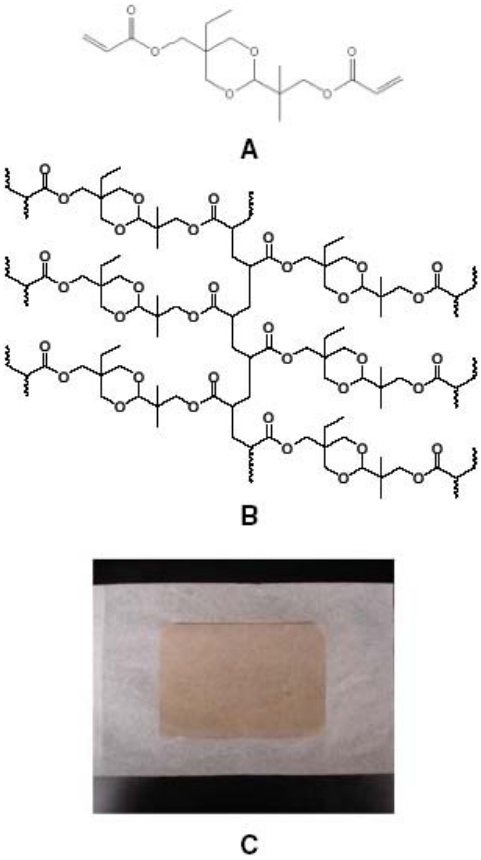

Figure 5. 1: (A) Chemical structure of the monomer 5-ethyl-5-(hydroxymethyl)-β,β-dimethyl-1,3dioxane-2-ethanol diacrylate (EHD). (B) Chemical structure of the resulting crosslinked EH network. (C) An EH network sheet made with a 0.58M BP solution.

EH network's novel property is that it lacks the ester groups present in many other biodegradable polymers and, therefore, as EH degrades it produces less acidic byproducts.[22, 58, 60] Thus, premature scaffold degradation due to high acidity is prevented and the inflammatory response of skeletal muscle tissue surrounding the implant is decreased.

The work presented here intends to investigate the skeletal muscle regeneration on the surface of an EH network. Skeletal muscle regeneration begins with satellite cells, the progenitor cell of skeletal muscle. These mononuclear cells are present in skeletal, smooth, and cardiac muscles. In skeletal muscle specifically, the mononuclear satellite cells reside between the myofiber and the basal lamina and are able to move freely.[88-91] When trauma to the musculature occurs, available satellite cells become activated and migrate to the site of the defect, where they proliferate. The newly produced cells then have one of two roles: to replenish the satellite cells' reserve and return to quiescence or to remain activated at the site of the defect. Activated satellite cells mature into myoblasts that align parallel with each other and with the remaining myofibers in a process that parallels muscle development. Myoblast fusion then begins, after which the resulting myotubes undergo a maturation process to become functioning myofibers. The importance of this process in the regeneration of tissues has been the focus of several studies defining cell signaling pathways, migration, attachment, proliferation, and differentiation of several types of cells.[120-122]

One such cell-signaling pathway that has been studied extensively in conjunction with skeletal muscle development and regeneration is that of insulin-like

growth factor-1 (IGF-1). IGF-1 is a polypeptide hormone that has been shown to function as autocrine and paracrine signals that affect skeletal muscle growth and development.[133-135] More specifically, when IGF-1 binds to the IGF-1 receptor (IGF-1R) that is present on activated satellite cells, it produces an increase in the cell's proliferative capabilities as well as its differentiation.[135-137] Overall, increasing the amount of IGF-1 present in the skeletal muscle produces an increase in both the skeletal muscle DNA and protein content.[136] Therefore, the use of IGF-1 may be critical to activating and guiding satellite cell behavior in skeletal muscle regeneration.[135]

To date, there have been only modest investigations into the use of biomaterials in guided skeletal muscle regeneration. As satellite cells are not present within the prosthesis prior to implantation, they must migrate and compete with the granulation tissue and foreign body giant cells to enter the matrix. With such an inadequate number of satellite cells available compared with the competing cells, the musculature is often replaced almost solely by fibrous scar tissue as opposed to skeletal muscle.[95, 113] Given this issue, we investigated what initial steps would permit creation of an EH scaffold that would facilitate skeletal muscle regeneration. To begin, we examined the effects of initiator concentration on the mechanical properties of the radically crosslinked EH networks so as to confirm their utility in soft tissue applications. Next, we investigated the effects of initiator concentration on cell attachment to characterize the interactions between the network and our skeletal myoblast population. Then, the effect of exogenous IGF-1 in the growth media on cell proliferation was tested on attached myoblasts to ensure that the IGF-1 protein

signaling was unaffected by the scaffold. Finally, the effects of increasing the concentration of adsorbed IGF-1 on release and myoblast proliferation were characterized to determine the ability of the EH scaffold to serve as a delivery system for IGF-1.

Materials and Methods

Materials

Benzoyl peroxide (BP), N,N-dimethyl-p-toluidine (DMT), 5-ethyl-5-(hydroxymethyl)-β,β-dimethyl-1,3-dioxane-2-ethanol diacrylate (EHD), and bovine serum albumin were obtained from Sigma-Aldrich (Milwaukee, WI). Reagent grade acetone was purchased from Fisher Scientific (Pittsburgh, PA). F-10 Ham media (F-10), fetal bovine serum (FBS), penicillin/streptomycin (Pen/Strep), and trypsin/ethylenediamine tetraacetic acid (EDTA) were received from Invitrogen (Carlsbad, CA). Collagenase P was obtained from Roche Applied Sciences (Indianapolis, IN). Recombinant human insulin-like growth factor-1 was acquired from R&D Systems (Minneapolis, MN).

EH Network Synthesis

EH sheets were fabricated in a glass plate mold. To assemble this mold, capillary tubes were secured onto one of two glass plates with vacuum grease. Together, the plate and capillaries made up the walls and bottom of a rectangular well. With this completed, a 0.81 M stock solution of BP in acetone was prepared.

Subsequently from this stock, working solutions based on desired fabrication parameters were made. EHD monomer was then mixed with the working initiator solution until one phase was present. The accelerant N,N-dimethyl- p-toluidine was added to the solution at a concentration of 0.5 μL/g of EHD monomer. The solution was mixed again and poured into the well of the previously prepared plate. A second plate was used to cover the solution and the system was placed in an oven at 30°C for 20 min. A uniform thickness of approximately 0.8 mm was achieved.

Skeletal Myoblast Isolation and Harvest

Skeletal muscle was harvested and isolated from the hind limbs of Wistar Hannover GALAS rats. Once removed, each muscle was rinsed three times with F-10 Ham media containing 10% Pen/Strep, diced, and then digested in 10 mL of collagenase P solution for 2 h at 37°C and 5% CO_2. After incubation, 100 μL of trypsin/EDTA solution was mixed into the cell solution and placed back into the incubator for 30 min at 37°C and 5% CO_2. The trypsin and collagenase P solution was neutralized with 22 mL of growth media, composed of F-10 Ham media containing 10% FBS and 1% Pen/Strep. The cell suspension was passed through three filters with 100 μm, 70 μm, and 40 μm mesh sizes, respectively. The remaining cells were centrifuged, and the pellet was again resuspended in growth media. This procedure was completed twice more, once with F-10 Ham media only and finally with growth media. The resulting suspension was plated on a T-25 culture flask and was placed in the incubator at 37°C and 5% CO_2. The resulting cell population is a putative rat skeletal myoblast population, and will be referred to henceforth as

myoblasts. The growth media was changed the day after harvest. At day 3, the cells were passaged and reseeded onto a new T-25 culture flask. Growth media was changed again at day 6. Finally on day 8 the cells were washed twice with phosphate-buffered saline (PBS), trypsinized, and seeded according to the study parameters.

Dynamic Mechanical Analysis

The mechanical properties of EH networks were analyzed by dynamic mechanical analysis, reflecting the dynamic mechanical forces experienced in the abdominal wall. Three different networks were formed using initiator solution concentrations of 0.08, 0.23, and 0.81 M. During fabrication 2.25 mL of the desired initiator solution was used for every 2.0 g of EHD monomer. The resulting sheets were cut into 13 mm × 30 mm rectangles. Using the Q-800 Dynamic Mechanical Analyzer (TA Instruments, New Castle, DE) the samples were placed in the single cantilever clamp and held isothermally at 37°C. One end of the network was then oscillated over a frequency range of 1–100 Hz at an amplitude of 15 μm. This experiment was run with a sample size of six and the values for the complex modulus were reported as a mean and standard deviation of these samples at a frequency of 10 Hz.

Skeletal Myoblast Attachment

Skeletal myoblast attachment was investigated on EH networks that were formed using 0.75 mL of either 0.34 M or 0.58 M initiator solution for every 2.0 g of EHD. These resulting networks were cut into disks with a diameter of 2.0 cm. The disks were subsequently washed three times for 15 min each with PBS, acetone, PBS again, and then sterilized by exposure to UV light overnight. Each disk was placed in a 12-well plate. Stainless steel inserts were fabricated by cutting 1.5 cm length sections from a 3/4 in. stainless steel polished pipe purchased from Stainless Steel Stock (Friend, NE). These inserts were filed down until their edges were smooth, and then they were washed thoroughly and sterilized through autoclaving. The stainless steel inserts were then placed onto the EH networks to prevent them from floating in the culture media. A population of myoblasts was seeded into the center of the EH disks, confined by the stainless steel insert, at a seeding density of 100,000 cells per network. After 4 and 6 h the disks were washed twice with PBS and the remaining cells were lifted with trypsin/EDTA and counted using a hemacytometer.

Dosed IGF-1 Induced Myoblast Proliferation

To examine the effect of EH networks on IGF-1 signaling, skeletal myoblasts were isolated and networks made from the 0.58 M initiator solution were prepared. Myoblasts, seeded at an initial density of 1.0×10^6 cells, were cultured on each disk for 48 h to allow cellular attachment before testing for cellular proliferation. After 48 h, growth media was changed and IGF-1 was added at concentrations of 0 ng/mL (control group), 10 ng/mL, and 15 ng/mL of IGF-1. (Please note that all myoblast

culture studies, including those with exogenous IGF-1, used media containing 10% FBS despite the fact that FBS does contain multiple growth factors, including IGF-1. FBS was nevertheless incorporated into the cell culture media for two significant reasons. First, FBS is generally required for long term cell adhesion to a purely synthetic material in an *in vitro* study. Second, FBS replicates some of the aspects of the chemically complex environment that will be observed by the proposed constructed when used clinically. After 3 and 5 d, the cells were lifted and counted using a hemacytometer. This experiment was done in triplicate and the values are reported as the mean and standard deviation of the total number of cells for each group.

Adsorbed IGF-1 Release Profile and its Effect on Myoblast Proliferation

To determine the activity of IGF-1 adsorbed on the surface of EH networks, IGF-1 was physically adsorbed onto the network, and both IGF-1 release and myoblast proliferation were characterized. IGF-1 was reconstituted in PBS with 0.1% bovine serum albumin to a concentration of 100 μg/mL. Solutions of the IGF-1 stock were diluted to 10 ng/mL, 50 ng/mL, and 100 ng/mL. One mL of the IGF-1 working solutions was then added to the surface of the network and allowed to evaporate overnight in a sterile laminar flow hood. Once the networks dried, 2 mL of fresh PBS were added to each sample. The networks were then placed in the incubator at 37°C and 5% CO_2. At 0.25, 0.5, 0.75, 1, 2, 4, 6, 12, 24, and 48 h, a 300 μL sample was removed and fresh PBS was added to maintain a constant total volume. All sample aliquots were stored at 4°C until analysis. The samples were

analyzed using a human IGF-I Quantikine enzyme-linked immunosorbent assay Kit (R&D Systems, Minneapolis, MN). To investigate proliferation, myoblasts were cultured on the IGF-1 loaded disks with growth media being changed on day 3. All media was supplemented with FBS as was done in the previous proliferation study. After 3 and 5 d, the cells were lifted and counted using a hemacytometer. Both studies were done in triplicate and the values were reported as the mean and standard deviation of the absolute amount of IGF-1, the percent of loaded IGF-1 released from the network, and the total number of cells on each network, respectively.

Statistical Analysis

Statistical analysis was performed on all data using analysis of variance and Tukey's multiple comparison tests.

Results

The objective of this work was to determine the feasibility of a 5-ethyl-5-(hydroxymethyl)-β,β-dimethyl-1,3-dioxane-2-ethanol diacrylate network as a biomaterial for skeletal muscle regeneration and therefore abdominal wall hernia repair. Specifically, we looked at the physical properties of the biomaterial itself as well as its use as a degradable scaffold for the delivery of IGF-1 to a skeletal myoblast population.

In the mechanical study, the frequency at which the sample was oscillated was varied between 1 and 100 Hz. Initial data analysis indicated that EH networks had a

complex modulus that demonstrated less than 8% variance across the entire frequency range. Therefore, reported values were chosen from the middle of the experimental range at 10 Hz to eliminate any end effects. As can be seen in Fig. 2, the complex modulus of the network made with 0.23 M BP solution was found to be statistically similar to both of the networks made with 0.08 and 0.81 M BP solutions. However, comparison of the 0.08 and 0.81 M BP solution networks show that the complex modulus decreased significantly from $4.7 \times 10^2 \pm 1.2 \times 10^2$ MPa to $2.5 \times 10^2 \pm 0.1 \times 10^2$ MPa, respectively.

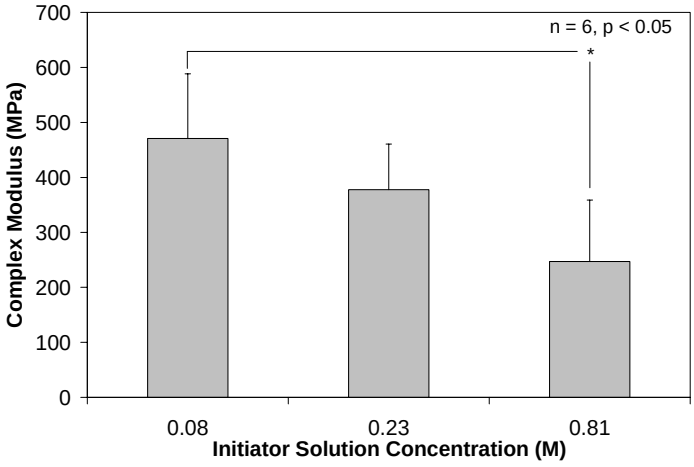

Figure 5. 2: Complex modulus as a function of initiator concentration. A frequency sweep of 1–100 Hz was run on a Q-800 dynamic mechanical analyzer (TA Instruments) with parameters of 37°C and 15 µm amplitude. Results for 10 Hz are reported in this graph.

To determine the ability of EH scaffolds to support a cell population, four different studies were conducted with putative rat skeletal myoblasts. First, myoblast attachment was tested. Figure 3 shows that when comparing the 0.34 and 0.58 M BP networks, there is a slight increase in myoblast attachment as the initiator content is increased. However, closer study revealed this trend was not found to be statistically

significant. Results also indicated that the percent of myoblasts attached to the experimental group and the tissue culture polystyrene (TCPS) were statistically similar at all time points, indicating that initial myoblast attachment occurs at a rate and extent similar to the control.

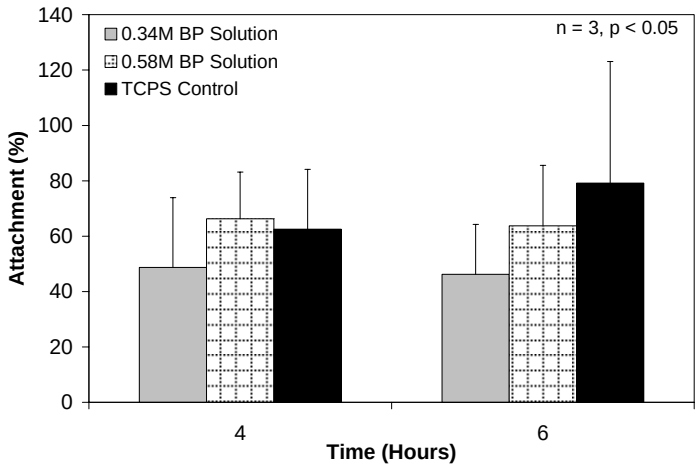

Figure 5. 3: Myoblast cell attachment on EH networks with varied initiator concentrations. All groups were found to be statistically similar.

Next, in an effort to promote cell proliferation, IGF-1 was added to the culture media at concentrations of 0 ng/mL (control group), 10 ng/mL, and 15 ng/mL. As mentioned earlier, myoblasts were allowed to attach to the EH network for 48 h prior to IGF-1 addition; therefore, all results were normalized to data taken on the day of IGF-1 addition (day 0). As indicated in Fig. 4, at day 3, the cell numbers for the control, 5 ng/mL and 10 ng/mL groups were as follows: $0.65 \times 10^6 \pm 0.10 \times 10^6$, $0.61 \times 10^6 \pm 0.11 \times 10^6$, and $0.64 \times 10^6 \pm 0.13 \times 10^6$ cells per network. No significant difference among all groups at day 3 was found. However, by day 5 the groups containing growth media supplemented with IGF-1 had significantly more cells than the control group: the values for the control and experimental groups were 0.65×10^6

± 0.17 × 10^6, 1.03 × 10^6 ± 0.34 × 10^6, and 1.08 × 10^6 3± 0.28 × 10^6 cells per well, respectively. While there were no statistical differences among the experimental groups at these doses, this study demonstrates the result that the supplementation of IGF-1 to the growth media induces attached myoblast proliferation.

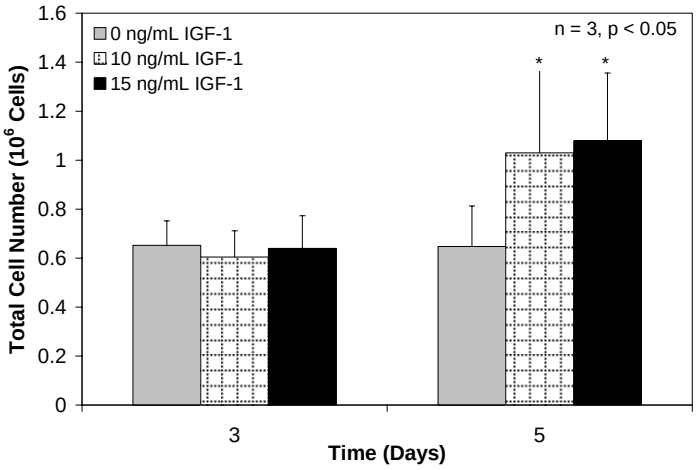

Figure 5. 4: Total number of cells attached to EH networks after 3 and 5 days. It was shown in this study that only the IGF-1 groups at day 5 were statistically different from all groups in both time points.

Next, the study of this material as a delivery device was initiated as IGF-1 was physically adsorbed onto the EH surface and allowed to release into fresh PBS over time. To obtain release profiles of the IGF-1, three concentrations of 10, 50, and 150 ng were adsorbed onto the network and release was characterized over 48 h. Figure 5A displays the absolute amount of IGF-1 released. The 50 and 150 ng loading groups released 16.19 ± 0.32 ng and 17.07 ± 0.12 ng IGF-1, respectively, over 48 h. These two groups follow a similar temporal profile and are significantly similar for all points, except at 2 and 48 h. Alternatively, the 10 ng loading group released 1.65 ± 0.03 ng over 48 h. This group was statistically lower than the other higher loading

groups at all time points, as expected. Considering percent release, the 50 ng loading group released a significantly higher percent of IGF-1 than the 10 ng loading group after 48 h (Fig. 5B). Moreover, compared with the 150 ng loading group, the 10 ng loading group released a significantly higher percent of IGF-1. Here, release after 48 h was 32.38 ± 0.63%, 16.52 ± 0.29%, and 11.38 ± 0.08% IGF-1 loaded, respectively.

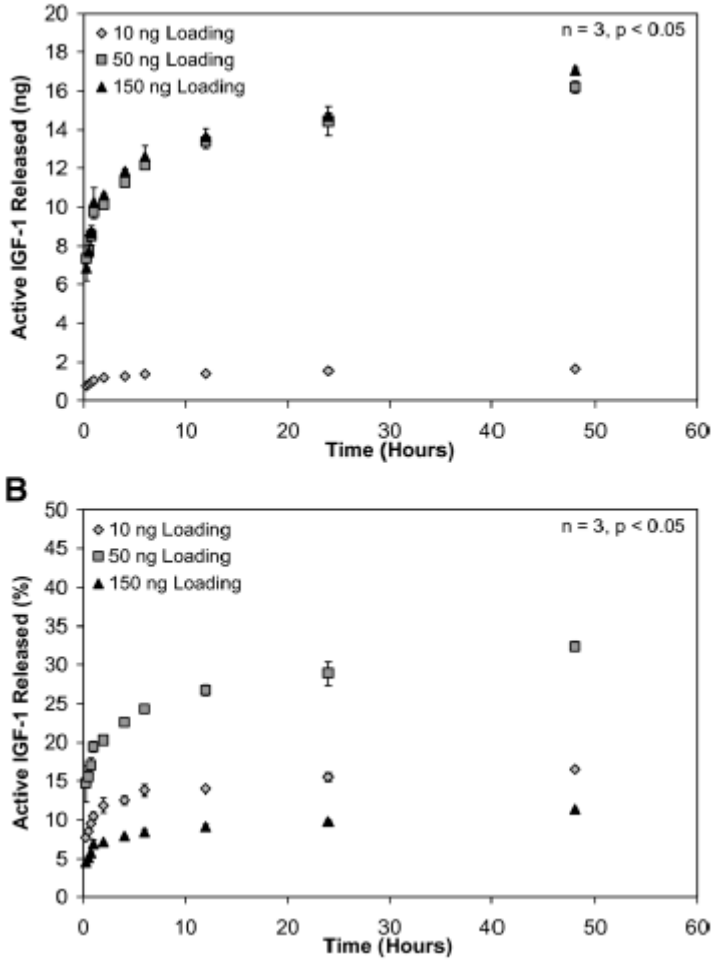

Figure 5. 5: (A) Total IGF-1 released from the surface of the EH network. The 10 ng loading group showed a significantly lower amount of IGF-1 released than the 50 and 150 ng loading groups. The 50 and 150 ng groups were statistically similar for all time points except 2 and 48 h. (B) Percent IGF-1 release from the surface of the EH network. The 10 ng loading group released a significantly higher percent of the loaded IGF-1 than the 150 ng loading group. The 50 ng

group released the highest percent of the loaded IGF-1 and was statistically different from both the 10 ng and 50 ng loading groups.

Last, the functionality of the adsorbed IGF-1 was examined. Myoblasts were seeded onto IGF-1 loaded EH networks and the IGF-1 induced proliferation investigated. Figure 6 showed that the 50 and 150 ng loaded networks had significantly more cells attached to the networks than either the 10 ng loading group or the control at day 3. By day 5, all groups were shown to be statistically similar. Also, the control at day 5 was statistically higher than at day 3, showing a slower increase in cell numbers than the IGF-1 loaded network groups.

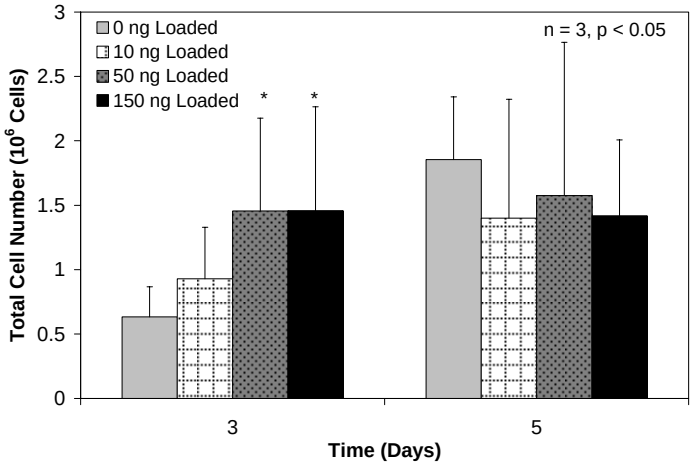

Figure 5. 6: Total number of cells attached to IGF-1 loaded EH networks after 3 and 5 days. It was shown in this study that only the networks that contained 50 and 150 ng of IGF-1 had more cells attached at day 3 than the 10 ng and control groups. It was also found that by day 5 all groups had leveled off and were statistically similar.

Discussion

This work seeks to develop EH networks as a platform for skeletal muscle regeneration within abdominal hernias. As an initial concern, any biomaterial developed for abdominal hernia repair must have physical properties that are suitable for the abdominal environment. In particular, the material must withstand the force of the abdominal cavity, while allowing for free movement. Previous work with EH networks has shown that by altering the fabrication parameters, properties such as the gelation time, sol fraction, and swelling degree could all be varied.[22] Therefore, it was hypothesized that by altering the fabrication parameters, specifically the initiator concentration, we could alter the mechanical properties as well. Results showed that complex modulus did decrease significantly as initiator concentration was reduced from 0.81 to 0.08 M and, thus, EH network mechanical properties may be controlled by alternations in initiator concentration (Fig. 2). This control over material mechanical properties is a key attribute, allowing an implant to be fabricated with the mechanical properties necessary for a particular application. Nevertheless, it must be noted that abdominal wall skeletal muscle has been reported to possess a Young's modulus of 42.5 ± 9.0 kPa in the transverse plane and 22.5 ± 2.6 kPa in the sagittal plane.[138] Thus, the EH networks studied here have a modulus approximately 100-fold greater than skeletal muscle. Although this may be a concern, it must be emphasized that the networks studied here were solid sheets, while clinically relevant implants would be fabricated as porous meshes with significantly lower mechanical properties. Porous EH networks are easily fabricated using any of a number of strategies, including porogen leaching, phase separation, and gas foaming. Following a porogen

leaching strategy[139-142], we have fabricated porous EH networks, although they are not considered in the present work.

The biological functionality of EH networks, specifically cellular interactions, was then investigated by determining the effects of increasing initiator concentration on myoblast attachment. Myoblasts were expected to have a similar percent attachment to the EH networks as the tissue culture polystyrene control. Results showed that the 0.58 M initiator system had a slightly higher percent of cell attachment than the 0.34 M BP system; however, all groups were statically similar at both 4 and 6 h (Fig. 3). Previous studies have shown that during network formation, the 0.58 M BP solution reacts more completely, leaving behind less unreacted and presumably more cytotoxic materials.[22] Therefore, the trend of increasing myoblast attachment with increased initiator concentration may be due to the reduction of unreacted components in the system. Due to the results of this study, the higher initiator formulation was used for subsequent experiments.

The retention of IGF-1 signaling pathways by myoblasts attached to EH networks was then investigated by augmenting culture media with exogenous IGF-1. Results demonstrated that at day 3, all groups of IGF-1 concentrations had significantly similar cell growth (Fig. 4). However, by day 5, both the 10 ng/mL and 15 ng/mL group had significantly more cells than the control group, as well as similar cell numbers to each other. The results indicate that repeated exposure to IGF-1 has a long-term effect on the cell proliferation. Furthermore, it also implies that increasing the concentration from 10 to 15 ng/mL did not have a significant effect on the cell proliferation, an outcome that may be due to the small difference between

concentrations. Finally, this study demonstrates that the EH network does not affect the myoblast's ability to use the IGF-1 protein to induce mitotic signaling pathways.

However, to be an effective delivery vehicle, the EH scaffold should be able to deliver the IGF-1 protein in an active form, so as to ultimately induce myoblast proliferation *in vivo*. Therefore, the release rate of adsorbed IGF-1 from EH networks was subsequently characterized. In particular, the effect of physically adsorbing increasing concentrations of IGF-1 on the total IGF-1 released into PBS over time was measured (Fig. 5). Results demonstrated that the loading of low levels of IGF-1 allow for release over 2 h, while higher loading levels sustained release after 12 h. Furthermore, as this study used an enzyme-linked immunosorbent assay to detect IGF-1 release, it may be inferred that the released IGF-1 retained its structurally active form. It must be noted, however, that a relatively low percentage of IGF-1 was released from the EH networks. Finally, this data does demonstrate that EH networks can be functionalized to release IGF-1 into the local environment, therefore inferring their ability to deliver IGF-1 to native skeletal muscle *in vivo*.

The final work aimed to demonstrate the ability of IGF-1 loaded EH networks to induce skeletal myoblast proliferation (Fig. 6). Results showed that after 3 d, EH networks loaded with 50 and 150 ng of IGF-1 had significantly more myoblasts than the control and 10 ng loaded networks. By day 5, however, all of the groups had significantly similar levels of myoblast proliferation. At this later time point, there was likely no additional IGF-1 being released from any of the networks (see results in Fig. 5) and, thus, it would be expected that IGF-1 induced proliferation had slowed. As the results with IGF-1 augmented media demonstrated that continuous IGF-1

delivery is needed for enhanced myoblast proliferation (Fig. 4), this work confirms that EH networks loaded with IGF-1 can release the growth factor at early time points so as to induce myoblast proliferation in the initial healing stages. Furthermore, contrasting the results in Figs. 4 and 6, it appears that skeletal myoblasts exposed to continuous IGF-1 delivery demonstrate a delayed increase in cell proliferation. However, when a similar amount of IGF-1 was delivered in a burst due to EH network release, a short-term increase in myoblast proliferation was observed. Overall, a similar increase in cell proliferation was seen in both studies, with adsorbed IGF-1 exhibiting an increase in proliferation at earlier time points than IGF-1 supplemented culture media. In clinical applications, it may be that the burst release of IGF-1 from EH networks is preferred, so that myoblast proliferation is initiated early, however this is speculative and would need to be confirmed by controlled *in vivo* studies.

The results of this work demonstrated fundamental relationships between EH networks, IGF-1, and myoblasts. In particular, EH networks allow for myoblast adhesion, IGF-1 surface absorption, and subsequent release, as well as IGF-1 induced myoblast proliferation. While this initial work focused upon *in vitro* studies, we can speculate that *in vivo* EH networks should allow for the local delivery of an active form of IGF-1 and that this delivery can be sustained for up to 12 h.

These successful results also indicate future directions for this work. In particular, the fabrication of porous EH networks as well as the interaction of porous architectures with myoblasts should be considered. Comprehensive mechanical studies, including tensile strength, burst strength, and suture retention strength would

demonstrate whether the mechanical properties of porous EH meshes are suitable for the abdominal wall environment. The results described here also indicate that *in vivo* studies of EH materials may be warranted, as well as contrasting their efficacy with meshes currently in use for abdominal hernia repair. Finally, future work will need to evaluate the proposed strategy of skeletal muscle regeneration for hernia repair and, in particular, contrasting this approach with current strategies that focus upon fibroblast proliferation and collagen matrix production.

Conclusions

This work examined the ability of the novel cyclic acetal biomaterial to function as an abdominal wall hernia repair implant. Tissue engineering principles were used to examine EH networks in regards to their mechanical and biological compatibility. In particular, mechanical properties, cellular attachment, IGF-1 release, and IGF-1 induced proliferation were examined. Results showed that the concentration of initiator solution used during fabrication altered the mechanical property of these networks. Additionally, results show that myoblasts attach to the networks in a manner similar to the tissue culture polystyrene control and proliferate upon these networks in the presence of IGF-1. Finally, results demonstrate that IGF-1 can be released from the network after adsorption and will continue to induce myoblast proliferation. These studies suggest that the EH scaffold would be a favorable material for facilitated myoblast attachment and proliferation. When combined with fabrication and degradation properties of EH networks, this biomaterial is a promising scaffold for tissue engineering, specifically a skeletal muscle engineering strategy.

Acknowledgments

This work was supported by the National Science Foundation through a Career Award to JPF (no. 0448684). The authors acknowledge the editorial contributions provided by Rosemary Klein of the Division of General Surgery at the University of Maryland Medical Center. In addition, we would also like to thanks Dr. Arthur Cresce from the lab of Dr. Peter Kofinas for his help with the Dynamic Mechanical Analysis.

Chapter 6: Fabrication and Characterization of Porous EH Scaffolds and EH-PEG Bilayers

Introduction

Synthetic polymers have been extensively studied for use in biomedical and tissue engineering applications.[1-3] Several current clinical applications include medical devices such as vascular stents and hernia repair meshes as well as polymer therapeutics such as polymer-protein conjugates and drug delivery devices.[1, 17, 143, 144] These applications are all possible due to the ease with which a synthetic polymer's chemical and physical properties can be modified. One of the most common modifications made for tissue engineering applications specifically is to polymer scaffold architecture.[9-11] Techniques such as porogen leaching, electrospinning, and micropatterning are often used.[123, 124, 140, 145, 146] To determine a polymer's utility and clinical relevance, mechanical and chemical properties of the fabricated scaffolds must be investigated.

This paper addresses the use of a cyclic acetal monomer, 5-ethyl-5-(hydroxymethyl)-β,β-dimethyl-1,3-dioxane-2-ethanol diacrylate (EHD), in the formation of a crosslinked porous EH scaffolds for abdominal wall hernia repair. Abdominal wall hernias are a prevalent condition with approximately 500,000 new cases developed each year in the United States.[132] While several synthetic meshes have been developed to aid in the repair of abdominal wall hernias, there is yet to be an ideal candidate that can effectively prevent recurrence in all patients. In fact, even with synthetic mesh placement hernia recurrence occurs in 20-50% of patients.[84]

In an effort to lower hernia recurrence rates, a tissue engineering strategy was developed to encourage skeletal muscle regeneration within the hernia defect. To achieve this, two aspects must be investigated: wound healing and mechanical stability. Current studies have demonstrated that recurrent hernia patients almost always exhibit incomplete or immature wound healing.[84, 93] During skeletal muscle wound healing, satellite cells become activated and migrate to the defect site where they begin to proliferate. If the defect is blocked by a polymer scaffold however, neither the satellite cells nor inflammatory cells can infiltrate the defect. This results in the prosthetic mesh becoming encapsulated in fibrous scar tissue.[107] Previous work has shown that EH networks are biocompatible with a rat skeletal muscle myoblastic cell population and that they support the attachment and proliferation of these cells.[59] Therefore a macroporous EH monolayer was designed to allow for cell infiltration into the network. Once populated with satellite cells, the cells can attach and align with each other to fuse into myotubes and mature into functioning myofibers. For this strategy to be successful however, the polymeric scaffold must degrade on the same time scale as muscle is regenerated.

To further create a functional hernia repair device, EH monolayers were coated with poly(ethylene glycol) diacrylate (EH-PEG bilayers) in an attempt to create an abdominal adhesion barrier. Abdominal adhesions are a common clinical complication in hernia repair.[103, 104, 118, 130, 131, 147] It has been found that adhesions can lead to intestinal obstruction, chronic pain, female infertility and entercutaneous fistulas.[103, 132, 147] To successfully prevent reoccurrence and other post-operative complication, an ideal hernia repair device must address this concern. As for

mechanical stability, previous studies have showed that solid EH networks had a 100 fold greater modulus than that of skeletal muscle.[59] Therefore it is hypothesized that by creating a more porous architecture one can alter the mechanical properties as well.

To this end, the studies presented here aim to characterize porous EH networks for the application of abdominal wall hernia repair. EH scaffolds with different architectures were fabricated and were degraded in buffer (pH 7.4) to determine the percent mass lost as well as the change in pH of the buffer solution over 85 days. In addition, the effect of changes in the scaffold architecture on the Young's modulus and flexural strength was measured.

Materials and Methods

Materials

Benzoyl peroxide (BP), N,N-dimethyl-p-toluidine (DMT), 5-ethyl-5-(hydroxymethyl)-β,β-dimethyl-1,3-dioxane-2-ethanol diacrylate (EHD), isobutyraldehyde, formaldehyde (37% aqueous solution), trimethylolpropane, triethylamine, hydroquinone, acryloyl chloride, ammonium persulfate (APS), N,N,N',N'-tetramethylethylenediamine (TEMED) and PEG diacrylate (PEGDA) were obtained from Sigma-Aldrich (Milwaukee, WI, USA). Reagent grade acetone, potassium carbonate, sodium sulfate, ethyl ether, silica gel (60-200 mesh) and sodium chloride (salt) were purchased from Fisher Scientific (Pittsburg, PA, USA).

5-ethyl-5-(hydroxymethyl)-β,β-dimethyl-1,3-dioxane-2-ethanol diacrylate Synthesis

EHD was synthesized based on the protocols described by Kaihara et al. Potassium carbonate (18.9 g, 0.25 equiv) was added to isobutyraldehyde (50 ml, 1 equiv) and formaldehyde (37% aqueous solution, 40.8 ml, 1 equiv) and the solution was stirred at 0°C overnight. The product 3-hydroxy-2,2-dimethylpropinaldehyde (HDP) was extracted three times with chloroform and then washed with water and brine. The chloroform layers were combined and dried with sodium sulfate and the solvent was evaporated under reduced pressure to obtain solid HDP. HDP (32.9 g, 1 equiv) and trimethylolpropane (86.6 g, 2 equiv) were dissolved in 1 M hydrochloric acid (200 ml) and stirred for 2 h at 80°C. The solution was then neutralized with sodium hydroxide and the product 5-ethyl-5-(hydroxymethyl)-*β*,*β*-dimethyl-1,3-dioxane-2-ethanol (HEHD) was extracted three times with chloroform and washed with water and brine. The chloroform layers were combined and again dried with sodium sulfate and evaporated under reduced pressure to obtain solid HEHD. The HEHD was purified using an ethyl ether wash to remove undesired byproducts and was dried under reduced pressure. HEHD (31.3 g, 1 equiv) was dissolved in chloroform and triethylamine (65.4 ml, 3 equiv) and hydroquinone (0.034 g, 0.002equiv) were added. Acryloyl chloride (38.1 ml, 3 equiv) was added dropwise as the reaction was stirred at 0°C for 2 h. The insoluble salts were removed through filtration and the product, 5-ethyl-5-(hydroxymethyl)-*β*,*β*-dimethyl-1,3-dioxane-2-ethanol diacrylate (EHD), was extracted three times with chloroform and washed with water and brine. The chloroform layers were combined and dried with sodium sulfate and evaporated under reduced pressure. The EHD was further purified by silica gel

column chromatography using a chloroform/ethanol (10:1, v/v) as the eluent. The fractions that contained EHD were determined by thin layer chromatography and NMR.

Solid EH Network Formation

Solid EH networks were fabricated in a glass plate mold. To assemble this mold, capillary tubes were secured onto one of two glass plates with vacuum grease to create a 1 mm thick well. BP was added to acetone to create a 0.826 M solution. 2 g of EHD monomer was then mixed with 0.75 mL of BP solution and 16 μL of DMT was added. This mixture was vortexed and poured directly into the mold. The network was covered with a second plate and placed in an oven at 60°C for 20 min. The resulting sheet was removed, cut into the required shape and placed into DI water for 48 h with the water change after 24 h.

Solution Formed Porous EH Monolayer Formation

Solution formed porous EH networks (SOLN EH monolayers) were made using a leachable porogen strategy. 7 × 4.3 cm rectangular cavities were cut out of 1.4 mm thick plastic sheets in order to form frames. A glass plate was placed under the frames to form a well, which was filled with 7.8 g of salt. Salt was wetted with 2.445 mL 85% acetone and spread with another glass plate to fill the frame. Salt-filled frames were dried on an 85 °C hot plate for 1 h in order to produce an

interconnected salt network that was attached to the plastic frame. The salt-filled frame was allowed to cool 10 min before removal from the glass plate.

The mass of the salt network was measured to determine the amount of polymer solution required to achieve the desired porosities of 75 and 80 wt% salt. Active EHD solution was prepared by mixing each gram of EHD with 375 μL of 0.826 M BP in acetone and 8 μL DMT. The salt-filled frame was suspended over a weighing dish such that the salt network was solely supported by the frame and active EHD solution was delivered drop wise onto the salt cake.

The frame was then placed in a 60°C oven for 20 min to promote polymer gelling. Once gelled, the SOLN EH network was transferred to DI water to leach out salt. After 20 min the networks were removed from the frame to prevent cracking and the salt was leached out for 48 h with a water change at 24 h.

Solid PEG Monolayer Formation

PEG networks were prepared with 30 wt% PEGDA, 20 mM APS, 20 mM TEMED and 5% acetone. Two stacks of three cover slips were placed on top of a glass sheet to control the PEG network thickness. PEGDA, APS, TEMED, water and acetone were vortexed and poured quickly in between the cover glass stacks. A second glass sheet was then placed on top of the cover slips, pressing the PEG solution between the two layers of glass. After curing, 10 mm wide samples were cut from the PEG network.

EH-PEG Bilayer Production

SOLN EH networks were made as described above. Networks were removed from the water after 48 h and dried overnight on a paper towel. 20 mM solutions of the water soluble radical initiators ammonium persulfate (APS) and N,N,N',N'-tetramethylethylenediamine (TEMED) were made as well as a 30% solution of PEG diacrylate (PEGDA) in 5% acetone. Two stacks of three coverslips were placed on a glass plate to control the thickness of the PEGDA layer on the EH network. After combining the PEGDA, APS, and TEMED the solution was vortexed and poured quickly in between the coverslips. The dried SOLN EH network was placed on top of the coverslips and the PEGDA was allowed to crosslink with the network. After the PEGDA was gelled the network was removed from the plate and the excess PEG was removed. The bilayers could then be cut into any shape desired.

Scanning Electron Microscopy

To obtain SEM images, networks were fabricated as mentioned above. The samples were positioned to expose both the top surface and cross section of each scaffold and the samples were coated with gold before imaging. Images were obtained using a Hitachi Field Emission Scanning Electron Microscope fitted with an X-Ray Analysis System.

Degradation Study

Solid networks, two SOLN EH monolayers and two EH-PEG bilayers were all fabricated as described above. 5 samples for each of the 5 groups for each time point were cut into 1 cm^2 networks and were immediately weighed after fabrication. During storage the network dispelled water so on day 0 all networks were prewetted with ethanol using the following protocol. The networks were put in a falcon tube of 100% ethanol and placed under vacuum. Once the air was removed and the pores were filled, the networks were allowed to soak for 20 min. The ethanol was then replaced with PBS over a series of three 20 min washes. 20 mL of PBS was then added each vial and the networks were placed in the oven at 37°C for 1 to 85 days. At each time point the networks were weighed and the pH of the PBS was measured.

Mechanical Analysis

Two SOLN EH monolayers and two EH-PEG bilayers were fabricated as described above. Solid PEG layers were also formed as discussed above as a control. Samples were cut into 1 x 6.5 cm strips. 5 samples from each group where then tested according to ASTM 790 Procedure A for three point bending for reinforced and unreinforced polymers, with the following modifications: samples were tested wet in order to better represent physiological conditions, the support span for all specimens was 30 mm and samples were preloaded with 0.01 N prior to testing.

Results

The objective of this work was to investigate the degradation rate and mechanical properties of solid EH networks, porous SOLN EH monolayers, and EH-PEG bilayers. Initially, SEM images were obtained to qualitatively assess the differences in network structure. Then, the networks were degraded in PBS buffer (pH 7.4) at 37°C for 85 days and the mass lost and buffer pH change was measured. In addition, 3 point bending mechanical analysis was performed to determine the Young's modulus and flexural strength of the networks.

Solid EH networks, porous SOLN EH monolayers, and EH-PEG bilayers were successfully constructed and cut into 1 cm^2 squares. Figure 1 shows the top and cross sectional views of (A) a solid EH network, (B) a 75 wt% SOLN EH network and (C) a 80 wt% SOLN EH network. Figure 1A (top) shows that the solid EH networks were defect free on the top surface. The cross sectional image (bottom) however displays some ridges which are artifacts from the cutting of the networks. Figures 1B and 1C show the porous structure created by the porogen leaching method. Qualitatively, the pores on the top surface of the 75 wt% SOLN EH monolayer (figure 1B top) appear more uniformly spaced as illustrated by the thicker wall between pores and the grid-like alignment of pores, which was not observed for the 80 wt% SOLN EH network (figure 1C top). However, when comparing cross sections (1B and 1C bottom), the pores are evident through the entire cross sectional area of both groups.

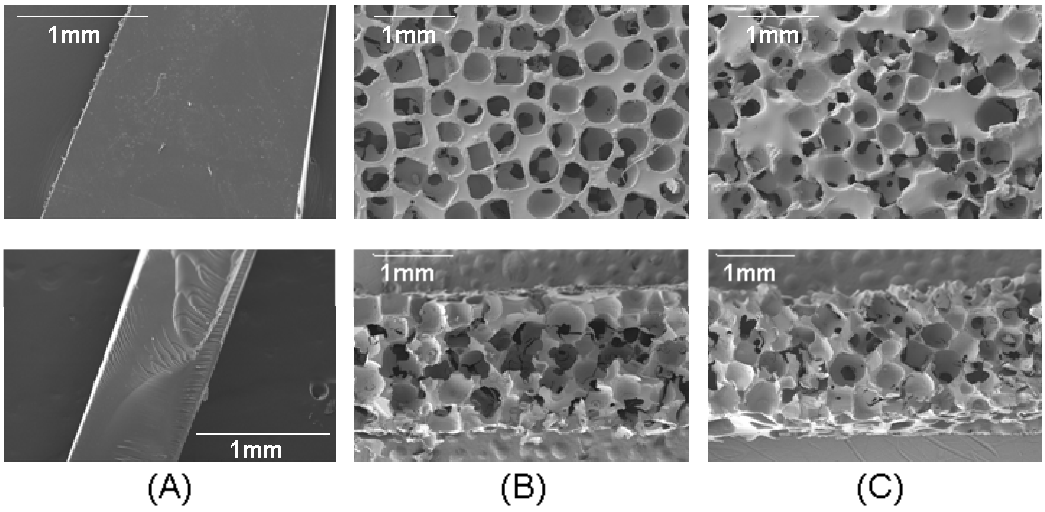

Figure 6. 1: (A) SEM image of the surface (top) and cross section (bottom) of a solid EH network (B) SEM image of the surface (top) and cross section (bottom) of a 75 wt% SOLN EH monolayer (C) SEM image of the surface (top) and cross section (bottom) of a 80 wt% SOLN EH monolayer.

To determine how the degradation of these networks was impacted by these architectural changes, scaffolds were made and cut into 1 cm^2 squares. The networks were weighed and submerged in PBS buffer (pH 7.4) for 85 days. Figure 2 shows that the solid EH networks lost the majority of their mass during the first 4 days in solution. Between days 4 and 85 no significant changes were observed. By day 85 the solid EH networks lost 12.290 ± 0.663% of their total mass. The 75 wt% SOLN EH monolayer exhibited a significant loss in mass only during the first day in solution before the mass stabilized. After 85 days 29.209 ± 7.181% of the network's mass was lost. The 80 wt% SOLN EH monolayers lost the majority of its mass during the first 4 days of the study. While this was similar to the solid networks, the total mass loss was significantly less in the solid networks than in the porous SOLN EH

monolayers. This group however did not remain stable though the study. The mass oscillated slightly between day 4 and 85 with a total percent mass loss of 25.028 ± 5.920% at 85 days. Both of the 75 and 80 wt% EH-PEG bilayers exhibited no significant mass loss during the 85 day study. At day 85 the total recorded mass lost for these groups were 3.032 ± 3.157 % and 8.995 ± 3.088 % respectively. Overall, at day 85 it was found the SOLN EH monolayers lost significantly more percent mass than the solid EH networks and the EH-PEG hydrogels.

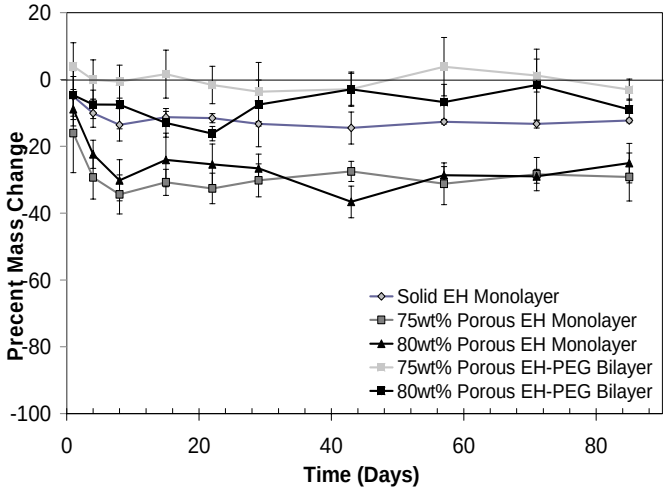

Figure 6. 2: Percent mass change of solid EH networks, 75 and 80 wt% SOLN EH monolayers and 75 and 80 wt% EH-PEG bilayers degraded in PBS buffer over 85 days. The 75 and 80 wt% EH-PEG bilayers did not lose a significant percent of its mass over the course of this study. The solid EH networks lost 12.290 ± 0.663 % of their mass which was statistically different than at day 1, but was not statistically different than the 75 and 80 wt% bilayers. The 75 and 80 wt% SOLN EH monolayers lost the most percent mass having lost 29.209 ± 7.181 % and 25.028 ± 5.920 % respectively.

In addition to the percent mass change, the change in buffer pH was recorded at each time point. The pH of the solution varied by approximately 1.4 pH units over

the course of the study, as can be seen in Figure 3. The solid EH networks had a significant decrease in pH over the majority of study. By day 29 the pH leveled off and was found to be 6.98 ± 0.06 at day 85. The pH of the 75 wt% SOLN EH networks did not vary significantly over the course of the study. The pH at 85 days was found to be 6.87 ± 0.05. As with the percent mass loss data, the pH of the 80 wt% SOLN EH monolayers displayed a similar trend to the solid EH networks. The pH at 85 days for this group was 7.01 ± 0.06 which was significantly lower than the starting pH of 7.4. The group that had the most significant decrease in pH over time was the 75 wt% EH-PEG bilayer group. This group showed significant differences throughout the whole study. In the end, at day 85 the pH for this group was 5.87 ± 0.14. The 80 wt% EH-PEG bilayer also exhibited a strong decrease in pH but it was not as strong as the 75 wt% EH-PEG bilayer group. The 75 wt% EH-PEG bilayer group showed a pH of 6.406 ± 0.17 at 85 days. Overall, at day 85 the degradation buffer solution from the solid EH networks and the 75 and 80 wt% SOLN EH monolayer groups had a statistically higher pH than that of the 75 and 80 wt% EH-PEG bilayers. The 80 wt% EH-PEG bilayers also had a statistically higher pH than the 75 wt% EH-PEG bilayers as well.

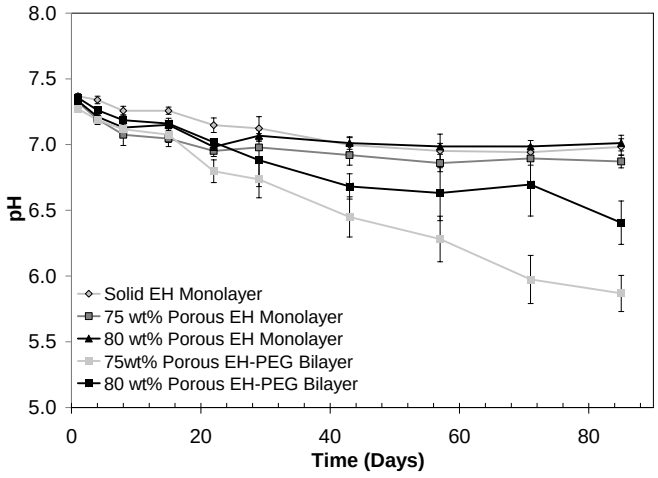

Figure 6. 3: pH change of PBS buffer solution from solid EH networks, 75 and 80 wt% SOLN EH monolayers and 75 and 80 wt% EH-PEG bilayers degraded over 85 days. The pH of the 75 wt% SOLN EH networks did not vary significantly over the course of the study. The solid EH networks and the 80 wt% SOLN EH monolayers however did show a significant decrease in pH to 6.98 ± 0.06 and 7.01 ± 0.06 respectively at day 85. Both of the 75 and 80 wt% EH-PEG bilayer groups showed the largest drops in pH from 7.4 to 5.87 ± 0.14 and 6.406 ± 0.17 respectively.

In an effort to characterize the effect of the scaffold architecture on mechanical properties, three point bending mechanical analysis was performed. Briefly, the 75 and 80 wt% SOLN EH monolayers and the 75 and 80wt% EH-PEG bilayer groups were fabricated and cut into 1 x 6 cm strips. These were then tested to determine the Young's modulus and flexural strength of the networks. The bilayers were tested on both sides to determine if there was a significant different in mechanical properties based on which material the force was applied to. All bilayer results are reported with the values of the EH side up first and the PEG side up second. Solid PEG scaffolds were used as a control. Figure 4 shows that the solid PEG networks had a Young's modulus of 8.310 ± 1.552MPa. The 80 wt% bilayers

showed similar numbers at 9.698 ± 3.338 MPa and 7.088 ± 3.871 MPa when the force was applied to the EH side and the PEG side respectively. The 80 wt% SOLN EH monolayer and the 75 wt% EH-PEG bilayers were statistically higher than the previous groups. The values for these groups were 20.824 ± 4.731 MPa for the solid networks and 20.929 ± 2.227 MPa and 20.683 ± 2.448 MPa when the force was applied to the EH side and the PEG side of the bilayers respectively. The 75 wt% SOLN EH monolayer was statistically higher than all other groups with a Young's modulus of 29.915 ± 6.103 MPa.

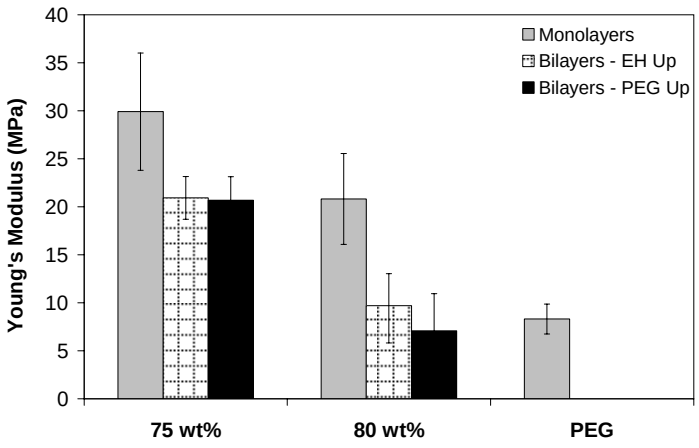

Figure 6. 4: The Young's modulus was found for 75 and 80 wt% SOLN EH monolayers, 75 and 80 wt% EH-PEG bilayers and a solid PEG control network. Results indicate the modulus for the 75 wt% SOLN EH monolayers was statistically higher than the 75 wt% EH-PEG bilayers and 80 wt% SOLN EH monolayers. In addition, the modulus for the 80 wt% EH-PEG bilayers and solid PEG control networks were statistically lower than all of the other groups. EH UP refers to when the force was being applied to the EH layer and PEG UP refers to when the force was being applied to the PEG layer.

When looking at the flexural strength a different trend was exhibited. The flexural strength of the 75 wt% SOLN EH monolayer and the 75wt% bilayers were 0.598 ± 0.107 MPa, 0.632 ± 0.095 MPa and 0.618 ± 0.090 MPa respectively. These values were found to be significantly higher than the 80 wt% EH-PEG bilayers and the solid PEG control which had values of 0.323 ± 0.097 MPa, 0.253 ± 0.114 MPa and 0.204 ± 0.030 MPa. The 80 wt% SOLN EH monolayer had a flexural strength of 0.528 ± 0.168 MPa which was only significantly higher than the 80 wt% bilayer when the force was applied to the PEG layer and the solid PEG control.

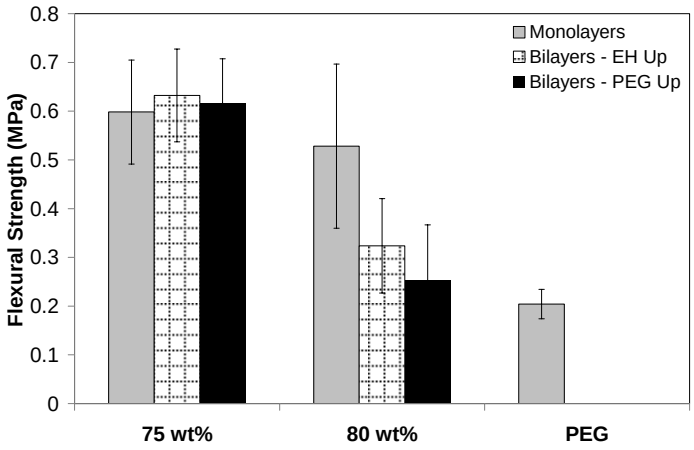

Figure 6. 5: The flexural strength was found for 75 and 80 wt% SOLN EH monolayers, 75 and 80 wt% EH-PEG bilayers and a solid PEG control network. Results indicate the 75 wt% SOLN EH monolayers, 75 wt% EH-PEG bilayers and the 80 wt% SOLN EH monolayers were not statistically different. In addition it was found that the 80 wt% EH-PEG bilayers and solid PEG control network was significantly lower than all of the other groups. EH UP refers to when the force was being applied to the EH layer and PEG UP refers to when the force was being applied to the PEG layer.

Discussion

This work seeks to characterize EH polymer scaffolds for the application of abdominal wall hernia repair. Previous studies have shown that solid EH scaffolds were a favorable material for facilitated myoblast attachment and proliferation. However, one of the drawbacks of this work was the high complex modulus exhibited by the solid networks during dynamic mechanical analysis.[59] Therefore in an effort to increase the EH scaffolds utility, porous SOLN EH monolayers, and EH-PEG bilayers were fabricated using a porogen leaching strategy. SEM images were taken after porogen leaching to qualitatively analyze the different network architectures. The solid EH scaffolds showed cracks during fabrication after the sheet was removed from the mold. SEM images were used to examine the extent of these defects within the solid scaffolds. Figure 1A shows the top view (top) and cross section (bottom) of the solid EH networks. No microscale defects were found in these images. The ridges that are evident on the cross section (1A bottom) occur during the cutting process of the polymer sheet after gelation and are visible to the naked eye. The porous EH scaffolds in Figures 1B and 1C show the surface pore architecture (top) and the pore distribution (bottom) formed due to the porogen leaching technique. Figure 1B (top) shows individual pores arranged across the top surface of the network as opposed to the clumped pores that are shown in Figure 1C (top). This is due to the lower percent of porogen, 75 wt% compared to 80 wt%, contained with the scaffolds during fabrication. Overall, the images show that solid networks are defect free and that both of the 75 and 80 wt% SOLN EH networks show highly porous structures

that are have different surface architectures with pores dispersed throughout the network.

To begin to characterize these scaffolds, polymer degradation in PBS buffer (pH 7.4) was investigated. Cyclic acetal monomers lack the ester linkages present in other hydrolytically degradable materials thereby eliminating the production of acidic degradation products. This study investigates the percent mass lost and pH change as a function of scaffold architecture over 85 days. EH networks are highly hydrophobic and thus must be prewetted to completely submerge the network. It is hypothesized that by exposing a larger surface area of the network to the buffer through the introduction of pores into the scaffold that the percent mass lost can be greatly enhanced. This effect can be seen in Figure 2 where the SOLN EH monolayers lost significantly more mass than any other group. However, it was found that there were no significant differences between the 75 wt% and 80 wt% SOLN EH monolayer groups throughout the study. As expected, the increase in scaffold surface area produced a large change in percent mass lost over the solid networks. These results are supported by the pH data shown in Figure 3. Both the solid networks and the 75 wt% SOLN EH monolayers had a significant decrease in pH over the 85 day study. This pH decrease was due to an additional degradation product. During fabrication, a radical initiator is used to break the double bond of the acrylate group which then bonds to other acrylate groups on other molecules. During hydrolysis, the carbon – oxygen bond is targeted. While the cyclic acetal unit degrades into non-acidic degradation products the newly bound acrylate groups form an additional carboxylic

acid degradation product. This product can alter the pH of the PBS buffer solution as was seen in the previous result.

While the solid EH networks and the SOLN EH monolayers exhibited expected behavior, the EH-PEG bilayers did not. These networks maintained their mass throughout the study. It is hypothesized that this is a result of the hydrophilic and non-degradable nature of the PEG layer. PEG is known to swell in PBS buffer solution and fabrication constraints prevent the use of dry weights for this study. More specifically, it was found that the EH-PEG bilayers must remain hydrated after fabrication to prevent the delamination of the bilayers due to dehydration. Therefore, the wet weights must be measured at each time point and the gel swelling effects cannot be completely eliminated. When fabricating the EH-PEG hydrogels, the hydrophobicity of the SOLN EH monolayers is used as the mechanism to prevent the PEGDA from filling the pores before gelation. While this is an effective technique, there are still some pores that can become filled with PEG. It is speculated that these PEG filled pores as well as the chemical bonds between the EH and the PEG can hinder the gel swelling. Then as the SOLN EH monolayer degrades (as is shown in Figure 2) the PEG layer becomes free to take up more PBS buffer therefore recovering or exceeding the mass lost through EH degradation. One indication that EH degradation is occurring within these bilayers, besides the SOLN EH monolayer data, is displayed in Figure 3. The bilayers exhibited a significant drop in pH over the time of the experiment, indicating the possible presence of the carboxylic acid degradation product that was discussed earlier.

To test the different mechanical properties of these networks three point bending tests were performed on the SOLN EH networks and the EH-PEG bilayers. A solid PEG network was used as a control. As expected the 75 wt% SOLN EH monolayers displayed the highest Young's modulus of the group at 29.915 ± 6.103 MPa. This number is still an order of magnitude higher than the modulus of skeletal muscle which is reported to be 42.5 ± 9.0 kPa in the transverse plane and 22.5 ± 2.6 kPa in the sagittal plane.[138] By coating the SOLN EH monolayers with PEG to create EH-PEG bilayers however, the Young's modulus was decreased significantly to 20.929 ± 2.227 MPa and 20.683 ± 2.448 MPa when the force was applied to the EH side and the PEG side of the bilayers respectively. There was no significant difference found when the force was applied to one side of the bilayer over the other. During flexural deformation, microcracks can be seen and heard within the network. These cracks accumulate and the integrity of the scaffold is compromised over time. `The addition of the PEG helped to reinforce these networks, increasing its capacity for elastic deformation and lowering the networks overall stiffness. The 80 wt% SOLN EH monolayer displayed similar properties to the 75 wt% EH-PEG bilayers with a Young's modulus of 20.824 ± 4.731 MPa. This is significantly lower than the 75 wt% SOLN EH monolayer and it indicates that by altering the weight percent of porogen within a network that the stiffness of that material can be controlled. This trend is also evident in materials such as metals and ceramics. As with the 75 wt% EH-PEG bilayers, the 80 wt% EH-PEG bilayers were statically lower than their monolayer counterpart as well as the 75 wt% SOLN EH monolayers and EH-PEG bilayers. This group was not statistically different from the solid PEG control

network which had a Young's modulus of 8.310 ± 1.552 MPa. Again, the same phenomenon that was displayed in the 75 wt% EH-PEG bilayers can be seen here. Overall, while the Young's modulus of this material is still greater than skeletal muscle, it has been shown that these properties can be altered significantly based on scaffold architecture.

In addition to the stiffness of the material, flexural strength was also measured. This property demonstrates the maximum stress at which fracture within the sample occurs. It was found that the PEG control had the lowest flexural strength when compared to the 75 and 80 wt% SOLN EH monolayers. In addition, the 80 wt% SOLN EH monolayers showed a drop in flexural strength but it was not significant. These results indicate that when fabricating the EH-PEG bilayers, the EH layer will control the scaffold's strength. The 75 wt% EH-PEG bilayers followed this expected trend as the addition of PEG to the SOLN EH monolayer did not significantly affect the flexural strength. For the 80 wt% EH-PEG bilayers however, a significant decrease in strength from the 75 wt% monolayers and EH-PEG bilayers was observed. A significant difference was found between the 80 wt% EH-PEG bilayers and the 80 wt% monolayer, but only when the force was applied to the PEG layer. It is hypothesized that this is a result of the change in the network's surface architecture and the composite's interface. Qualitatively, Figures 1B and 1C show that there are larger pores formed from the grouping of individual pores on the surface of the 80 wt% SOLN EH monolayers than on the surface of the 75 wt% SOLN EH monolayers. This presents a greater opportunity for the PEGDA to infiltrate the 80 wt% SOLN EH monolayers than the 75 wt% SOLN EH monolayer

before gelling. In addition, as mentioned earlier, the pore walls of the 80 wt% SOLN EH monolayers are thinner than in the 75 wt% SOLN EH monolayers. Thus providing less EH surface area for the PEG layer to bind to. It is thought that this thinning of EH pore walls could contribute significantly to the differences in flexural strength between the 80 wt% bilayers and the other experimental groups. Overall, this group was not found to be statistically different than the solid PEG control.

The successful characterization of these EHD based biomaterials show its utility in the field of tissue engineering. These samples were designed for the specific application of skeletal muscle regeneration within abdominal wall hernia repair. Future work will investigate the use of these porous architectures to better deliver therapeutic proteins to enhance skeletal muscle regeneration. By improving the biological functionality of these scaffolds as well as optimizing the material properties a new strategy for abdominal wall hernia repair can be implemented.

Conclusions

This work seeks to further advance the use of EH cyclic acetal biomaterials as an abdominal wall hernia repair device. The effect of scaffold architecture on the degradation properties and mechanical properties were evaluated. Results showed that by altering the porosity of the scaffolds, both percent mass loss and mechanical properties could be altered. More specifically, it was found the porous 75 and 80 wt% SOLN EH monolayers loss significant more mass than the solid EH network and 75 and 80 wt% EH-PEG bilayers over 85 days. In addition, it was found that the mass of the 75 and 80 wt% EH-PEG bilayers did not change significantly over time.

Mechanical testing showed that by adding the PEG layer to SOLN EH monolayers, the stiffness of the networks could be greatly reduced as did adding more porogen to the SOLN EH networks during fabrication. When looking at the flexural strength however, the EH was found to be the main contributor to the overall strength of the networks. All together, these results showed that changing the architecture of the porous SOLN EH monolayers and EH-PEG bilayers we can control the chemical and mechanical properties of scaffolds.

Acknowledgments

This work was supported by the National Science Foundation (NSF) through a CAREER Award to JPF (#0448684) as well as the Maryland NanoCenter and its NispLab. The NispLab is supported in part by the NSF and as a MRSEC Shared Experimental Facility. The authors would like to acknowledge Dr, Abhay Pandit and his lab at the National Centre for Biomedical Engineering Sciences at the National University of Ireland, Galway for the use of the SEM to take the photos of the solid EH networks.

Chapter 7: Porous EH Monolayers and EH-PEG Bilayers as a Gene Delivery Device for Abdominal Wall Hernias Repair

Introduction

Abdominal wall hernias are among the most common pathological conditions affecting humans. Approximately one million repair surgeries are performed annually in the US alone.[77-80] Several repair techniques are available, including xenografts, allografts and autografts, but the most common technique is the implantation of synthetic or natural prosthetic meshes.[105, 106, 118, 127-130] Polypropylene, polytetrafluoroethylene and many polyesters are the most utilized synthetic materials while natural polymers such as sodium hyaluronate and carboxymethylcellulose are often added to augment the implant's integration with the host tissue. Despite these various options, hernia recurrence rates vary between 20-50%.[84]

In an effort to lower the hernia recurrence rates, a synthetic polymer scaffold was designed to deliver a therapeutic plasmid to the abdominal wall defect. This work addresses two major aspects of hernia repair: mechanical support and defect wound healing. Mechanical support of the hernia defect during repair is critical as the repair device must be able to sustain significant changes in intra-abdominal pressure during healing.[83, 92] Synthetic polymer systems are ideal for this application due to the ease of which their physical properties can be tailored. Some commonly controlled properties include pore size, shape and distribution as well as pliability and strength.[103, 117] The cyclic acetal monomer, 5-ethyl-5-(hydroxymethyl)-β,β-dimethyl-

1,3-dioxane-2-ethanol diacrylate (EHD), is an attractive option for repair scaffolds due to ease of scaffold production and biodegradable chemistry. [22, 58, 148]

Wound healing, on the other hand, is more complicated. Current studies showed that recurrent hernia patients almost unanimously exhibited incomplete or immature wound healing at and around the hernia defect site.[84, 93] During skeletal muscle wound healing, satellite cells become activated and migrate to the defect site where they begin to proliferate. A population of these cells align with remaining myofibers and each other and fuse to form multinucleated myotubes. The myotubes then mature to become fully functional myofibers. In the event of large defects such as abdominal wall hernias however satellite cells must compete with granulation tissue and foreign body giant cells to fill the defect. With a limited number of satellite cells, fibrous scar tissue is almost always formed over skeletal muscle. When the scar tissue produced is immature or abnormal, as is seen in recurrent hernia patients, a significant difference in scar strength and overall wound strength can be observed.[93] In an effort to lower recurrence, this paper investigates the use of a degradable biomaterial scaffold to encourage skeletal muscle regeneration over scar tissue formation through gene delivery.

Skeletal muscle has been extensively studied for gene therapy applications. Many trials look to use skeletal muscle as a mechanism to continuously distribute secreted therapeutic proteins systemically for the treatment of muscular genetic diseases and ischemia as well as for DNA vaccines.[149] These studies have shown some success with the biggest hurdles being low transfection efficiency and only localized protein production. While these hurdles hinder gene therapy for traditional

pathologies they can be overcome or used as an advantage in abdominal wall hernia repair. Transfection efficiency was found to increase in regenerating muscle as opposed to uninjured muscle for a week after transfection.[150] These results indicate a more effective short term administration of the gene of interest which could be applied during the healing of an abdominal wall defect and in the case of abdominal wall hernia repair, localized transfection and protein production is ideal. With the optimum gene and delivery system in place, skeletal muscle regeneration within abdominal wall defects could be realized.

The studies presented here investigate the use of scaffolds fabricated from EHD monomers as a release mechanism for the delivery of a therapeutic plasmid containing an insulin-like growth factor 1 green fluorescent protein fusion gene (IGF-1 GFP). To this end, different scaffold architectures were fabricated and the release curves and plasmid viability were recorded. IGF-1 was chosen as the gene of interest as it has been shown that IGF-1 functions as both autocrine and paracrine signals that effect skeletal muscle growth and development.[133-135] More specifically, IGF-1 binds to activated satellite cells and increases both cell proliferation and differentiation.[135-137] Increasing IGF-1 levels in skeletal muscle also leads to an increase in both DNA and protein content within the target muscle.[136] Therefore, IGF-1 may be critical to activating and guiding satellite cell behavior in skeletal muscle regeneration.[135]

Materials and Methods

Materials

Benzoyl peroxide (BP), N,N-dimethyl-p-toluidine (DMT), 5-ethyl-5-(hydroxymethyl)-β,β-dimethyl-1,3-dioxane-2-ethanol diacrylate (EHD), isobutyraldehyde, formaldehyde (37% aqueous solution), trimethylolpropane, triethylamine, hydroquinone, acryloyl chloride, ammonium persulfate (APS), N,N,N',N'-tetramethylethylenediamine (TEMED), PEG diacrylate (PEGDA), agar and LB media were obtained from Sigma-Aldrich (Milwaukee, WI, USA). Reagent grade acetone, potassium carbonate, sodium sulfate, ethyl ether, silica gel (60-200 mesh) and sodium chloride (salt) were purchased from Fisher Scientific (Pittsburg, PA, USA). Lipofectin Transfection Reagent, Opti-MEM I Reduced Serum Media (OM), Vivid Colors™ pcDNA™ 6.2/C-EmGFP-GW/TOPO® Mammalian Expression Vector, One Shot® TOP10 chemically competent E. coli, Lipofectamine 2000 Transfection Reagent were received from Invitrogen (Carlsbad, CA, USA). FuGENE Transfection Reagent was purchased from Roche Applied Science (Indianapolis, IN, USA). Human skeletal muscle myoblasts, skeletal muscle cell growth media and BulletKit, trypsin/EDTA and trypsin neutralization solution were obtained from Lonza (Walkersville, MD, USA).

5-ethyl-5-(hydroxymethyl)-β,β-dimethyl-1,3-dioxane-2-ethanol diacrylate Synthesis

EHD was synthesized based on the protocols described by Kaihara et al. Potassium carbonate (18.9 g, 0.25 equiv) was added to isobutyraldehyde (50 ml, 1

equiv) and formaldehyde (37% aqueous solution, 40.8 ml, 1 equiv) and the solution was stirred at 0°C overnight. The product 3-hydroxy-2,2-dimethylpropinaldehyde (HDP) was extracted three times with chloroform and then washed with water and brine. The chloroform layers were combined and dried with sodium sulfate and the solvent was evaporated under reduced pressure to obtain solid HDP. HDP (32.9 g, 1 equiv) and trimethylolpropane (86.6 g, 2 equiv) were dissolved in 1 M hydrochloric acid (200 ml) and stirred for 2 h at 80°C. The solution was then neutralized with sodium hydroxide and the product 5-ethyl-5-(hydroxymethyl)-*β*,*β*-dimethyl-1,3-dioxane-2-ethanol (HEHD) was extracted three times with chloroform and washed with water and brine. The chloroform layers were combined and again dried with sodium sulfate and evaporated under reduced pressure to obtain solid HEHD. The HEHD was purified using an ethyl ether wash to remove undesired byproducts and was dried under reduced pressure. HEHD (31.3 g, 1 equiv) was dissolved in chloroform and triethylamine (65.4 ml, 3 equiv) and hydroquinone (0.034 g, 0.002equiv) were added. Acryloyl chloride (38.1 ml, 3 equiv) was added dropwise as the reaction was stirred at 0°C for 2 h. The insoluble salts were removed through filtration and the product, 5-ethyl-5-(hydroxymethyl)-*β*,*β*-dimethyl-1,3-dioxane-2-ethanol diacrylate (EHD), was extracted three times with chloroform and washed with water and brine. The chloroform layers were combined and dried with sodium sulfate and evaporated under reduced pressure. The EHD was further purified by silica gel column chromatography using a chloroform/ethanol (10:1, v/v) as the eluent. The fractions that contained EHD were determined by thin layer chromatography and NMR.

Slurry Formed Porous EH Monolayer Formation

Slurry former porous EH networks (SLRY EH monolayers) were fabricated using a porogen leaching strategy. To begin, a glass mold was fabricated by attaching capillary tubes to a glass plate creating a 1 mm thick well. BP was added to acetone to create a 0.58 M solution. 2 g of EHD monomer was then mixed with 0.75 mL of BP solution and 1 μL of DMT. This mixture was quickly added to the salt, vortexed and spread into the mold. The network was covered with a second plate and placed in an oven at 30°C until it was gelled. The resulting networks contained 75 wt% salt. The sheet was removed from the mold and placed into DI water for 72 h and the water was changed ever 24 h. The resulting porous sheets were cut into circles with a diameter of 2 cm.

Solution Formed Porous EH Monolayer Formation

Solution formed porous EH networks (SOLN EH monolayers) were made using a leachable porogen strategy. 7 × 4.3 cm rectangular cavities were cut out of 1.4 mm thick plastic sheets in order to form frames. A glass plate was placed under the frames to form a well, which was filled with 7.8 g of salt. Salt was wetted with 2.445 mL 85% acetone and spread with another glass plate to fill the frame. Salt-filled frames were dried on an 85 °C hot plate for 1 h in order to produce an interconnected salt network that was attached to the plastic frame. The salt-filled frame was allowed to cool 10 min before removal from the glass plate.

The mass of the salt network was measured to determine the amount of polymer solution required to achieve the desired porosities of 75 and 80 wt% salt.

Active EHD solution was prepared by mixing each gram of EHD with 375 μL of 0.826 M BP in acetone and 8 μL DMT. The salt-filled frame was suspended over a weighing dish such that the salt network was solely supported by the frame and active EHD solution was delivered drop wise onto the salt cake.

The frame was then placed in a 60°C oven for 20 min to promote polymer gelling. Once gelled, the SOLN EH monolayer was transferred to DI water to leach out salt. After 20 min the networks were removed from the frame to prevent cracking and the salt was leached out for 48 h with a water change at 24 h.

EH-PEG Bilayer Production

SOLN EH monolayers were made as described above. Networks were removed from the water after 48 h and dried overnight on a paper towel. 20 mM solutions of the water soluble radical initiators ammonium persulfate (APS) and N,N,N',N'-tetramethylethylenediamine (TEMED) were made as well as a 30% solution of PEG diacrylate (PEGDA) in 5% acetone. As was done in the solid networks, two stacks of three coverslips were placed on a glass plate to control the thickness of the PEGDA layer on the EH network. After combining the PEGDA, APS, and TEMED the solution was vortexed and poured quickly in between the coverslips. The dried SOLN EH monolayer was placed on top of the coverslips and the PEGDA was allowed to crosslink with the network. After the PEGDA was gelled the network was removed from the plate and the excess PEG was removed. The bilayers could then be cut into any shape desired.

Scanning Electron Microscopy

To obtain SEM images, networks were fabricated as mentioned above. The samples were positioned to expose both the top surface and cross section of each scaffold and were coated with gold before imaging. Images were obtained using a Hitachi Field Emission Scanning Electron Microscope fitted with an X-Ray Analysis System.

Single Gene Lipoplex Formation

Single gene lipoplexes (SG lipoplexes) were formed using a GFP plasmid supplied from Dr. Pandit's lab as well as Lipofectin Transfection Reagent at a ratio of 1:7 using the standard protocols. Briefly, Lipofectin and DNA were each diluted into 100 μL of Opti-MEM I Reduced Serum Media (OM) and allowed to sit for approximately 30 min. The DNA solution was then added to the diluted Lipofectin and mixed gently. The complexes were then incubated at room temperature for an additional 10 min before use.

Dose Dependent SG Lipoplex Release from SLRY EH Monolayers

Porous EH networks were formed as mentioned above. Before seeding the networks were washed three times for 15 min each with PBS, acetone, PBS again. The networks were placed on a paper towel to remove any PBS. They were then pre-wetted and sterilized using the following protocol. The networks were put in a falcon tube of 100% ethanol and placed under vacuum. Once the air was removed and the

pores were filled, the networks were allowed to soak for 20 min during which time there were moved into a biosafety hood to maintain sterility. The ethanol was then replaced with PBS over a series of five 20 min washes. The networks were placed in a 12 well plate and the 200 μL SG lipoplex solution was added to the top surface of the network. The solution was allowed to fill the pores undisturbed in an incubator at 37°C and 5% CO_2 for 4 h after which time any displaced PBS was collected for loading efficiency calculations. 1 mL of PBS was added to completely submerge each network and the media was collected and replaced at each time point.

IGF-1 GFP Fusion Plasmid Construction

To produce the IGF-1 GFP fusion plasmid, RNA was isolated from human skeletal muscle myoblasts (hSkMMs). cDNA was created using reverse transcription and the IGF-1 gene was amplified by performing a polymerase chain reaction (PCR). The PCR product was then purified though agarose gel electrophoresis and the desired cDNA was removed from the gel. This product was mixed with the Vivid Colors™ pcDNA™ 6.2/C-EmGFP-GW/TOPO® Mammalian Expression Vector and then used to transform One Shot® TOP10 chemically competent E. Coli. The cells were spread onto agar plates containing 100 μg/mL of ampicillin and were left in the incubator at 37°C for 12-14 h at which time they were moved to 4°C for storage. Colonies were chosen from the plates and grown in LB media containing 100 μg/mL of ampicillin for 12-16 h. Using a Promega Endotoxin Free Midi Prep Kit the plasmid was harvested from the cells and concentration was determined using the NanoDrop spectrophotometer. To ensure proper insertion of the PCR product into

the TOPO vector, the inserted product was again amplified using PCR and purified using gel electrophoresis. The sample was then sent to DNA sequencing as another check.

Fusion Gene Complex Formation

Fusion gene complexes (FG complexes) were formed using the FuGENE Transfection Reagent. DNA was diluted in OM to a concentration of 2 ng/μL. FuGENE was then added to the solution at a ratio of 6:2 (FuGENE(μL):DNA(μg)) and mixed gently. The solution was incubated at room temperature for 15 min before use.

Fusion Gene Lipoplex Formation

Fusion gene lipoplexes (FG lipoplexes) were formed using the Lipofectamine 2000 Transfection Reagent. Desired amount of DNA was diluted in 50 μL of OM and Lipofectamine 2000 was diluted in 50 μL of OM in a ratio of 6:2 (Lipofectamine 2000:DNA). After a 5 min incubation at room temperature the DNA was added to the Lipofectamine 2000 and the lipoplexes were incubated at room temperature for an additional 20 min before use.

Transfection Efficiency and Dose Dependence

To test the transfection efficiency and dose dependence of the plasmid hSkMMs were cultured to passage 4 and then seeded in a 24 well plate at a density of

60,000 cells per well (approximately 80-90% confluence). After 24 h the media was changed to OM and either lipoplexes, complexes or nothing were added to the media of the wells at concentrations of 0.5, 1 and 5 μg of plasmid DNA per well. The media was replaced 5 h and 24 h after transfection. 46 h after transfection and 22 h after the media change the media was collected and a Quantikine ELISA assay (R&D Systems, Minneapolis, MN) was performed.

Architecture Guided FG Complex Release

SOLN EH monolayers and EH-PEG bilayers with two different porosities were formed as mentioned above. Before seeding the networks they were pre-wetted and sterilized as explained in the dose dependent SG Lipoplex release study. The networks were then placed in a 12 well plate and the complex solution was added to the top surface of the network. The solution was allowed to fill the pores and any displaced PBS was collected for loading efficiency calculations. 1.4 mL of PBS was added to completely submerge each network and 400 μL of PBS was removed at each time point and replaced with fresh PBS to maintain a constant volume. Picogreen was then used to determine the concentration of the released DNA.

Statistical Analysis

Statistical analysis was performed on all data using analysis of variance (ANOVA) and Tukey's multiple comparison tests.

Results

The objective of this work was to investigate the use porous SLRY and SOLN EH monolayer scaffolds as plasmid delivery devices for abdominal wall hernia repair. To this end, plasmid release was measured as a function of scaffold architecture. Initially, the architecture of both the SLRY EH monolayers and the SOLN EH monolayers was characterized. The dose based SG lipoplex release was measured for plasmids that produced a single reporter gene, GFP. In an effort to test the scaffolds utility as a functional release device, plasmids that produced IGF-1 GFP fusion proteins were constructed and plasmid performance was evaluated. Finally, a release study was performed to test the effect of scaffold architecture on FG complex release rate.

In this study, SLRY EH monolayers were made using the glass plate system described above. Samples were collected and photographed to visualize both the macroscopic structure (Figure 1A) and the microscopic structure (Figures 1B, C and D) as described in the methods. The top surface in Figure 1A and 1B shows that there are few pores on the outer surfaces. However, Figures 1C and 1D show that the pores are located throughout the scaffold and are cubic in shape.

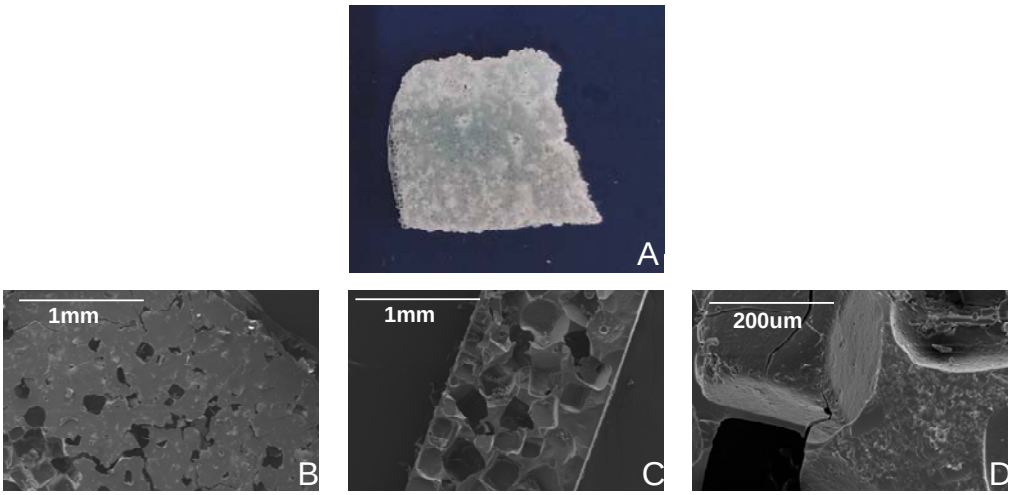

Figure 7. 1: (A) Image of a 75 wt% porous SLRY EH monolayer. (B) SEM image of the surface of a 75 wt% SLRY EH monolayer. (C) SEM image of the cross section of a 75 wt% SLRY EH monolayer. (D) Higher magnification SEM image of pores in a 75 wt% SLRY EH monolayer.

In addition, porous SOLN EH monolayers were fabricated using the frame method described previously and the scaffolds were imaged to qualitatively show the changes in architecture from the previous scaffolds. Figure 2A shows a highly porous surface, so much so that the architecture could be observed under 10x magnifications with a Zeiss Inverted Microscope (Figure 2B). In addition, Figures 2C-E showed that the pores were more evenly distributed throughout the scaffold and that the pores were more spherical in shape.

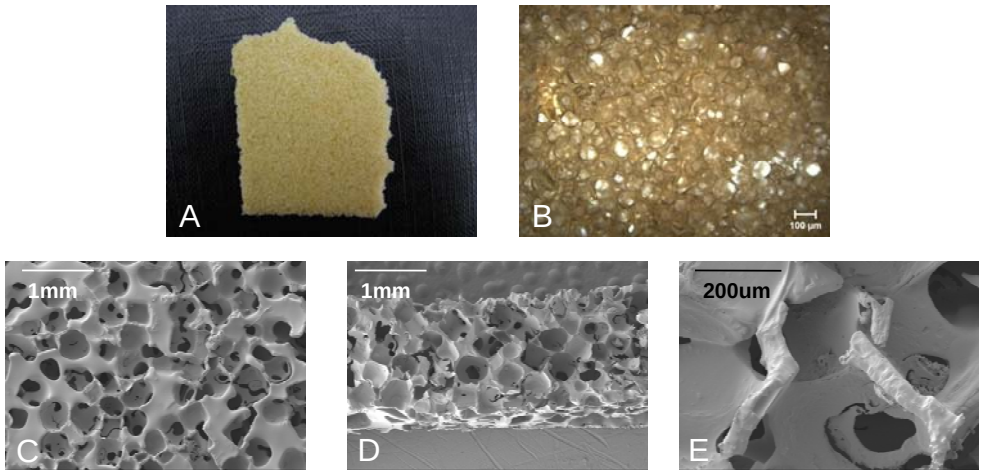

Figure 7. 2: (A) Image of an 80 wt% SOLN EH monolayer. (B) 10x magnification of an 80 wt% SOLN EH monolayer. (C) SEM image of the surface of an 80 wt% SOLN EH monolayer. (D) SEM image of the cross section of an 80 wt% SOLN EH monolayer. (E) Higher magnification SEM image of a single pore in an 80 wt% SOLN EH monolayer.

To determine dose based release profiles of SG lipoplexes from SLRY EH monolayers, three different concentrations of SG lipoplexes were released from the network over 24 h. Figure 3 shows that the lipoplexes exhibit an initial burst release for the first hour. From 1 to 24 h the plasmid concentration continued to increase but at a much slower rate than during the first hour. In addition, it was shown that while the loading efficiency was 98.6 ± 0.1 % or greater only 4.6 ± 0.1 % of the originally loaded plasmid was released at maximum. The 25 µg loading group released the most plasmid with 444.0 ± 0.7 ng being released at 24 h. The 10 µg and 5 µg loading groups each released 351.0 ± 16.6 ng and 226.1 ± 11.5 ng respectively. The 25 µg and 10 µg loading groups were statistically higher than the 5 µg loading groups at all

time points. They were not statistically different from each other until the 2 h time point.

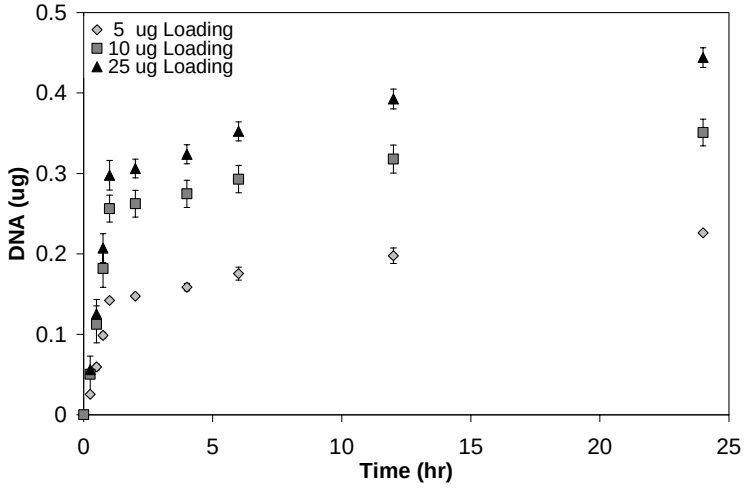

Figure 7. 3: Total SG plasmid DNA released from a 75 wt% porous SLRY EH monolayer. The 25 µg loading group released the most plasmid at 24 h followed by the 10 µg and 5 µg loading groups respectively. The 25 µg and 10 µg loading groups were statistically higher than the 5 µg loading groups at all time points. They were not statistically different from each other until the 2 h time point.

In an effort to create a more functional protein, plasmid DNA was created that fuses IGF-1 to emGFP. To test the plasmids utility and dose dependent transfection FG complexes and FG lipoplexes were added to hSkMMs at different concentrations. 46 h after transfection the change in IGF-1 concentrations in the supernatant was measured via an ELISA assay. Figures 4A-C show the GFP production within cells transfected with FG complexes. Figures 4A and 4B show expression in wells that were seeded at a density of 20,000 and 40,000 cells/well respectively whereas figure 4C shows transfection in fused myoblasts. Figure 4D shows that IGF-1 production is

only affected slightly by plasmid dose with a statistically higher amount of protein being produced with the highest concentration of FG complexes.

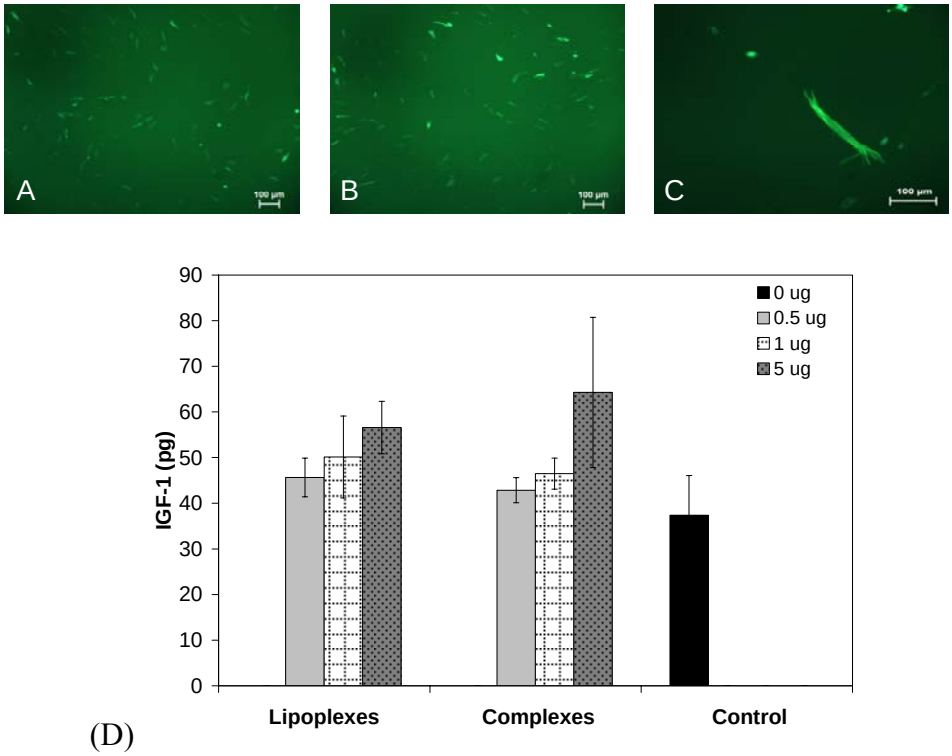

Figure 7. 4: (A) GFP expression within hSkMMs seeded at a density of 20,000 cells/well. (B) GFP expression within hSkMMs seeded at a density of 40,000 cells/well. (C) GFP expression within fused hSkMMs in culture. (D) Amount of IGF-1 produced from transfected hSkMMs. The general trend shows that there is a slight dose response over the DNA range used. In addition the lipoplexes and the complexes performed similarly at all doses. The 5 µg FuGENE complex group was statistically higher than the control group.

To determine the effects of architecture on plasmid release rate both SOLN EH monolayers and EH-PEG bilayers were fabricated. Complexes were loaded onto the different scaffolds and DNA concentration in the supernatant was measured over 24 h. Figure 5 shows that the release profile was similar to previous study with a burst release over the first hour which levels off to 24 h. Overall all groups

performed similarly however general trends show that the 75 wt% SOLN EH monolayer released more complex over 24 h than its less porous counterpart. In addition, the bilayers retained more complex than the monolayers of the same porosity for the first 2 h. The 75 wt% EH-PEG bilayers continued to release more than its monolayer counterpart, however the 80 wt% monolayer released more than the EH-PEG bilayer after 2 h.

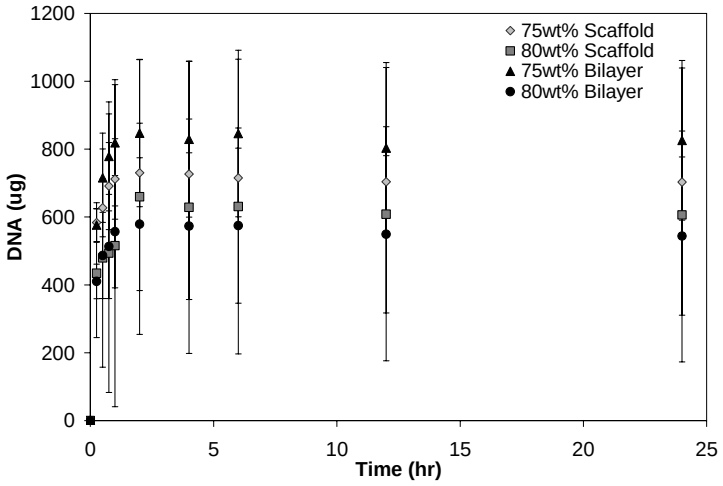

Figure 7. 5: Total IGF-1 GFP plasmid release from SOLN EH monolayers and bilayers. Trends showed that 80 wt% SOLN EH monolayers released more plasmid than the 75 wt% SOLN EH monolayers. It was also observed that the porous bilayers released more plasmid than their monolayer counterparts.

Discussion

This work seeks to develop an EH scaffold for the release of IGF-1 GFP fusion plasmids for abdominal wall hernia repair. Previous work has focused on the mechanical properties and biocompatibility of the EH scaffolds. It was found that solid EH networks had a modulus approximately 100 fold greater than that of skeletal

muscle and that these scaffolds could release active IGF-1 over a 48 h period of time.[59] In addition, by changing the scaffold architecture it was found the modulus of the scaffolds could be decreased by an order of magnitude. To further this work it was hypothesized that IGF-1 could be delivered more effectively using a porous scaffold. Networks were fabricated using a porogen leaching strategy and SEM photos were taken after the porogen was leached to qualitatively determine pore interconnectivity and distribution (Figures 1 and 2). Interconnectivity was also established quantitatively by monitoring the mass lost during leaching. It was found that the 75 wt% and 80 wt% SLRY EH monolayers lost 62.09 ± 8.29 % and 66.57 ± 11.9 % of their overall mass respectively (Table 1). This demonstrates that the pores are not completely interconnected and it is evident in Figures 1B and 1C that there are few pores on the top surfaces of the network. In addition, it can be seen that the pores are not evenly distributed throughout the cross-section of the scaffold. This is an artifact of the fabrication technique where the porogen settles to the bottom of the glass mold before the scaffold is fully gelled.

To increase the pore distribution of the scaffolds however, the glass plate system was abandoned and salt frames were made to maintain porous surfaces. As can be seen in Figure 2, SOLN EH monolayers were fabricated where the number of pores exposed at the surface as well as throughout the cross section was increased. In addition, Table 1 shows that 80 wt% SOLN EH monolayers lost 86.67 ± 0.635 % of their overall mass after 48 h. A greater amount of mass was lost than porogen was added in these samples. It is speculated that this is due to the removal of unreacted monomers and initiator during leaching. The SLRY EH monolayers required

additional washing steps to remove these components. This increase in pore interconnectivity was also observed during the following gene delivery studies both in the loading and release of the plasmid complexes.

Fabrication Technique	wt% NaCL Added During Scaffold Fabrication	Pecent Mass Lost During Leaching
SLRY	75	62.09 ± 8.29%
	80	66.57 ± 11.9%
SOLN	80	86.87 ± 0.63%

Table 7.1: The percent mass lost during leaching for two different SLRY and a SOLN EH monolayer. It was found that the SOLN fabrication technique produced scaffolds with higher pore interconnectivity than the SLRY fabrication technique.

In an effort to further alter the scaffold architecture and create a more functional scaffold for hernia repair, one side of the porous scaffolds was coated with a layer of PEG. Adhesions of the abdominal viscera to the abdominal defect area are a common clinical setback in prosthetic mesh placement.[103, 104, 118, 130, 131] By adding a PEG layer to this scaffold the dual benefit of blocking the pores on one surface of the network and creating an adhesion barrier for the scaffold is achieved.

To advance the protein delivery aspect of the previous work, gene delivery was investigated. Gene delivery is a promising technique in producing therapeutic proteins within skeletal muscle.[149] These initial studies were carried out with a GFP reporter plasmid complexed with a liposomal carrier. This SG lipoplex was chosen over naked DNA due to the known difficulty of transfecting primary skeletal myoblasts. Results showed that the plasmid was released in a burst release for the first hour as expected. Continued release of the plasmid was observed at a steady but

much slower rate over the next 23 h. During this study the plasmid concentration did not plateau. It was found that the 10 and 25 μg loading groups released significantly more plasmid than the 5 μg loading group over all time points. By 24 h however all group were statistically different with the 25 μg loading group releasing 444.0 ± 0.7 ng, the 10 μg loading group releasing 351.0 ± 16.6 ng and the 5 μg loading group releasing 226.1 ± 11.5 ng. This corresponds to 1.8, 3.5 and 4.6 % of the initially loaded plasmid respectively for each group. It is hypothesized that due to the limited pore distribution and presence of so few pores on the surface of the networks that once complexes entered the network, they became trapped within the pores. This is evident through the continual and gradual increase of plasmid release rate with no plateau reached during the 24 h. In an effort to expand upon these results and obtain a higher release percentage over 24 h the effect of scaffold architecture on FG complex release was studied.

To produce a therapeutic protein, an IGF-1 GFP fusion plasmid was constructed and released from the networks. Transfection studies were performed with human skeletal muscle myoblasts (hSkMMs) to test the utility and transfection ability of both the FG complexes and FG lipoplexes. Both GFP production and IGF-1 production were observed using fluorescent microscopy and ELISA assays. Figures 4A-C show cells transfected with FG complexes were Figure 4D shows the amount of IGF-1 produced over a 22 h incubation period. Overall, the FG lipoplexes and FG complexes performed equally. There is a slight trend of increasing IGF-1 as plasmid dose increases. The only group that was statistically higher than the control however was the 5 μg plasmid loading group. While this is a large amount of DNA to provide

to the cells, primary cells are notoriously hard to transfect. Overall, the production of both GFP and IGF-1 confirm that the plasmid was functional.

Finally, to test the delivery capabilities of the SOLN EH monolayer and bilayer scaffolds, release studies were performed. While there were no statistical differences after 24 h, obvious trends were evident in the data. The 75 wt% EH-PEG bilayers released the most plasmid followed by its monolayer counterpart. From the results achieved in the previous SG lipoplex study this was expected as more plasmid would be trapped within the network with fewer pores on the surface to leach out from. In addition, by blocking the pores with the PEG hydrogel layer more plasmid can be retained in the network during initial loading. A similar trend was exhibited by the 80 wt% SOLN EH monolayers and bilayers during the first 2 h of release. After this point, the bilayer release leveled off and the monolayers release more complexes. Due to the high interconnectivity of these scaffolds as well as the hydrophobicity of the polymer EH, loading efficiencies were reduced to approximately 87 % and 70 % in the 75 wt% scaffolds and 80 wt% scaffolds respectively. Therefore the loading efficiency is hypothesized to be a significant factor in the overall release rate.

These results demonstrate promise for the use of porous EH scaffolds as a gene delivery vehicle. It has been shown that the release of plasmid complexes and lipoplexes can be altered based on varying scaffold architecture. By tailoring the architecture of the scaffold to hold the desired quantity of plasmid complexes or lipoplexes one can effectively alter the complex release time and dose. Future directions involve the addition of hSkMMs to these loaded networks to determine cell

behavior in the presence of SOLN EH monolayer and EH-PEG bilayer scaffolds as well as evaluating this scaffold *in vivo* as a therapeutic gene delivery device for hernia repair.

Conclusions

This work seeks to further advance the use of EH cyclic acetal biomaterials as an abdominal wall hernia repair device. The effect of scaffold architecture on the release of plasmid lipoplexes and complexes was evaluated. Results showed that by altering the porosity of the scaffolds, especially at the surface of the network, the release of plasmids over time could be altered. More specifically, it was shown that having highly porous network surfaces provided fast loading and lower retention than those networks with blocked pores or fewer surface pores. In addition, a therapeutic plasmid was constructed to deliver an IGF-1 GFP fusion gene to hSkMMs. When combined, these results saw a promising tunable delivery method for gene delivery to the abdominal wall skeletal muscle.

Acknowledgments

This work was supported by the National Science Foundation through a CAREER Award to JPF (#0448684) as well as the Maryland NanoCenter and its NispLab. The NispLab is supported in part by the NSF and as a MRSEC Shared Experimental Facility. The authors would like to acknowledge the help of Joshua Chetta and the gift of Lipofectamine 2000 transfection reagent from the lab of Dr.

Sameer Shah at the University of Maryland as well as the gift of ampicillin from the lab of Dr. Adam Hsieh at the University of Maryland. We would also like to thank Chen-Yu Tsao, Chi-Wei Hung and Hsuan-Chen Wu from the lab of Dr. William Bentley at the University of Maryland for their contributions.

Chapter 8: Summary

Synthetic biomaterials are widely used in clinical application. As technology advances, these materials are being tailored to suit many tissue engineering and drug delivery needs. Currently however, their efficacy is limited as many materials are not biologically inert. In an effort to develop alternative materials, extensive research is being done to synthesize polymers with more biological functionality. Cyclic acetals are an increasingly versatile group of materials used for both soft and hard tissue repair. They have been demonstrated to show a varying range of mechanical, chemical and biological properties both *in vitro* and *in vivo*. Therefore this material was chosen to investigate skeletal muscle regeneration within an abdominal wall hernia.

Despite various attempts to lower both primary hernia occurrence and recurrence an ideal solution has not been found. Currently technologies aim to patch the defect without fully addressing the underlying cause of the problem, imperfect wound healing. There has been little success, therefore a tissue engineering strategy was employed to aid in skeletal muscle regeneration as oppose to scar tissue formation.

First, the mechanical and biological compatibility of the EH networks was investigated. In particular solid EH networks were fabricated and mechanical properties, cellular attachment and IGF-1 protein release and viability were tested. Results showed that the mechanical properties of the networks could be altered by increasing the initiator concentration during fabrication. The mechanical strength of

these networks was approximately 100 fold greater than that of native skeletal muscle. In addition, these networks were able to maintain a proliferating rat myoblast population and release active IGF-1 from their surface. Overall, this work showed the utility and biofunctionality of a cyclic acetal biomaterial made from EHD.

Next, in an effort to make networks with more relevant mechanical properties and to characterize its chemical properties, scaffolds with different architectures were fabricated. The effect of this change on the scaffold's degradation properties as well as the Young's modulus and flexural strength were evaluated. Results showed that by adding pores to the solid EH networks from the previous work that mass lost during degradation could be greatly increased. In addition, by adding a layer of PEG to these monolayers during fabrication, the mass lost during degradation could be counteracted. Mechanical testing showed that adding this layer of PEG, as well as increasing overall scaffold porosity can significantly decrease the stiffness of the scaffold. The strength however was found to remain the same as it was shown that the EH layer provides the majority of the strength to the scaffolds. Overall, this work demonstrated the effect of changing scaffold architecture on the physical and mechanical properties of EH scaffolds.

Last, the utility of the previously made EH scaffolds as a gene delivery device was evaluated. More specifically, the effect of scaffold architecture on the release of plasmid lipoplexes and complexes was determined. Results showed that by creating scaffolds with highly dispersed and interconnected pores, that the release of SG lipoplexes and FG complexes could be altered. The biggest effects on release were due to the changes in surface architecture and pore interconnectivity of the networks.

To further the functionality of the scaffold, a therapeutic plasmid that produces IGF-1 GFP fusion proteins was constructed. hSkMMs were transfected with this plasmid and functionality was demonstrated using fluorescent microscopy and ELISA.

Overall, this project shows the biocompatibility of the cyclic acetal based EH scaffold as well as the effects of scaffold architecture on physical, mechanical and biological properties. Through further optimization of the surface and bulk architecture of these scaffolds, a gene delivery device can be fabricated to aid and guide in the skeletal muscle regeneration within an abdominal wall hernia defect.

References

1. Delie, F. and M.J. Blanco-Prieto, *Polymeric particulates to improve oral bioavailability of peptide drugs.* Molecules, 2005. **10**(1): p. 65-80.
2. Hoffman, A.S., *"Intelligent" polymers in medicine and biotechnology.* Artif Organs, 1995. **19**(5): p. 458-67.
3. Galaev, I.Y. and B. Mattiasson, *'Smart' polymers and what they could do in biotechnology and medicine.* Trends Biotechnol, 1999. **17**(8): p. 335-40.
4. De Laporte, L. and L.D. Shea, *Matrices and scaffolds for DNA delivery in tissue engineering.* Adv Drug Deliv Rev, 2007. **59**(4-5): p. 292-307.
5. Harrison, B.S., et al., *Oxygen producing biomaterials for tissue regeneration.* Biomaterials, 2007. **28**(31): p. 4628-34.
6. Nakabayashi, N., *Dental biomaterials and the healing of dental tissue.* Biomaterials, 2003. **24**(13): p. 2437-9.
7. Huang, Y.C. and Y.Y. Huang, *Biomaterials and strategies for nerve regeneration.* Artif Organs, 2006. **30**(7): p. 514-22.
8. Patel, M. and J.P. Fisher, *Biomaterial Scaffolds in Pediatric Tissue Engineering.* Pediatr Res, 2008.
9. Raghunath, J., et al., *Biomaterials and scaffold design: key to tissue-engineering cartilage.* Biotechnol Appl Biochem, 2007. **46**(Pt 2): p. 73-84.
10. Lendlein, A., K. Kratz, and S. Kelch, *Smart implant materials.* Med Device Technol, 2005. **16**(3): p. 12-4.
11. Sachlos, E. and J.T. Czernuszka, *Making tissue engineering scaffolds work. Review: the application of solid freeform fabrication technology to the production of tissue engineering scaffolds.* Eur Cell Mater, 2003. **5**: p. 29-39; discussion 39-40.
12. An, Y.H., S.K. Woolf, and R.J. Friedman, *Pre-clinical in vivo evaluation of orthopaedic bioabsorbable devices.* Biomaterials, 2000. **21**(24): p. 2635-52.
13. Cohen, S.R., et al., *Clinical experience with a new fast-resorbing polymer for bone stabilization in craniofacial surgery.* J Craniofac Surg, 2006. **17**(1): p. 40-3.
14. Brandl, F., F. Sommer, and A. Goepferich, *Rational design of hydrogels for tissue engineering: impact of physical factors on cell behavior.* Biomaterials, 2007. **28**(2): p. 134-46.
15. Allen, C., et al., *Controlling the physical behavior and biological performance of liposome formulations through use of surface grafted poly(ethylene glycol).* Biosci Rep, 2002. **22**(2): p. 225-50.
16. Bohner, M., *Physical and chemical aspects of calcium phosphates used in spinal surgery.* Eur Spine J, 2001. **10 Suppl 2**: p. S114-21.
17. Haag, R. and F. Kratz, *Polymer therapeutics: concepts and applications.* Angew Chem Int Ed Engl, 2006. **45**(8): p. 1198-215.
18. Stayton, P.S., et al., *Control of protein-ligand recognition using a stimuli-responsive polymer.* Nature, 1995. **378**(6556): p. 472-4.

19. Cascone, M.G., B. Sim, and S. Downes, *Blends of synthetic and natural polymers as drug delivery systems for growth hormone.* Biomaterials, 1995. **16**(7): p. 569-74.
20. Stenzl, A. and K.D. Sievert, *A quantitative method for evaluating the degradation of biologic scaffold materials.* Int Braz J Urol, 2007. **33**(6): p. 871-2.
21. Gilbert, T.W., A.M. Stewart-Akers, and S.F. Badylak, *A quantitative method for evaluating the degradation of biologic scaffold materials.* Biomaterials, 2007. **28**(2): p. 147-50.
22. Moreau, J.L., D. Kesselman, and J.P. Fisher, *Synthesis and properties of cyclic acetal biomaterials.* J Biomed Mater Res A, 2006.
23. Schacht, E., et al., *Polyacetal and poly(ortho ester)-poly(ethylene glycol) graft copolymer thermogels: preparation, hydrolysis and FITC-BSA release studies.* J Control Release, 2006. **116**(2): p. 219-25.
24. Heffernan, M.J. and N. Murthy, *Polyketal nanoparticles: a new pH-sensitive biodegradable drug delivery vehicle.* Bioconjug Chem, 2005. **16**(6): p. 1340-2.
25. Kaihara, S., et al., *Synthesis of poly(L-lactide) and polyglycolide by ring-opening polymerization.* Nat Protoc, 2007. **2**(11): p. 2767-71.
26. Gunatillake, P.A. and R. Adhikari, *Biodegradable synthetic polymers for tissue engineering.* Eur Cell Mater, 2003. **5**: p. 1-16; discussion 16.
27. Middleton, J.C. and A.J. Tipton, *Synthetic biodegradable polymers as orthopedic devices.* Biomaterials, 2000. **21**(23): p. 2335-46.
28. Taylor, M.S., et al., *Six bioabsorbable polymers: in vitro acute toxicity of accumulated degradation products.* J Appl Biomater, 1994. **5**(2): p. 151-7.
29. Lam, K.H., et al., *The effect of phagocytosis of poly(L-lactic acid) fragments on cellular morphology and viability.* J Biomed Mater Res, 1993. **27**(12): p. 1569-77.
30. Periti, P., T. Mazzei, and E. Mini, *Clinical pharmacokinetics of depot leuprorelin.* Clin Pharmacokinet, 2002. **41**(7): p. 485-504.
31. Takada, S. and Y. Ogawa, *[Design and development of controlled release of drugs from injectable microcapsules]*. Nippon Rinsho, 1998. **56**(3): p. 675-9.
32. Sartor, O., et al., *An eight-month clinical study of LA-2575 30.0 mg: a new 4-month, subcutaneous delivery system for leuprolide acetate in the treatment of prostate cancer.* Urology, 2003. **62**(2): p. 319-23.
33. Sinha, V.R., et al., *Poly-epsilon-caprolactone microspheres and nanospheres: an overview.* Int J Pharm, 2004. **278**(1): p. 1-23.
34. Al Malyan, M., et al., *Polymer-based biodegradable drug delivery systems in pain management.* J Craniofac Surg, 2006. **17**(2): p. 302-13.
35. Bramfeldt, H., P. Sarazin, and P. Vermette, *Characterization, degradation, and mechanical strength of poly(D,L-lactide-co-epsilon-caprolactone)-poly(ethylene glycol)-poly(D,L-lactide-co-epsilon-caprolactone).* J Biomed Mater Res A, 2007. **83**(2): p. 503-11.
36. Kim, T.G., D.S. Lee, and T.G. Park, *Controlled protein release from electrospun biodegradable fiber mesh composed of poly(epsilon-*

caprolactone) and poly(ethylene oxide). Int J Pharm, 2007. **338**(1-2): p. 276-83.
37. Mundargi, R.C., et al., *Development and evaluation of novel biodegradable microspheres based on poly(d,l-lactide-co-glycolide) and poly(epsilon-caprolactone) for controlled delivery of doxycycline in the treatment of human periodontal pocket: in vitro and in vivo studies.* J Control Release, 2007. **119**(1): p. 59-68.
38. Poletto, F.S., et al., *Rate-modulating PHBHV/PCL microparticles containing weak acid model drugs.* Int J Pharm, 2007. **345**(1-2): p. 70-80.
39. Gunatillake, P., R. Mayadunne, and R. Adhikari, *Recent developments in biodegradable synthetic polymers.* Biotechnol Annu Rev, 2006. **12**: p. 301-47.
40. Timmer, M.D., C.G. Ambrose, and A.G. Mikos, *Evaluation of thermal- and photo-crosslinked biodegradable poly(propylene fumarate)-based networks.* J Biomed Mater Res A, 2003. **66**(4): p. 811-8.
41. Timmer, M.D., et al., *Effect of physiological temperature on the mechanical properties and network structure of biodegradable poly(propylene fumarate)-based networks.* J Biomater Sci Polym Ed, 2003. **14**(4): p. 369-82.
42. Timmer, M.D., C.G. Ambrose, and A.G. Mikos, *In vitro degradation of polymeric networks of poly(propylene fumarate) and the crosslinking macromer poly(propylene fumarate)-diacrylate.* Biomaterials, 2003. **24**(4): p. 571-7.
43. Behravesh, E., et al., *Synthetic biodegradable polymers for orthopaedic applications.* Clin Orthop Relat Res, 1999(367 Suppl): p. S118-29.
44. Shi, X., et al., *Injectable nanocomposites of single-walled carbon nanotubes and biodegradable polymers for bone tissue engineering.* Biomacromolecules, 2006. **7**(7): p. 2237-42.
45. Sitharaman, B., et al., *Injectable in situ cross-linkable nanocomposites of biodegradable polymers and carbon nanostructures for bone tissue engineering.* J Biomater Sci Polym Ed, 2007. **18**(6): p. 655-71.
46. Mistry, A.S., A.G. Mikos, and J.A. Jansen, *Degradation and biocompatibility of a poly(propylene fumarate)-based/alumoxane nanocomposite for bone tissue engineering.* J Biomed Mater Res A, 2007. **83**(4): p. 940-53.
47. Suggs, L.J., et al., *In vitro cytotoxicity and in vivo biocompatibility of poly(propylene fumarate-co-ethylene glycol) hydrogels.* J Biomed Mater Res, 1999. **46**(1): p. 22-32.
48. Katti, D.S., et al., *Toxicity, biodegradation and elimination of polyanhydrides.* Adv Drug Deliv Rev, 2002. **54**(7): p. 933-61.
49. Kumar, N., R.S. Langer, and A.J. Domb, *Polyanhydrides: an overview.* Adv Drug Deliv Rev, 2002. **54**(7): p. 889-910.
50. Burkoth, A.K. and K.S. Anseth, *A review of photocrosslinked polyanhydrides: in situ forming degradable networks.* Biomaterials, 2000. **21**(23): p. 2395-404.
51. Brem, H., et al., *The safety of interstitial chemotherapy with BCNU-loaded polymer followed by radiation therapy in the treatment of newly diagnosed malignant gliomas: phase I trial.* J Neurooncol, 1995. **26**(2): p. 111-23.

52. Uppal, P., et al., *Pharmacokinetics of etoposide delivery by a bioerodible drug carrier implanted at glaucoma surgery.* J Ocul Pharmacol, 1994. **10**(2): p. 471-9.
53. Papisov, M.I., et al., *Semisynthetic hydrophilic polyals.* Biomacromolecules, 2005. **6**(5): p. 2659-70.
54. Lam, K.H., et al., *The influence of surface morphology and wettability on the inflammatory response against poly(L-lactic acid): a semi-quantitative study with monoclonal antibodies.* J Biomed Mater Res, 1995. **29**(8): p. 929-42.
55. Schlosser, M., et al., *Antibody response to collagen after functional implantation of different polyester vascular prostheses in pigs.* J Biomed Mater Res A, 2005. **72**(3): p. 317-25.
56. Daniels, A.U., et al., *Toxicity of absorbable polymers proposed for fracture fixation devices.* Transactions of the orthopaedic research society, 1992. **17**(1): p. 88.
57. Betz, M.W., et al., *Cyclic acetal hydrogel system for bone marrow stromal cell encapsulation and osteodifferentiation.* J Biomed Mater Res A, 2008. **86**(3): p. 662-70.
58. Kaihara, S., S. Matsumura, and J.P. Fisher, *Synthesis and characterization of cyclic acetal based degradable hydrogels.* Eur J Pharm Biopharm, 2008. **68**(1): p. 67-73.
59. Falco, E.E., J.S. Roth, and J.P. Fisher, *EH Networks as a scaffold for skeletal muscle regeneration in abdominal wall hernia repair.* J Surg Res, 2008. **149**(1): p. 76-83.
60. Kaihara, S., S. Matsumura, and J.P. Fisher, *Synthesis and properties of Poly[poly(ethylene glycol)-co-cyclic acetal] based hydrogels.* Macromolecules, 2007. **40**: p. 7625-7632.
61. Betz, M.W., et al., *Tissue response and orbital floor regeneration using cyclic acetal hydrogels.* J Biomed Mater Res A, 2008.
62. Tamada, Y. and Y. Ikada, *Fibroblast growth on polymer surfaces and biosynthesis of collagen.* J Biomed Mater Res, 1994. **28**(7): p. 783-9.
63. van Wachem, P.B., et al., *Adhesion of cultured human endothelial cells onto methacrylate polymers with varying surface wettability and charge.* Biomaterials, 1987. **8**(5): p. 323-8.
64. Heller, J. and J. Barr, *Poly(ortho esters)--from concept to reality.* Biomacromolecules, 2004. **5**(5): p. 1625-32.
65. Nomura, M., S. Shuto, and A. Matsuda, *Synthesis of the cyclic and acyclic acetal derivatives of 1-(3-C-ethynyl-beta-D-ribo-pentofuranosyl)cytosine, a potent antitumor nucleoside. Design of prodrugs to be selectively activated in tumor tissues via the bio-reduction-hydrolysis mechanism.* Bioorganic & Medicinal Chemistry, 2003. **11**(11): p. 2453-2461.
66. Vicent, M.J., et al., *Polyacetal-diethylstilboestrol: a polymeric drug designed for pH-triggered activation.* J Drug Target, 2004. **12**(8): p. 491-501.
67. Lee, S., et al., *Polyketal microparticles: a new delivery vehicle for superoxide dismutase.* Bioconjug Chem, 2007. **18**(1): p. 4-7.
68. Tomlinson, R., et al., *Polyacetal-doxorubicin conjugates designed for pH-dependent degradation.* Bioconjug Chem, 2003. **14**(6): p. 1096-106.

69. Tomlinson, R., et al., *Pendent chain functionalized polyacetals that display pH-dependent degradation: A platform for the development of novel polymer therapeutics.* Macromolecules, 2002. **35**(2): p. 473-480.
70. Khaja, S.D., S. Lee, and N. Murthy, *Acid-degradable protein delivery vehicles based on metathesis chemistry.* Biomacromolecules, 2007. **8**(5): p. 1391-5.
71. Lemcoff, N.G. and B. Fuchs, *Toward novel polyacetals by transacetalation techniques: dendrimeric diacetals.* Org Lett, 2002. **4**(5): p. 731-4.
72. Gillies, E.R., T.B. Jonsson, and J.M.J. Frechet, *Stimuli-responsive supramolecular assemblies of linear-dendritic copolymers.* Journal of the American Chemical Society, 2004. **126**(38): p. 11936-11943.
73. Thompson, M.S., M.D. Northmore-Ball, and K.E. Tanner, *Tensile mechanical properties of polyacetal after one and six months' immersion in Ringer's solution.* J Mater Sci Mater Med, 2001. **12**(10-12): p. 883-7.
74. Strazar, K., A. Cor, and V. Antolic, *Biological impact of polyacetal particles on loosening of isoelastic stems.* Biomacromolecules, 2006. **7**(9): p. 2507-11.
75. Kurtz, S.M., C.L. Muhlstein, and A.A. Edidin, *Surface morphology and wear mechanisms of four clinically relevant biomaterials after hip simulator testing.* Journal of Biomedical Materials Research, 2000. **52**(3): p. 447-459.
76. Lee, K.I. and M.J. Choi, *Phase velocity and normalized broadband ultrasonic attenuation in Polyacetal cuboid bone-mimicking phantoms.* J Acoust Soc Am, 2007. **121**(6): p. EL263-9.
77. *Discharge Survey*. 1996, National Survey of Ambulatory Surgery and National Hospital.
78. *Advanced data*. 1998, Vital and health statistics of the Centers for Disease Control and Prevention.
79. *Patient information for Laparoscopic Ventral Hernia Repair*. 2004, Society of American Gastrointestinal and Endoscopic Surgeons (SAGES).
80. *Patient information for Laparoscopic Inguinal Hernia Repair*. 2004, Society of American Gastrointestinal and Endoscopic Surgeons (SAGES).
81. Kimber, D.C., *Textbook of anatomy and physiology*. 13th ed. 1955, New York: Macmillan. 183-5.
82. Mudge, M. and L.E. Hughes, *Incisional hernia: a 10 year prospective study of incidence and attitudes.* Br J Surg, 1985. **72**(1): p. 70-1.
83. Yahchouchy-Chouillard, E., et al., *Incisional hernias. I. Related risk factors.* Dig Surg, 2003. **20**(1): p. 3-9.
84. Jansen, P.L., et al., *The biology of hernia formation.* Surgery, 2004. **136**(1): p. 1-4.
85. Lindner, H.H., *Clinical Anatomy*. 1989, Norwalk, Connecticut; San Mateo, California: Appleton & Lange. 283-95.
86. Thomas, C.L. and C.W. Taber, *Taber's cyclopedic medical dictionary*, F.A. Davis Co.: Philadelphia. p. v.
87. Hinkelman, L.M., et al., *The effect of abdominal wall morphology on ultrasonic pulse distortion. Part I. Measurements.* J Acoust Soc Am, 1998. **104**(6): p. 3635-49.
88. Campion, D.R., *The muscle satellite cell: a review.* Int Rev Cytol, 1984. **87**: p. 225-51.

89. Hashimoto, N., et al., *Muscle reconstitution by muscle satellite cell descendants with stem cell-like properties.* Development, 2004. **131**(21): p. 5481-90.
90. Machida, S. and F.W. Booth, *Increased nuclear proteins in muscle satellite cells in aged animals as compared to young growing animals.* Exp Gerontol, 2004. **39**(10): p. 1521-5.
91. Holterman, C.E. and M.A. Rudnicki, *Molecular regulation of satellite cell function.* Semin Cell Dev Biol, 2005.
92. Santora, T.A. and J.J. Roslyn, *Incisional hernia.* Surg Clin North Am, 1993. **73**(3): p. 557-70.
93. Franz, M.G., *The biology of hernia formation.* Surg Clin North Am, 2008. **88**(1): p. 1-15, vii.
94. Chen, H.Y., M.H. Sheu, and L.M. Tseng, *Bicycle-handlebar hernia: a rare traumatic abdominal wall hernia.* J Chin Med Assoc, 2005. **68**(6): p. 283-5.
95. Anderson, J.M., *Biological Responses to Materials.* Annu Rev Mater Res, 2001. **31**: p. 81-110.
96. Heniford, B.T., et al., *Laparoscopic repair of ventral hernias: nine years' experience with 850 consecutive hernias.* Ann Surg, 2003. **238**(3): p. 391-9; discussion 399-400.
97. Luijendijk, R.W., et al., *A comparison of suture repair with mesh repair for incisional hernia.* N Engl J Med, 2000. **343**(6): p. 392-8.
98. Sahin, M., et al., *Comparison of prosthetic materials used for abdominal wall defects or hernias (an experimental study).* Acta Chir Hung, 1995. **35**(3-4): p. 291-5.
99. Bower, C.E., et al., *Complications of laparoscopic incisional-ventral hernia repair: the experience of a single institution.* Surg Endosc, 2004. **18**(4): p. 672-5.
100. Johnson, J., et al., *The history of open inguinal hernia repair.* Curr Surg, 2004. **61**(1): p. 49-52.
101. Roth, J.S., et al., *Current laparoscopic inguinal hernia repair.* Curr Surg, 2004. **61**(1): p. 53-6.
102. Scott, N.W., et al., *Open mesh versus non-mesh for repair of femoral and inguinal hernia.* Cochrane Database Syst Rev, 2002(4): p. CD002197.
103. Gonzalez, R., et al., *Resistance to adhesion formation: a comparative study of treated and untreated mesh products placed in the abdominal cavity.* Hernia, 2004. **8**(3): p. 213-9.
104. Borrazzo, E.C., et al., *Effect of prosthetic material on adhesion formation after laparoscopic ventral hernia repair in a porcine model.* Hernia, 2004. **8**(2): p. 108-12.
105. Badylak, S., et al., *Morphologic study of small intestinal submucosa as a body wall repair device.* J Surg Res, 2002. **103**(2): p. 190-202.
106. Badylak, S., et al., *Strength over time of a resorbable bioscaffold for body wall repair in a dog model.* J Surg Res, 2001. **99**(2): p. 282-7.
107. Rauth, T.P., et al., *A comparative analysis of expanded polytetrafluoroethylene and small intestinal submucosa--implications for patch repair in ventral herniorrhaphy.* J Surg Res, 2007. **143**(1): p. 43-9.

108. Xu, H., et al., *Host Response to Human Acellular Dermal Matrix Transplantation in a Primate Model of Abdominal Wall Repair.* Tissue Eng Part A, 2008.
109. Silverman, R.P., et al., *Ventral hernia repair using allogenic acellular dermal matrix in a swine model.* Hernia, 2004. **8**(4): p. 336-42.
110. Kolker, A.R., et al., *Multilayer reconstruction of abdominal wall defects with acellular dermal allograft (AlloDerm) and component separation.* Ann Plast Surg, 2005. **55**(1): p. 36-41; discussion 41-2.
111. Saltzman, W.M., *Tissue engineering : engineering principles for the design of replacement organs and tissues*. 2004, Oxford ; New York: Oxford University Press. xiv, 523 p.
112. Conconi, M.T., et al., *Homologous muscle acellular matrix seeded with autologous myoblasts as a tissue-engineering approach to abdominal wall-defect repair.* Biomaterials, 2005. **26**(15): p. 2567-74.
113. Marzaro, M., et al., *Autologous satellite cell seeding improves in vivo biocompatibility of homologous muscle acellular matrix implants.* Int J Mol Med, 2002. **10**(2): p. 177-82.
114. Pittenger, M., et al., *Adult mesenchymal stem cells: potential for muscle and tendon regeneration and use in gene therapy.* J Musculoskelet Neuronal Interact, 2002. **2**(4): p. 309-20.
115. Stern-Straeter, J., et al., *Advances in skeletal muscle tissue engineering.* In Vivo, 2007. **21**(3): p. 435-44.
116. Pittenger, M.F., et al., *Multilineage potential of adult human mesenchymal stem cells.* Science, 1999. **284**(5411): p. 143-7.
117. Danino, A.M., et al., *A scanning electron microscopical study of the two sides of polypropylene mesh (Marlex) and PTFE (Gore Tex) mesh 2 years after complete abdominal wall reconstruction. A study of 15 cases.* Br J Plast Surg, 2005. **58**(3): p. 384-8.
118. Kayaoglu, H.A., et al., *Comparison of adhesive properties of five different prosthetic materials used in hernioplasty.* J Invest Surg, 2005. **18**(2): p. 89-95.
119. Demir, U., et al., *Comparison of prosthetic materials in incisional hernia repair.* Surg Today, 2005. **35**(3): p. 223-7.
120. Allen, R.E. and L.K. Boxhorn, *Regulation of skeletal muscle satellite cell proliferation and differentiation by transforming growth factor-beta, insulin-like growth factor I, and fibroblast growth factor.* J Cell Physiol, 1989. **138**(2): p. 311-5.
121. Santa Maria, L., C.V. Rojas, and J.J. Minguell, *Signals from damaged but not undamaged skeletal muscle induce myogenic differentiation of rat bone-marrow-derived mesenchymal stem cells.* Exp Cell Res, 2004. **300**(2): p. 418-26.
122. Jones, N.C., et al., *The p38alpha/beta MAPK functions as a molecular switch to activate the quiescent satellite cell.* J Cell Biol, 2005. **169**(1): p. 105-16.
123. Huang, N.F., et al., *Myotube assembly on nanofibrous and micropatterned polymers.* Nano Lett, 2006. **6**(3): p. 537-42.
124. Shen, J.Y., et al., *UV-embossed microchannel in biocompatible polymeric film: Application to control of cell shape and orientation of muscle cells.*

Journal of Biomedical Materials Research Part B-Applied Biomaterials, 2006. **77B**(2): p. 423-430.
125. Falco, E.E., J.S. Roth, and J.P. Fisher, *EH Networks as a Scaffold for Skeletal Muscle Regeneration in Abdominal Wall Hernia Repair.* J Surg Res, 2007.
126. Falco, E.E., M. Patel, and J.P. Fisher, *Recent Developments in Cyclic Acetal Biomaterials for Tissue Engineering Applications.* Pharm Res, 2008.
127. Clarke, K.M., et al., *Intestine submucosa and polypropylene mesh for abdominal wall repair in dogs.* J Surg Res, 1996. **60**(1): p. 107-14.
128. Pu, L.L., *Small intestinal submucosa (Surgisis) as a bioactive prosthetic material for repair of abdominal wall fascial defect.* Plast Reconstr Surg, 2005. **115**(7): p. 2127-31.
129. Patton, J.H., Jr., S. Berry, and K.A. Kralovich, *Use of human acellular dermal matrix in complex and contaminated abdominal wall reconstructions.* Am J Surg, 2007. **193**(3): p. 360-3; discussion 363.
130. Ko, R., et al., *Tensile strength comparison of small intestinal submucosa body wall repair.* J Surg Res, 2006. **135**(1): p. 9-17.
131. Matthews, B.D., et al., *Assessment of adhesion formation to intra-abdominal polypropylene mesh and polytetrafluoroethylene mesh.* J Surg Res, 2003. **114**(2): p. 126-32.
132. Burger, J.W., et al., *Evaluation of new prosthetic meshes for ventral hernia repair.* Surg Endosc, 2006. **20**(8): p. 1320-5.
133. DeVol, D.L., et al., *Activation of insulin-like growth factor gene expression during work-induced skeletal muscle growth.* Am J Physiol, 1990. **259**(1 Pt 1): p. E89-95.
134. Beguinot, F., et al., *Distinct biologically active receptors for insulin, insulin-like growth factor I, and insulin-like growth factor II in cultured skeletal muscle cells.* J Biol Chem, 1985. **260**(29): p. 15892-8.
135. Barton-Davis, E.R., D.I. Shoturma, and H.L. Sweeney, *Contribution of satellite cells to IGF-I induced hypertrophy of skeletal muscle.* Acta Physiol Scand, 1999. **167**(4): p. 301-5.
136. Adams, G.R. and S.A. McCue, *Localized infusion of IGF-I results in skeletal muscle hypertrophy in rats.* J Appl Physiol, 1998. **84**(5): p. 1716-22.
137. Barton-Davis, E.R., et al., *Viral mediated expression of insulin-like growth factor I blocks the aging-related loss of skeletal muscle function.* Proc Natl Acad Sci U S A, 1998. **95**(26): p. 15603-7.
138. Song, C., et al., *Mechanical properties of the human abdominal wall measured in vivo during insufflation for laparoscopic surgery.* Surg Endosc, 2006. **20**(6): p. 987-90.
139. Fisher, J.P., et al., *Synthesis and properties of photocross-linked poly(propylene fumarate) scaffolds.* J Biomater Sci Polym Ed, 2001. **12**(6): p. 673-87.
140. Fisher, J.P., et al., *Photoinitiated cross-linking of the biodegradable polyester poly(propylene fumarate). Part II. In vitro degradation.* Biomacromolecules, 2003. **4**(5): p. 1335-42.

141. Fisher, J.P., et al., *Photoinitiated cross-linking of the biodegradable polyester poly(propylene fumarate). Part I. Determination of network structure.* Biomacromolecules, 2003. **4**(5): p. 1327-34.
142. Fisher, J.P., et al., *Soft and hard tissue response to photocrosslinked poly(propylene fumarate) scaffolds in a rabbit model.* J Biomed Mater Res, 2002. **59**(3): p. 547-56.
143. Higashiura, W., et al., *Prevalence, factors, and clinical impact of self-expanding stent fractures following iliac artery stenting.* J Vasc Surg, 2009. **49**(3): p. 645-52.
144. Falco, E.E., J.S. Roth, and J.P. Fisher, *Skeletal muscle tissue engineering approaches to abdominal wall hernia repair.* Birth Defects Res C Embryo Today, 2008. **84**(4): p. 315-21.
145. Kumbar, S.G., et al., *Electrospun nanofiber scaffolds: engineering soft tissues.* Biomed Mater, 2008. **3**(3): p. 034002.
146. Choi, J.S., et al., *The influence of electrospun aligned poly(epsilon-caprolactone)/collagen nanofiber meshes on the formation of self-aligned skeletal muscle myotubes.* Biomaterials, 2008. **29**(19): p. 2899-906.
147. Emans, P.J., et al., *Polypropylene meshes to prevent abdominal herniation. Can stable coatings prevent adhesions in the long term?* Ann Biomed Eng, 2009. **37**(2): p. 410-8.
148. Kaihara, S., S. Matsumura, and J.P. Fisher, *Synthesis and Properties of Poly[Poly(Ethylene Glycol)-co-Cyclic Acetal] Based Hydrogels.* Macromolecules, 2007. **40**: p. 7625-32.
149. Braun, S., *Muscular gene transfer using nonviral vectors.* Curr Gene Ther, 2008. **8**(5): p. 391-405.
150. Vitadello, M., et al., *Gene transfer in regenerating muscle.* Hum Gene Ther, 1994. **5**(1): p. 11-8.